General Disclaimer

One or more of the Following Statements may affect this Document

- This document has been reproduced from the best copy furnished by the organizational source. It is being released in the interest of making available as much information as possible.

- This document may contain data, which exceeds the sheet parameters. It was furnished in this condition by the organizational source and is the best copy available.

- This document may contain tone-on-tone or color graphs, charts and/or pictures, which have been reproduced in black and white.

- This document is paginated as submitted by the original source.

- Portions of this document are not fully legible due to the historical nature of some of the material. However, it is the best reproduction available from the original submission.

THE BEHAVIOR OF LASER MODES IN A MEDIUM WITH TIME VARYING DIELECTRIC CONSTANT

by

COLIN GORDON WHITNEY

MASSACHUSETTS INSTITUTE OF TECHNOLOGY
DEPARTMENT OF ELECTRICAL ENGINEERING
MATERIALS THEORY GROUP
CAMBRIDGE, MASSACHUSETTS 02139

TECHNICAL REPORT NO. 9

ARMY RESEARCH OFFICE
CONTRACT NO. DA-31-214-ARO(D)-92
ADVANCED RESEARCH PROJECTS AGENCY
CONTRACT NO. SD-90
NATIONAL AERONAUTICS AND SPACE ADMINISTRATION
ELECTRONICS RESEARCH CENTER

TECHNICAL REPORT NO. 9 August 25, 1970

Title: THE BEHAVIOR OF LASER MODES IN A MEDIUM WITH TIME VARYING DIELECTRIC CONSTANT

Sponsored by:

Army Research Office Contract No.: DA-31-124-ARO(D)-92

Department of the Army Project No.: 2001051B 700

Advanced Research Projects Agency Contract No.: SD-90

National Aeronautics and Space Administration/Electronics Research Center.

Name of Contractor:

Massachusetts Institute of Technology

Cambridge, Massachusetts 02139

Principal Investigator:

G.W. Pratt, Jr.

Author:

C.G. Whitney

MASSACHUSETTS INSTITUTE OF TECHNOLOGY

MATERIALS THEORY GROUP

ELECTRICAL ENGINEERING DEPARTMENT

Technical Report No. 9 August 25, 1970

THE BEHAVIOR OF LASER MODES IN A MEDIUM WITH TIME VARYING DIELECTRIC CONSTANT

by

Colin Gordon Whitney

This report is identical to a thesis submitted to the Physics Department, M.I.T., May 14, 1970, in partial fulfillment of the requirements for the degree of Doctor of Philosophy.

ABSTRACT

The effect, on semiconductor laser modes, of a time-varying modulation of the complex dielectric constant of the active region of the laser, is considered. It is seen that the main effect is to produce frequency modulation associated with modulation of the real part of the dielectric constant while modulation of the imaginary part gives rise to amplitude modulation. Two methods for producing the modulation are considered. The first, pressure via ultrasonic waves, produces pure frequency modulation in impure material. The second, modulation of the injection, results in both amplitude and frequency modulation.

Experiments to confirm this analysis were carried out on a cw GaAs injection laser. The modulated laser spectrum was observed with a Fabry-Perot Interferometer. Pressure modulation was seen to give frequency modulation with little distortion, while for injection modulation, ratio of the amplitude modulation index to frequency modulation index was found to be about 0.1.

High resolution measurements on the pulsed spectral shift of a GaAs laser at 77°K and 4.2°K were performed using a Fabry-Perot interferometer. The feasibility of detecting modulation on a pulsed semiconductor laser was demonstrated.

Acknowledgments

I wish to thank Professor George W. Pratt, Jr., for suggesting this research and for his guidance during its completion. I would also like to thank Dr. Michael S. Macrakis for his suggestions and support of the project, and Dr. Jose Ripper for supplying the lasers used and for the many discussions we have had. Thanks go to Dr. Melville Clark, Jr., for many fruitful discussions, to Mr. Ernest Corrado and Mr. Frank Wilson for their help with the experimental work, and to Miss Diane Sinausky for her excellent typing of this report. I wish also to express my sincere gratitude and love for my wife, Caroline, who has been a constant aid and inspiration to me and, without whose help, this work would not have been completed.

I am also grateful to the National Aeronautics and Space Administration/ Electronics Research Center, the Advanced Research Projects Agency, and the Army Research Office (Durham) for their financial support of this research.

Table of Contents

Table of Contents Cont.

List of Figures

List of Figures Cont.

List of Figures Cont.

List of Tables

CHAPTER I

THE UNMODULATED SEMICONDUCTOR LASER

1. Introduction

Considerable research has been performed in the field of laser communications because of the inherently large bandwidth associated with the laser. Many modulation schemes on different types of lasers have been developed but it is not clear that any one has a definite, overall advantage. Rather, the modulation scheme to be used, will depend on the specific application.

Here we report on two schemes for modulating a semiconductor injection laser, firstly by modulating the bias and secondly by modulating the pressure using ultrasonic waves. In Chapter I we derive the laser mode frequencies and amplitudes for the unmodulated laser. In Chapter II the effects of a general time dependent modulation on the laser are considered. Pressure modulation via ultrasonic waves is described in Chapter III and it is seen that the finite wavelength of the sound imposes an upper frequency limit on this form of modulation. Comparison with experiment is also made. In Chapter IV the same comparison is made for injection modulation. Finally in Chapter V, high resolution studies are made of the spectral shift of a pulsed semiconductor laser.

2. The Unmodulated Semiconductor Laser

Spontaneous emission, in semiconductors, arises when electrons in the conduction band or a nearby donor state, recombine spontaneously with holes in the valence band or an acceptor state, the energy lost by the electron being emitted as light. The spontaneous emission has a

fairly broad frequency range ($\approx$ 100Å for GaAs) and closely follows the behavior of the energy gap. Stimulated emission of light occurs, on the other hand, when the transition is aided by the radiation field present. From the well-known Statz-de Mars equations,[2] the threshold for laser action occurs when the population inversion $N_{th} = B_c^{-1} t_c^{-1}$ where B_c is the rate of stimulated emission into a single mode and t_c is the lifetime of a photon in the optical cavity.

The frequencies at which the laser will operate are determined by the (i) resonant frequencies of the optical cavity and (ii) the gain at these frequencies. The spontaneous emission gives roughly the spectral shape of the gain of the laser modes so that lasing action occurs near the peak of the spontaneous emission. In the following section the laser mode frequencies and amplitudes will be calculated for an unmodulated laser.

3. Mode Amplitudes and Frequencies

In this section we follow the treatment of Zachos and Ripper[1] in calculating the amplitudes and resonant frequencies of the laser modes. We start from the experimental observation that lasing action is not uniform across the laser mirror in the plane of the p-n junction of an injection laser. Instead, the light is broken up into filaments which lie along the junction. In general, to calculate the mode frequencies and amplitudes is exceedingly complex due to the randomness of these filaments. The choice of a focusing mechanism in the plane of the junction is thus difficult. If, however, the electron injection is confined to an area such that only one filament is present, the problem is greatly simplified. This can be achieved by using lasers of "stripe"

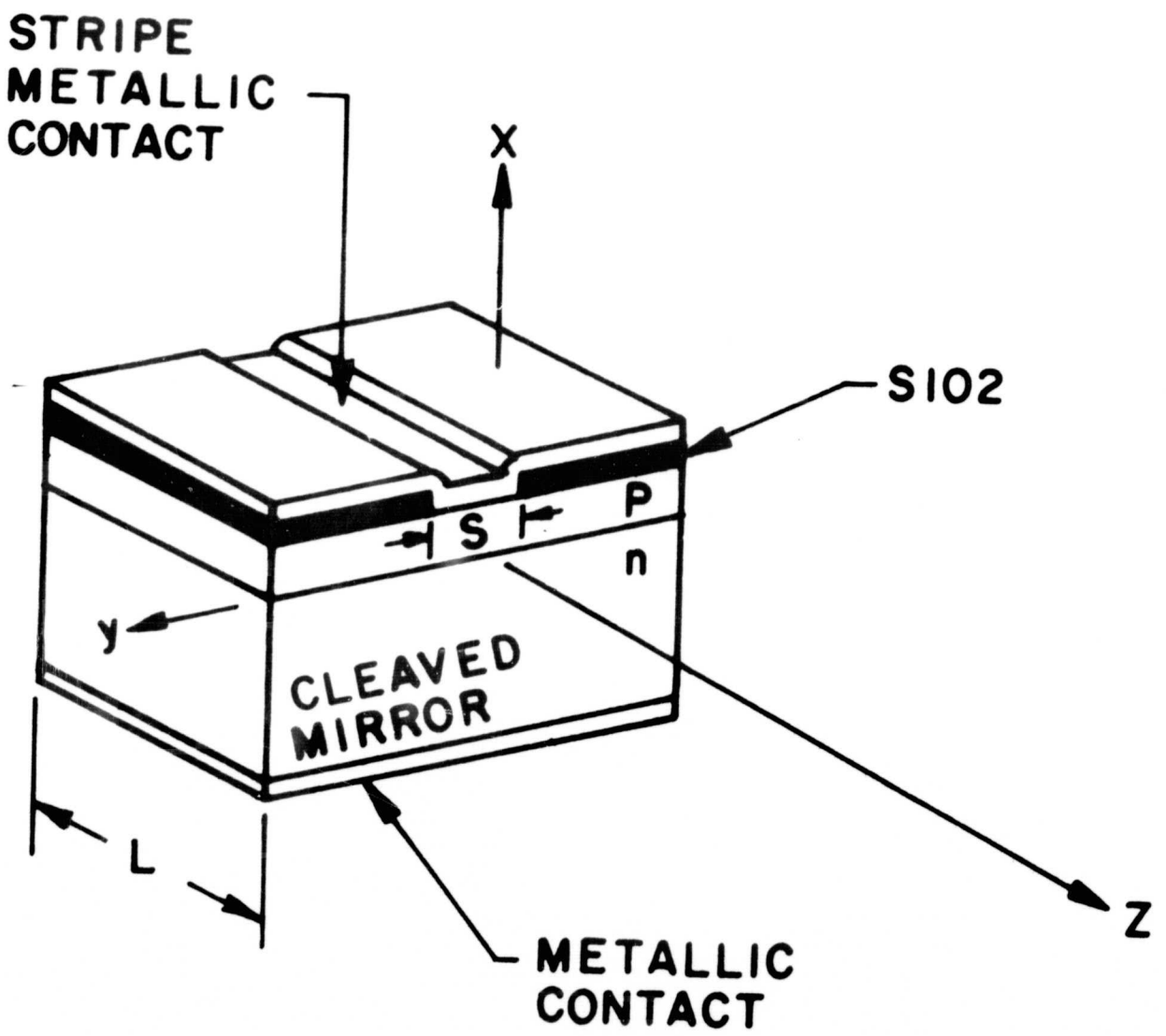

LASER GEOMETRY

FIGURE 1-1

geometry* as done in these experiments. (see fig. 1-1)

As a model for confinement of the laser radiation to a filament we thus assume a variation of the real part of the dielectric constant of the form

$$\varepsilon = \bar{n}^2 \varepsilon_o \left[1 - \left(\frac{x}{x_e}\right)^2 - \left(\frac{y}{y_e}\right)^2 \right] \quad 1\text{-}1$$

where $\bar{n}$ is the maximum value of $\varepsilon/\varepsilon_o$ and where ε_o is the dielectric constant of air, the z direction is the direction of propagation of the light beam with the mirrors at z = 0 and z = L the x-direction is perpendicular to the laser junction and y lies in the junction plane. We consider Maxwell's equations for a medium with spatially ranging dielectric constant

$$\nabla \times \vec{E} = -\mu_o \frac{\partial \vec{H}}{\partial t} \quad 1\text{-}2$$

$$\nabla \times \vec{H} = \vec{J} + \frac{\partial \vec{D}}{\partial t} \quad 1\text{-}3$$

taking the curl of 1-2 and the time derivative of 1-3

$$\nabla(\nabla \cdot \vec{E}) - \nabla^2 \vec{E} + \mu_o \varepsilon(x,y) \frac{\partial^2 \vec{E}}{\partial t^2} = -\mu_o \frac{\partial \vec{J}}{\partial t} \quad 1\text{-}4$$

assuming a time dependence $e^{\pm i\omega_o t}$

$$\left[\nabla^2 + \mu_o \varepsilon(x,y) \omega_o^2\right] \vec{E} = \mu_o \frac{\partial \vec{J}}{\partial t} + \nabla(\nabla \cdot \vec{E}) \quad 1\text{-}5$$

*Kindly supplied by Dr. J. E. Ripper at Bell Telephone Laboratories, Murray Hill, New Jersey.

Since $\frac{\partial J}{\partial t} = 0$ and $\rho = 0$ the right-hand side is small. We shall neglect this term and justify this assumption later.

The equation to be solved is thus

$$\left[\nabla^2 + \mu_0 \varepsilon(x,y)\,\omega_0^2\right]\vec{E} = 0 \qquad 1\text{-}6$$

We are looking for propagating solutions of the form which decays as x,y tend to infinity

$$\vec{E} = \vec{E}_0\, X(x)\, Y(y)\, e^{\pm i k \gamma z}\, e^{\pm i \omega_0 t} \qquad 1\text{-}7$$

the solutions to the equation are TEM modes where in one case $\vec{E} = E\hat{y}$ and $\vec{H} = \vec{H}\hat{x}$ while in the other $\vec{E} = \hat{E}x$ and $\vec{H} = \hat{H}y$. We can thus solve a scalar equation for $\vec{E}$ and 1-6 becomes

$$\frac{1}{X(x)}\frac{\partial^2 X(x)}{\partial x^2} + \frac{1}{Y(y)}\frac{\partial^2 Y(y)}{\partial y^2} - k^2\gamma^2 + k^2\bar{n}^2\left[1 - \left(\frac{x_c}{x_e}\right)^2 - \left(\frac{y_c}{y_e}\right)^2\right] = 0 \qquad 1\text{-}8$$

where

$$k = \frac{\omega_0}{c}\sqrt{\mu_0 \varepsilon_0} \qquad 1\text{-}9$$

rewriting 1-8

$$\left[\frac{1}{X(x)}\frac{\partial^2 X(x)}{\partial x^2} - k^2\bar{n}^2\frac{x_c^2}{x_e^2}\right] + \left[\frac{1}{Y(y)}\frac{\partial^2 Y(y)}{\partial y^2} - k^2\bar{n}^2\frac{y_c^2}{y_e^2}\right] = k^2\gamma^2 - k^2\bar{n}^2 \qquad 1\text{-}10$$

the first two terms are functions of x only while the second two are functions of y only so both must be separately constant. But these are just two harmonic oscillator problems

$$\frac{\partial^2 X(x)}{\partial x^2} - \frac{k^2 \bar{n}^2}{x_e^2} x^2 X(x) = K_1 X(x) \qquad 1\text{-}11$$

letting $$\alpha = \sqrt{\frac{k\bar{n}}{x_e}}\, x \qquad 1\text{-}12$$

$$\frac{\partial^2 X(\alpha)}{\partial \alpha^2} - \alpha^2 X(\alpha) = \frac{K_1}{\left(\frac{k\bar{n}}{x_e}\right)} X(\alpha) \qquad 1\text{-}13$$

choosing $$K_1 = -(2n+1)\frac{k\bar{n}}{x_e} \qquad 1\text{-}14$$

we find

$$X_n(\alpha) = e^{-\frac{1}{2}\alpha^2} H_n(\alpha) \qquad 1\text{-}15(a)$$

$$X_n(x) = e^{-\frac{1}{2}\frac{k\bar{n}}{x_e}x^2} H_n\left(\sqrt{\frac{k\bar{n}}{x_e}}\, x\right) \qquad 1\text{-}15(b)$$

where H_n is the Hermite Polynomial of order n

a similar result may be obtained for $Y_m\left(\sqrt{\frac{k\bar{n}}{y_e}}\, y\right)$

$$\therefore \quad \gamma^2 = \bar{n}^2\left[1 - \frac{2n+1}{k\bar{n}x_e} - \frac{2m+1}{k\bar{n}y_e}\right] \qquad 1\text{-}16$$

The definition of a mode requires that for say the wave propagating in the +z direction

$$\vec{E}^{+}(x,y,0) = \pm \vec{E}^{+}(x,y,L) \qquad 1\text{-}17$$

this requires

$$\gamma_{nmq} = \frac{q\pi}{kL} \qquad 1\text{-}18$$

By substituting 1-18 into 1-16 we can solve for the laser frequency

$$\nu_{nmq} = \frac{cq}{2L\bar{n}}\left\{1+\left[\frac{L}{2\pi q}\left(\frac{2n+1}{x_e}+\frac{2m+1}{y_e}\right)\right]^2\right\}^{\frac{1}{2}}+\frac{c}{4\pi\bar{n}}\left(\frac{2n+1}{x_e}+\frac{2m+1}{y_e}\right) \qquad 1\text{-}19$$

and the laser mode electric field may be written

$$\vec{E}_{nmq}(x,y,z,t) = \vec{E}_0 e^{-\frac{1}{2}\frac{k\bar{n}}{x_e}x^2} H_n\left(\sqrt{\frac{k\bar{n}}{x_e}}x\right) e^{-\frac{1}{2}\frac{k\bar{n}}{y_e}y^2} H_m\left(\sqrt{\frac{k\bar{n}}{y_e}}y\right)\cos\left(q\pi\frac{z}{L}\right) \times \cos(2\pi\nu_{nmq}t) \qquad 1\text{-}20$$

The first term in 1-19 for GaAs is ≈8,400Å while the second gives a small correction ≈4Å.

This model gives very good agreement with the experimental observations. For instance by differentiating 1-19 remembering that $\bar{n}$ is a function of frequency, the mode separation for low-order transverse modes where

$$\frac{L}{2\pi q}\left[\frac{2n+1}{x_e}+\frac{2m+1}{y_e}\right] << 1 \qquad 1\text{-}21$$

is given by

$$L\frac{\Delta\lambda}{\lambda^2} = -\frac{1}{2\bar{n}_e}\left[\frac{L}{\pi x_e}\Delta n + \frac{L}{\pi y_e}\Delta m + \Delta q\right] \qquad 1\text{-}22$$

$$\text{where}\quad \bar{n}_e = \bar{n}\left(1-\frac{\lambda}{\bar{n}}\frac{\partial\bar{n}}{\partial\lambda}\right) \qquad 1\text{-}23$$

Longitudinal mode separation gives

$$(\Delta\lambda)_q = -\frac{\lambda^2}{2\bar{n}_e L}\Delta q \qquad 1\text{-}24$$

While transverse mode separation are given by

$$(\Delta\lambda)_n = -\frac{\lambda^2}{2\pi\bar{n}_e x_e}\Delta n \qquad 1\text{-}25(a)$$

$$(\Delta\lambda)_m = -\frac{\lambda^2}{2\pi\bar{n}_e y_e}\Delta m \qquad 1\text{-}25(b)$$

these values agree well with those observed experimentally. For the lasers used L = 380μ, and $\bar{n}_e \equiv 5.2$. The values x_e and y_e have been measured[1] as typically $x_e = 17\mu$ and $y_e = 1400\mu$. This figures give a longitudinal mode separation of 1.8Å while the transverse mode separations are given by

$$(\Delta\lambda)_n \approx 13\ \text{Å}\ \Delta n \qquad 1\text{-}26$$

and

$$(\Delta\lambda)_m \approx 0.18\ \text{Å}\ \Delta m \qquad 1\text{-}27$$

respectively.

Neglect of the term $\nabla(\nabla\cdot E)$ on the right-hand side of 1-5 can be shown to lead to neglect of terms of order $\frac{2n}{kx_e}$ and $\frac{2m}{ky_e}$ with respect to unity. Using the values given above and $\lambda = 0.84\mu$ we find

$$\frac{2n}{kx_e} \approx 16 \times 10^{-3}\ n \qquad 1\text{-}28$$

and

$$\frac{2m}{ky_e} \approx 0.19 \times 10^{-3}\ m \qquad 1\text{-}29$$

thus justifying the assumption mode.

The model used above for calculating the mode structure of an unmodulated semiconductor postulates a dielectric constant which has a maximum at the junction and decreases on either side thus acting as a waveguide for the light produced. Both the unperturbed cavity mode amplitude and frequencies have been calculated and shown to give good agreement with experimental observations on the laser spectrum. The laser mode amplitudes will be used to calculate the effects of pressure modulation on the laser in Chapter III.

References

1. T. H. Zachos and J. E. Ripper, IEEE Journal of Quantum Electronics QE-5, 29 (1969).

2. See, for example, W. V. Smith and P. P. Sorokin, THE LASER, McGraw-Hill Book Company, p. 69 (1966).

CHAPTER II

MODULATION OF THE COMPLEX DIELECTRIC CONSTANT

1. Time Dependent Modulation of the Complex Dielectric Constant

In Chapter I the mode amplitudes and frequencies for the unmodulated laser were calculated.These are now used as the starting point in calculating the effect on the laser amplitudes and frequencies of modulating the complex dielectric constant.It will be seen that modulation of the real part of the dielectric constant gives rise to frequency modulation while modulation of the imaginary part leads to amplitude modulation. In the section which follows,it is assumed that the laser mode amplitudes are orthonormal and only a time variation in the modulated component of the complex dielectric constant is considered.In Chapter III, for pressure modulation,we shall consider a modulation of the form $\cos(\omega_s t - q_s x)$

Consider Maxwell's equations

$$\nabla \times \vec{E} = -\frac{\partial}{\partial t}(\mu_0 \vec{H}) \qquad 2\text{-}1$$

$$\nabla \times \vec{H} = \vec{J} + \frac{\partial}{\partial t}\vec{D} \qquad 2\text{-}2$$

write

$$\vec{D} = \varepsilon(\vec{r},t)\,\vec{E} \qquad 2\text{-}3$$

where ε is complex to take into account gain in the system and

$$\vec{J} = \sigma(\vec{r},t)\,\vec{E} \qquad 2\text{-}4$$

where σ accounts for losses.

Write the electric and magnetic fields as a sum of normal modes[1]

$$\vec{E} = -\sum_a \frac{P_a(t)}{\sqrt{\varepsilon_{AV}}}\,\vec{E}_a(\vec{r}) \qquad 2\text{-}5$$

$$\vec{H} = \sum_a \frac{\omega_a}{\sqrt{\mu_0}}\,q_a(t)\,\vec{H}_a(\vec{r}) \qquad 2\text{-}6$$

where ε_{AV} is the real part of the dielectric constant and E_a and ω_a are given in Chapter I.

Note, $$k_a \vec{E}_a = \nabla \times \vec{H}_a \qquad 2\text{-}7(a)$$

$$k_a \vec{H}_a = \nabla \times \vec{E}_a \qquad 2\text{-}7(b)$$

Where $k_a = \frac{\omega_a}{c}\sqrt{\frac{\varepsilon_{AV}}{\varepsilon_0}}$

From 2-1 we get

$$P_a = \dot{q}_a \qquad 2\text{-}8$$

From 2-2 and using 2-7

$$\sum_a \frac{\omega_a^2 \sqrt{\frac{\varepsilon_{AV}}{\varepsilon_0}}}{c\sqrt{\mu_0}} q_a(t)\, \vec{E}_a(\vec{r}) = -\sum_a \vec{E}_a(\vec{r}) \left[\frac{\sigma(\vec{r},t)}{\sqrt{\varepsilon_{AV}}} P_a(t) + \frac{1}{\sqrt{\varepsilon_{AV}}} \frac{\partial}{\partial t}\left[\varepsilon(\vec{r},t) P_a(t)\right] \right] \qquad 2\text{-}9$$

take the dot product of 2-9 with $\vec{E}_b$ and integrate using orthonormality

$$\sum_a \frac{\omega_a^2}{c\sqrt{\mu_0}} q_a(t) \int d^3\vec{r}\, \vec{E}_a(\vec{r}) \cdot \vec{E}_b(\vec{r}) = -\sum_a \frac{P_a(t)}{\sqrt{\varepsilon_{AV}}} \int d^3\vec{r}\, \sigma(\vec{r},t)\, \vec{E}_a(\vec{r}) \cdot \vec{E}_b(\vec{r})$$

$$\sum \frac{1}{\sqrt{\varepsilon_{AV}}} \frac{\partial}{\partial t}\left[P_a(t) \int d^3\vec{r}\, \varepsilon(\vec{r},t)\, \vec{E}_a(\vec{r}) \cdot \vec{E}_b(\vec{r})\right] \qquad 2\text{-}10$$

$$\omega_b^2 q_b(t) = -\sum_a P_a(t) \frac{1}{\varepsilon_{AV}} \int d^3\vec{r}\, \sigma \vec{E}_a \cdot \vec{E}_b - \sum_a \frac{\partial}{\partial t}\left[\frac{P_a(t)}{\varepsilon_{AV}} \int d^3\vec{r}\, \varepsilon \vec{E}_a \cdot \vec{E}_b\right] \qquad 2\text{-}11$$

let

$$S_{ab}(\vec{r},t) = \frac{1}{\varepsilon_{AV}} \int d^3\vec{r}\; \sigma(\vec{r},t)\, \vec{E}_a(\vec{r}) \cdot \vec{E}_b(\vec{r}) \qquad 2\text{-}12$$

$$T_{ab}(t) = \frac{1}{\varepsilon_{AV}} \int d^3\vec{r}\, \varepsilon(\vec{r},t)\, \vec{E}_a(\vec{r}) \cdot \vec{E}_b(\vec{r}) \qquad 2\text{-}13$$

Then

$$\omega_b^2 q_b(t) = -\sum_a P_a(t)\, S_{ab}(t) - \sum_a \frac{\partial}{\partial t}\left[P_a(t)\, T_{ab}(t)\right] \qquad 2\text{-}14$$

$$\text{put} \quad q_b(t) = \frac{1}{\sqrt{2\omega_b}}\left[C_b^* + C_b\right] \qquad 2\text{-}15$$

$$P_b(t) = i\sqrt{\frac{\omega_b}{2}}\left[C_b^* - C_b\right] \qquad 2\text{-}16$$

Then Equation 2-8 becomes

$$\dot{C}_b^* + \dot{C}_b = i\omega_b\left[C_b^* - C_b\right] \qquad 2\text{-}17$$

and 2-14 becomes

$$2\text{-}18$$

$$\omega_b\left[C_b^* + C_b\right] = -i\sum_a S_{ab}(t)\left[C_a^* - C_a\right] - i\sum_a \frac{\partial}{\partial t}\left[T_{ab}(t)\left[C_a^* - C_a\right]\right]$$

$$\sum_a \frac{\partial}{\partial t}\left[T_{ab}(t)\left(C_a^* - C_a\right)\right] = i\omega_b\left[C_b^* + C_b\right] - \sum_a S_{ab}(t)\left[C_a^* - C_a\right]$$

$$2\text{-}19$$

Let us assume that σ and the modulated components of ε are independent of position. Then the terms S_{ab} and T_{ab} which couple the modes, decouple

$$S_{ab}(t) = \frac{\sigma(t)}{\varepsilon_{AV}} S_{ab} \qquad 2\text{-}20$$

$$T_{ab}(t) = \frac{\varepsilon(t)}{\varepsilon_{AV}} S_{ab} \qquad 2\text{-}21$$

further assume

$$\sigma(t) = \sigma_0 + \sigma_1(t) \qquad 2\text{-}22$$

$$\varepsilon(t) = \left[\tilde{n}^2\varepsilon_0\left(1 - \left(\frac{x}{x_e}\right)^2 - \left(\frac{y}{y_e}\right)^2\right)\right]_{AV} + \varepsilon_1(t) \qquad 2\text{-}23(a)$$

$$= \varepsilon_{AV} + \varepsilon_1(t) \qquad 2\text{-}23(b)$$

Then 2-19 becomes neglecting terms of order $\frac{m}{\bar{n}kx_e}$ and $\frac{m}{\bar{n}ky_e}$ compared to unity

$$\frac{\partial}{\partial t}\left[\frac{\varepsilon(t)}{\varepsilon_{AV}}(c_b^* - c_b)\right] = i\omega_b\left[c_b^* + c_b\right] - \frac{\sigma(t)}{\varepsilon_{AV}}\left[c_b^* - c_b\right] \qquad 2\text{-}24$$

$$\dot{c}_b^* - \dot{c}_b = \left[i\omega_b - \frac{\sigma(t)}{\varepsilon_{AV}}\right]c_b^* + \left[i\omega_b + \frac{\sigma(t)}{\varepsilon_{AV}}\right]c_b - \frac{\partial}{\partial t}\left[\frac{\varepsilon_1(t)}{\varepsilon_{AV}}(c_b^* - c_b)\right] \qquad 2\text{-}25$$

$$\dot{c}_b^* - \dot{c}_b = \left[i\omega_b - \frac{\sigma(t)}{\varepsilon_{AV}} - \frac{\dot{\varepsilon}_1(t)}{\varepsilon_{AV}}\right]c_b^* + \left[i\omega_b + \frac{\sigma(t)}{\varepsilon_{AV}} + \frac{\dot{\varepsilon}_1(t)}{\varepsilon_{AV}}\right]c_b - \frac{\varepsilon_1(t)}{\varepsilon_{AV}}\left[\dot{c}_b^* - \dot{c}_b\right] \qquad 2\text{-}26$$

adding and subtracting 2-17 we find

$$\dot{c}_b = -\left[i\omega_b + \frac{\sigma(t)}{2\varepsilon_{AV}} + \frac{\dot{\varepsilon}_1(t)}{2\varepsilon_{AV}}\right]c_b + \left[\frac{\sigma(t)}{2\varepsilon_{AV}} + \frac{\dot{\varepsilon}_1(t)}{2\varepsilon_{AV}}\right]c_b^* + \frac{\varepsilon_1(t)}{2\varepsilon_{AV}}\left[\dot{c}_b^* - \dot{c}_b\right] \qquad 2\text{-}27$$

$$\dot{c}_b^* = -\left[-i\omega_b + \frac{\sigma(t)}{2\varepsilon_{AV}} + \frac{\dot{\varepsilon}_1(t)}{2\varepsilon_{AV}}\right]c_b^* + \left[\frac{\sigma(t)}{2\varepsilon_{AV}} + \frac{\dot{\varepsilon}_1(t)}{2\varepsilon_{AV}}\right]c_b + \frac{\varepsilon_1(t)}{2\varepsilon_{AV}}\left[\dot{c}_b - \dot{c}_b^*\right] \qquad 2\text{-}28$$

we may write

$$\varepsilon_1(t) = i\alpha + \varepsilon_2(t) + i\alpha_2(t) \qquad 2\text{-}29$$

$$\varepsilon_1(t) = i\alpha + \bar{\varepsilon}_2(t) \qquad 2\text{-}30$$

where α is related to the gain. Then we have

$$\left[1 + \frac{i\alpha}{2\varepsilon_{AV}}\right]\dot{c}_b = -\left[i\omega_b + \frac{\sigma_0 + \sigma_1 + \dot{\bar{\varepsilon}}_2}{2\varepsilon_{AV}}\right]c_b + \left[\frac{\sigma_0 + \sigma_1 + \dot{\bar{\varepsilon}}_2}{2\varepsilon_{AV}}\right]c_b^* - \frac{\bar{\varepsilon}_2}{2\varepsilon_{AV}}\dot{c}_b + \left[\frac{i\alpha + \bar{\varepsilon}_2}{2\varepsilon_{AV}}\right]\dot{c}_b^* \qquad 2\text{-}31$$

$$\left[1 + \frac{i\alpha}{2\varepsilon_{AV}}\right]\dot{c}_b^* = -\left[-i\omega_b + \frac{\sigma_0 + \sigma_1 + \dot{\bar{\varepsilon}}_2}{2\varepsilon_{AV}}\right]c_b^* + \left[\frac{\sigma_0 + \sigma_1 + \dot{\bar{\varepsilon}}_2}{2\varepsilon_{AV}}\right]c_b - \frac{\bar{\varepsilon}_2}{2\varepsilon_{AV}}\dot{c}_b^* + \left[\frac{i\alpha + \bar{\varepsilon}_2}{2\varepsilon_{AV}}\right]\dot{c}_b \qquad 2\text{-}32$$

Let

$$C_b^*(t) = D_b^*(t)\, e^{i\omega_b t - \frac{\sigma_0}{2\bar{\varepsilon}_{AV}} t + \gamma' t} \qquad 2\text{-}33$$

and

$$C_b(t) = D_b(t)\, e^{-i\omega_b t - \frac{\sigma_0}{2\bar{\varepsilon}_{AV}} t + \gamma t} \qquad 2\text{-}34$$

where $D_b(t)$ is a slowly varying function of time

$$\left[1 + \frac{i\alpha}{2\bar{\varepsilon}_{AV}}\right]\left[\dot{D}_b\, e^{-i\omega_b t - \frac{\sigma_0}{2\bar{\varepsilon}_{AV}} t + \gamma t} - \left(i\omega_b + \frac{\sigma_0}{2\bar{\varepsilon}_{AV}} - \gamma\right) C_b\right] = -\left[i\omega_b + \frac{\sigma_0}{2\bar{\varepsilon}_{AV}}\right] C_b$$

$$- \left[\frac{\sigma_1 + \dot{\bar{\varepsilon}}_2}{2\bar{\varepsilon}_{AV}}\right] C_b + \left[\frac{\sigma_0 + \sigma_1 + \dot{\bar{\varepsilon}}_2}{2\bar{\varepsilon}_{AV}}\right] C_b^* - \frac{\bar{\varepsilon}_2}{2\bar{\varepsilon}_{AV}} \dot{C}_b + \left[\frac{i\alpha + \bar{\varepsilon}_2}{2\bar{\varepsilon}_{AV}}\right] \dot{C}_b^* \qquad 2\text{-}35$$

Choose γ so that

$$-\left[1 + \frac{i\alpha}{2\bar{\varepsilon}_{AV}}\right]\left[i\omega_b + \frac{\sigma_0}{2\bar{\varepsilon}_{AV}} - \gamma\right] = -\left[i\omega_b + \frac{\sigma_0}{2\bar{\varepsilon}_{AV}}\right] \qquad 2\text{-}36$$

then

$$\gamma = \frac{\frac{\alpha}{2\bar{\varepsilon}_{AV}} \left\{ i\left[\frac{\sigma_0}{2\bar{\varepsilon}_{AV}} + \frac{\alpha\omega_b}{2\bar{\varepsilon}_{AV}}\right] - \left[\omega_b - \frac{\alpha}{2\bar{\varepsilon}_{AV}} \cdot \frac{\sigma_0}{2\bar{\varepsilon}_{AV}}\right]\right\}}{1 + \left(\frac{\alpha}{2\bar{\varepsilon}_{AV}}\right)^2} \qquad 2\text{-}37$$

if we put in 2-37 $\omega_b \to -\omega_b$ then $\gamma \to \gamma'$

and we have

$$\left[1 + \frac{i\alpha}{2\bar{\varepsilon}_{AV}}\right]\dot{D}_b\, e^{-i\omega_b t - \frac{\sigma_0}{2\bar{\varepsilon}_{AV}} t + \gamma t} = -\left(\frac{\sigma_1 + \dot{\bar{\varepsilon}}_2}{2\bar{\varepsilon}_{AV}}\right) D_b\, e^{-i\omega_b t - \frac{\sigma_0}{2\bar{\varepsilon}_{AV}} t + \gamma t} + \left(\frac{\sigma_0 + \sigma_1 + \dot{\bar{\varepsilon}}_2}{2\bar{\varepsilon}_{AV}}\right) D_b^*\, e^{i\omega_b t - \frac{\sigma_0 t}{2\bar{\varepsilon}_{AV}} + \gamma' t}$$

$$+ \left[\frac{i\alpha + \bar{\varepsilon}_2}{2\bar{\varepsilon}_{AV}}\right]\left[\dot{D}_b^* + \left(i\omega_b - \frac{\sigma_0}{2\bar{\varepsilon}_{AV}} + \gamma'\right) D_b\right] e^{i\omega_b t - \frac{\sigma_0 t}{2\bar{\varepsilon}_{AV}} + \gamma' t} \qquad 2\text{-}38$$

$$- \frac{\bar{\varepsilon}_2}{2\bar{\varepsilon}_{AV}}\left[\dot{D}_b + \left(-i\omega_b - \frac{\sigma_0}{2\bar{\varepsilon}_{AV}} + \gamma\right) D_b\right] e^{-i\omega_b t - \frac{\sigma_0 t}{2\bar{\varepsilon}_{AV}} + \gamma t}$$

$$\left[1 + \frac{i\alpha + \bar{\varepsilon}_2}{2\bar{\varepsilon}_{AV}}\right]\dot{D}_b = \left[\frac{\bar{\varepsilon}_2}{2\bar{\varepsilon}_{AV}}\left(i\omega_b + \frac{\sigma_0}{2\bar{\varepsilon}_{AV}} - \gamma\right) - \left(\frac{\sigma_1 + \dot{\bar{\varepsilon}}_2}{2\bar{\varepsilon}_{AV}}\right)\right] D_b + \left[\frac{i\alpha + \bar{\varepsilon}_2}{2\bar{\varepsilon}_{AV}}\right] D_b^*\, e^{2i\omega_b t + (\gamma' - \gamma)t}$$

$$+ \left[\left(\frac{i\alpha + \bar{\varepsilon}_2}{2\bar{\varepsilon}_{AV}}\right)\left(i\omega_b - \frac{\sigma_0}{2\bar{\varepsilon}_{AV}} + \gamma'\right) + \frac{\sigma_0 + \sigma_1 + \dot{\bar{\varepsilon}}_2}{2\bar{\varepsilon}_{AV}}\right] D_b^*\, e^{2i\omega_b t + (\gamma' - \gamma)t} \qquad 2\text{-}39$$

and

$$\left[1+\frac{i\alpha+\bar{\varepsilon}_2}{2\,\varepsilon_{AV}}\right]\dot{D}_b^{*}\,e^{2i\omega_b t+(\gamma'-\gamma)t}=\left[\frac{\bar{\varepsilon}_2}{2\,\varepsilon_{AV}}\left(-i\omega_b+\frac{\sigma_0}{2\varepsilon_{AV}}-\gamma'\right)-\frac{(\sigma_1+\dot{\bar{\varepsilon}}_2)}{2\varepsilon_{AV}}\right]D_b^{*}e^{2i\omega_b t+(\gamma'-\gamma)t}$$

$$+\left[\left(\frac{i\alpha+\bar{\varepsilon}_2}{2\,\varepsilon_{AV}}\right)\left(-i\omega_b-\frac{\sigma_0}{2\,\varepsilon_{AV}}+\gamma\right)+\frac{\sigma_0+\sigma_1+\dot{\bar{\varepsilon}}_2}{2\,\varepsilon_{AV}}\right]D_b+\left(\frac{i\alpha+\bar{\varepsilon}_2}{2\,\varepsilon_{AV}}\right)\dot{D}_b$$

2-40

Since we have assumed that D_b is slowly varying we can neglect the last two terms in 2-39 and write

$$\dot{D}_b=\frac{1}{\left[1+\frac{(i\alpha+\bar{\varepsilon}_2)}{2\,\varepsilon_{AV}}\right]}\left[\frac{\bar{\varepsilon}_2}{2\,\varepsilon_{AV}}\left(i\omega_b+\frac{\sigma_0}{2\,\varepsilon_{AV}}-\gamma\right)-\frac{\sigma_1+\dot{\bar{\varepsilon}}_2}{2\,\varepsilon_{AV}}\right]D_b$$

2-41

$$\therefore D_b=\exp\left\{\int dt\left[\frac{1}{1+\frac{i\alpha+\bar{\varepsilon}_2}{2\,\varepsilon_{AV}}}\left(\frac{\bar{\varepsilon}_2}{2\,\varepsilon_{AV}}\left(i\omega_b+\frac{\sigma_0}{2\,\varepsilon_{AV}}-\gamma\right)-\frac{\sigma_1+\dot{\bar{\varepsilon}}_2}{2\,\varepsilon_{AV}}\right)\right]\right\}$$

2-42

to first order in $\bar{\varepsilon}_2$ and σ_1 we have

$$D_b=\exp\left\{\left(\frac{1-\frac{i\alpha}{2\,\varepsilon_{AV}}}{1+\left(\frac{\alpha}{2\,\varepsilon_{AV}}\right)^2}\right)\left[\left(i\omega_b+\frac{\sigma_0}{2\,\varepsilon_{AV}}-\gamma\right)\int\frac{dt\,\bar{\varepsilon}_2}{2\,\varepsilon_{AV}}-\int dt\,\frac{(\sigma_1+\dot{\bar{\varepsilon}}_2)}{2\,\varepsilon_{AV}}\right]\right\}$$

2-43

$$=\exp\left\{\left(\frac{1-\frac{i\alpha}{2\,\varepsilon_{AV}}}{1+\left(\frac{\alpha}{2\,\varepsilon_{AV}}\right)^2}\right)\left[\frac{\left(i\omega_b+\frac{\sigma_0}{2\,\varepsilon_{AV}}-\gamma\right)}{2\,\varepsilon_{AV}}\int dt\,\bar{\varepsilon}_2+-\int\frac{dt\,\sigma_1}{2\,\varepsilon_{AV}}-\frac{\bar{\varepsilon}_2}{2\,\varepsilon_{AV}}\right]\right\}$$

2-44

$$\therefore C_b=\exp\left\{-\left(i\omega_b+\frac{\sigma_0}{2\varepsilon_{AV}}-\gamma\right)t+\frac{1}{2\varepsilon_{AV}}\left(\frac{1-\frac{i\alpha}{2\varepsilon_{AV}}}{1+\left(\frac{\alpha}{2\varepsilon_{AV}}\right)^2}\right)\left[\left(i\omega_b+\frac{\sigma_0}{2\varepsilon_{AV}}-\gamma\right)\int dt\,\bar{\varepsilon}_2-\int dt\,\sigma_1-\bar{\varepsilon}_2\right]\right\}$$

2-45

For a solution which does not either grow or decay exponentially with time we must have

$$\frac{\sigma_0}{2\,\bar{\epsilon}_{AV}} = \gamma \qquad 2-46$$

This implies from 2-37 that

$$\alpha\omega_b = -\,\sigma_0 \qquad 2-47$$

$$\therefore\quad C_b = e^{-i\omega_b t + \frac{1}{2\bar{\epsilon}_{AV}}\left[\frac{1-\frac{i\alpha}{2\bar{\epsilon}_{AV}}}{1+\left(\frac{\alpha}{2\bar{\epsilon}_{AV}}\right)^2}\right]\left\{i\omega_b\int\bar{\epsilon}_2\,dt - \int\bar{\sigma}_1\,dt - \bar{\epsilon}_2\right\}} \qquad 2-48$$

$$C_b = e^{-i\omega_b t + \frac{1}{2\bar{\epsilon}_{AV}}\left[\frac{1-\frac{i\alpha}{2\bar{\epsilon}_{AV}}}{1+\left(\frac{\alpha}{2\bar{\epsilon}_{AV}}\right)^2}\right]\left\{i\omega_b\int\epsilon_2\,dt - \int(\omega_b\alpha_2+\sigma_1)\,dt - (\epsilon_2+i\alpha_2)\right\}} \qquad 2-49$$

Thus we see that if we modulate the complex dielectric constant the laser modes are both amplitude and frequency modulated. We must now examine the quantities in 2-49.

2. Relationship Between the Real and Imaginary Parts of the Dielectric Constant

In general the real and imaginary parts of the dielectric constant are related via the Kramer-Kronig relation. Thus in 2-49, the modulation components may not be chosen arbitrarily. In order to examine the connection between them we assume that the displacement $\vec{D}$ and electric field $\vec{E}$ are linearly related. The most general linear relationship between $\vec{D}$ and $\vec{E}$ may be written[2]

$$\vec{D}(t) = \vec{E}(t) + \int_0^\infty f(\tau)\,\vec{E}(t-\tau)\,d\tau \qquad 2-50$$

where $f(\tau)$ describes the properties of the medium and the displacement $\vec{D}$ depends on the values of the electric field at previous times. Furthermore, by requiring that real electric fields give real displacements $f(\tau)$ must be

real. Taking the Fourier transform of 2-50

$$D(\omega) = \left[1 + \int_0^\infty f(\tau) e^{i\omega\tau} d\tau\right] E(\omega) \qquad 2\text{-}51$$

Hence the most general form of the complex dielectric constant is given by

$$\varepsilon(\omega) = 1 + \int_0^\infty f(\tau)\, e^{i\omega\tau} d\tau \qquad 2\text{-}52$$

note that 2-51 gives the relationship for real ω

$$\varepsilon(-\omega) = \varepsilon^*(\omega) \qquad 2\text{-}53$$

writing

$$\varepsilon(\omega) = \varepsilon'(\omega) + i\,\varepsilon''(\omega) \qquad 2\text{-}54$$

$$\varepsilon'(\omega) = 1 + \int_0^\infty f(\tau) \cos\omega\tau\, d\tau \qquad 2\text{-}55$$

$$\varepsilon''(\omega) = \int_0^\infty f(\tau) \sin\omega\tau\, d\tau \qquad 2\text{-}56$$

If $f(\tau)$ is now changed to $f(\tau) + \Delta f(\tau)$ then the same analysis applies with a new dielectric constant

$$\epsilon_1(\omega) = \varepsilon(\omega) + \Delta\varepsilon(\omega) \qquad 2\text{-}57(a)$$

$$\varepsilon_1(\omega) = \varepsilon'(\omega) + \Delta\varepsilon'(\omega) + i\left(\varepsilon''(\omega) + \Delta\varepsilon''(\omega)\right) \qquad 2\text{-}57(b)$$

thus

$$\Delta\varepsilon'(\omega) = \int_0^\infty \Delta f(\tau) \cos\omega\tau\, d\tau \qquad 2\text{-}58$$

$$\Delta\varepsilon''(\omega) = \int_0^\infty \Delta f(\tau) \sin\omega\tau\, d\tau \qquad 2\text{-}59$$

applying the Fourier transform to 2-58 and 2-59

$$f(t) + 2\pi\,\delta(t) = \int_{-\infty}^{\infty} d\omega\, e^{-i\omega t}\, \varepsilon(\omega) \qquad 2\text{-}60$$

$$\Delta f(t) = \int_{-\omega}^{\omega} d\omega\, e^{-i\omega t}\, \Delta\varepsilon(\omega) \qquad 2\text{-}61$$

making use of

$$\Delta \epsilon'(-\omega) = \Delta \epsilon'(\omega) \qquad 2-62$$

and

$$\Delta \epsilon''(-\omega) = -\Delta \epsilon''(\omega) \qquad 2-63$$

$$\Delta f(t) = 2\int_0^\infty d\omega \left[\Delta \epsilon'(\omega) \cos\omega t + \Delta \epsilon''(\omega) \sin\omega t\right] \qquad 2-64$$

It can be seen that there are two components to $\Delta f(\tau)$. The first comes from modulation of the real part of the dielectric constant while the second comes from modulation of the imaginary part of the dielectric constant. Since in this experiment an external modulation at a frequency ω_m is imposed, it must be that

$$\Delta \epsilon'(\omega) = \Delta \epsilon' \left[\delta(\omega-\omega_m) + \delta(-\omega-\omega_m)\right] \qquad 2-65$$

$$\Delta \epsilon''(\omega) = \Delta \epsilon'' \left[\delta(\omega-\omega_m) - \delta(-\omega-\omega_m)\right] \qquad 2-66$$

so that

$$\Delta f(t) = \Delta \epsilon' \cos\omega_m t + \Delta \epsilon'' \sin\omega_m t \qquad 2-67$$

Thus we note the important result that the modulation of the real and imaginary parts of the dielectric constant are out of phase by $\Pi/2$. This fact makes a profound difference to the spectrum of the modulated laser. It will be seen that it leads to an asymmetry between the high and low frequency sidebands while if the components were modulated in phase no asymmetry would result.

The conclusions reached here apply very generally to materials whose properties are modulated in some manner. The assumptions made are only (i) a linear relationship between the displacement and electric field and (ii) real electric fields give rise to real displacements.

3. Interband Absorption

There are three main contributions to the distributed losses in a semiconductor laser: (a) interband absorption, (b) free carrier absorption and (c) scattering by optical inhomogeneities in the active region of the laser. The two other main losses are (i) loss of light from the mirrors and (ii) diffraction losses. First we consider interband absorption and show how it can lead to a net gain.

Consider Schrodinger's equation in the presence of an electric field for an electron in a crystal.

$$\left[\frac{(\vec{p}-e\vec{A})^2}{2m} + V(\vec{r}) + \frac{\hbar^2}{4m^2c^2}\left(\nabla V \times (\vec{p}-e\vec{A})\right)\cdot\vec{\sigma}\right]\psi_k' = E_k\psi_k' \qquad 2\text{-}68$$

where $V(\vec{r})$ is the crystalline potential, $\vec{p}$ and $\vec{\sigma}$ are the momentum and spin operatures respectively, $\vec{A}$ is the vector potential of the electric field, e and m are the electric charge and mass, $\hbar$ and c are Plank's constant divided by 2Π and the velocity of light, E_k is the energy eigen value, and ψ_k are the Bloch functions

$$\psi_k = e^{i\vec{k}\cdot\vec{r}}\,u_k(\vec{r}) \qquad 2\text{-}69$$

Re-writing 2-68 and dropping the A^2 term

$$\left[H_o - \frac{e}{2m}(\vec{A}\cdot\vec{p} + \vec{p}\cdot\vec{A}) - \frac{e\hbar}{m}\vec{k}\cdot\vec{A} - \frac{e\hbar^2}{4m^2c^2}(\nabla V\times\vec{A}\cdot\vec{\sigma})\right]u_k' = E_k' u_k' \qquad 2\text{-}70$$

where

$$E_k' = E_k - \frac{\hbar^2k^2}{2m} \qquad 2\text{-}71(a)$$

$$H_o\psi_k = E_k\psi_k \qquad 2\text{-}71(b)$$

and

$$H_o = \frac{p^2}{2m} + V(\vec{r}) + \frac{\hbar^2}{4m^2c^2}(\nabla V \times \vec{p} \cdot \vec{\sigma}) \qquad 2\text{-}72$$

is the Hamiltonian for the electron in the absence of an applied electric field. The only term in 2-70 which can cause transitions between two states is

$$H' = \frac{e}{2m}(\vec{A}\cdot\vec{p} + \vec{p}\cdot\vec{A}) \qquad 2\text{-}73$$

For a plane wave we may write[3]

$$\vec{A} = Re\left[\vec{A_o}\, e^{i\vec{k}_{opt}\cdot\vec{r} - i\omega t}\right] \qquad 2\text{-}74$$

$$= Re\ \vec{\tilde{A}} \qquad 2\text{-}75$$

$$\therefore \quad H' = \frac{e}{4m}\left[\vec{\tilde{A}}\cdot\vec{p} + \vec{p}\cdot\vec{\tilde{A}} + \vec{\tilde{A}}^*\cdot\vec{p} + \vec{p}\cdot\vec{\tilde{A}}^*\right] \qquad 2\text{-}76$$

$$= \frac{e}{2m}\left[\vec{A}_o\cdot(\vec{p}+\tfrac{1}{2}\hbar\vec{k}_{opt})e^{i(\vec{k}_{opt}\cdot\vec{r}-\omega t)} + \vec{A}_o^*\cdot(\vec{p}-\tfrac{1}{2}\hbar\vec{k}_{opt})e^{-i(\vec{k}_{opt}\cdot\vec{r}-\omega t)}\right] \qquad 2\text{-}77$$

The first term causes transitions upward while the second term causes transitions downward. The time dependence will ensure energy conservation in the transition. Considering only upward transitions and noting that, since the electric field is transverse

$$\vec{A}\cdot\vec{k}_{opt} = 0 \qquad 2\text{-}78$$

the rate of transition is given by

$$\gamma = \frac{2\pi}{\hbar} \left| \langle \psi_m | \frac{e}{2m} \vec{A}_0 \cdot \vec{p}\, e^{i(\vec{k}_{opt}\cdot\vec{r} - \omega t)} | \psi_j \rangle \right|^2 \rho(E) \qquad 2\text{-}79$$

where $\rho(E)$ is the member of states for which $E_m - E_j$ lies between $\hbar\omega$ and $\hbar\omega + dE$. The total stimulated transition rate upwards is thus given by[4]

$$\gamma_{stim} = \frac{2\pi}{\hbar} \sum_j \left| \langle \psi_m | \frac{e}{2m} \vec{A}_0 \cdot \vec{p}\, e^{i(\vec{k}_{opt}\cdot\vec{r} - \omega t)} | \psi_j \rangle \right|^2 \rho(E_m - E_j) f_m(E_m)\left(1 - f_j(E_j)\right) \qquad 2\text{-}80$$

where the sum is over valence bands and spin. $f(E_c)$ is the occupation probability of a state at energy E_c in the conduction band and $f(E_v)$ is the probability of occupation in the valence band. Then net stimulated transiton rate is thus

$$\gamma_{stim} = \frac{2\pi}{\hbar} \sum_j \left| \langle \psi_m | \frac{e}{2m} \vec{A}_0 \cdot \vec{p}\, e^{i(\vec{k}_{opt}\cdot\vec{r} - \omega t)} | \psi_j \rangle \right|^2 \rho_j(\hbar\omega) \left[f_m(E_m)\left(1 - f_j(E_j)\right) - f_j(E_j)\left(1 - f_m(E_m)\right) \right] \qquad 2\text{-}81$$

$$= \frac{\pi}{\hbar} \frac{e^2}{2m^2} \sum_j \left| \langle \psi_m | \vec{A}_0 \cdot \vec{p}\, e^{i(\vec{k}_{opt}\cdot\vec{r} - \omega t)} | \psi_j \rangle \right|^2 \rho_j(\hbar\omega) \left[f_m(E_m) - f_j(E_j) \right] \qquad 2\text{-}82$$

where

$$E_m - E_j = \hbar\omega \qquad 2\text{-}83$$

The absorption coefficient (β) is related to the stimulated transition rate in the following manner

$$\beta = \frac{\hbar\omega\, \gamma_{stim}}{|\vec{S}|} \qquad 2\text{-}84$$

where

$$|\vec{S}| = \frac{1}{2} \left| Re\left(\vec{E}^* \times \vec{H}\right) \right| \qquad 2\text{-}85$$

$$= \frac{\varepsilon_{AV}^{\frac{1}{2}} \omega^2}{2 c \mu_0} |\vec{A}|^2 \qquad 2\text{-}86$$

is the poynting vector

$$\therefore \quad \beta = \frac{\pi c \mu_0}{\epsilon_{RV}^{1/2}\omega} \cdot \frac{e^2}{m^2} \sum_j |\langle \psi_m | \hat{a}_0 \cdot \vec{p} | \psi_j \rangle|^2 \rho_j(\hbar\omega)\left[f_n(E_m) - f_j(E_j)\right] \qquad 2\text{-}87$$

where $\hat{a}_o$ is a unit vector in the direction of polarization of the electric. The matrix element connecting the conduction and valence bands may be calculated using Kane's theory[5] applied to GaAs. The Hamiltonian in 2-72 is used in the Schrodinger equation for an electron in the crystal, and we obtain

$$\left[\frac{p^2}{2m} + V(\vec{r}) + \frac{\hbar}{m}\vec{k}\cdot\vec{p} + \frac{\hbar^2}{4m^2c^2}(\nabla V \times \vec{p}\cdot\vec{\sigma}) + \frac{\hbar^2}{4m^2c^2}(\nabla V \times \vec{k}\cdot\vec{\sigma})\right] u_k = E_k' u_k \qquad 2\text{-}88$$

$$\text{Where} \qquad E_k' = E_k - \frac{\hbar^2 k^2}{2m}$$

If the spin orbit coupling is neglected, 2-88 can be solved for a conduction band with Γ_1 symmetry and a valence band with Γ_{15} symmetry using the basis function iS for the conduction band and X, Y, Z for the valence bands. Writing

$$E_s = \langle iS | \frac{p^2}{2m} + V(\vec{r}) | iS \rangle \qquad 2\text{-}89$$

$$E_p = \langle \alpha | \frac{p^2}{2m} + V(\vec{r}) | \alpha \rangle \qquad 2\text{-}90$$

and

$$P = \frac{i\hbar}{m} \langle S | p_\alpha | \alpha \rangle \qquad 2\text{-}91$$

$$\text{where} \quad \alpha = x, y, \text{or } z$$

the 4x4 determinant may be solved exactly

$$E_1 = E_2 = E_p + \frac{\hbar^2 k^2}{2m} \qquad 2\text{-}92$$

$$E_3 = \frac{1}{2}(E_s + E_p) + \frac{\hbar^2 k^2}{2m} + \left[\frac{1}{4}(E_s - E_p)^2 + k^2 P^2\right]^{\frac{1}{2}} \qquad 2\text{-}93$$

$$E_4 = \frac{1}{2}(E_s + E_p) + \frac{\hbar^2 k^2}{2m} - \left[\frac{1}{4}(E_s - E_p)^2 + k^2 P^2\right]^{\frac{1}{2}} \qquad 2\text{-}94$$

at $\vec{k}=0$ these give a triply degenerate valence band at E_p and a conduction band at E_s. When the spin-orbit terms are taken into account, an 8x8 secular determinant must be solved. However, the spin-orbit energy is not diagonal in the $\vec{L},\vec{S}$ representation and the basis must be changed to the $\vec{J}$ representation. The problem is further simplified by choosing the following combinatiom of wave functions for the basis: $|S\downarrow\rangle$, $\left|\frac{(X-iY)}{\sqrt{2}}\uparrow\right\rangle$ $|Z\downarrow\rangle$, $\left|\frac{(X+iY)}{\sqrt{2}}\uparrow\right\rangle$ and $|S\uparrow\rangle$, $\left|\frac{(X-iY)}{\sqrt{2}}\downarrow\right\rangle$, $|Z\uparrow\rangle$, $\left|-\frac{(X+iY)}{\sqrt{2}}\downarrow\right\rangle$

If now $\vec{k}$ is chosen in the z direction and the last term on the left-hand side of 2-88 is neglected in comparison with the second to last, the 8x8 determinant breaks up into two 4x4 determinants

$$\begin{bmatrix} H & 0 \\ 0 & H \end{bmatrix} \qquad 2\text{-}95$$

where

$$H = \begin{bmatrix} E_s & 0 & kP & 0 \\ 0 & E_p - \frac{\Delta}{3} & \frac{\sqrt{2}}{3}\Delta & 0 \\ kP & \frac{\sqrt{2}}{3}\Delta & E_p & 0 \\ 0 & 0 & 0 & E_p + \frac{\Delta}{3} \end{bmatrix} \qquad 2\text{-}96$$

where

$$\Delta = \frac{3\hbar}{4m^2c^2} i \langle x | (\nabla v \times \vec{p})_z | y \rangle \qquad 2\text{-}97$$

is the spin orbit energy. Neglect of the last term on the left in 2-88 is justified since the spin orbit interaction takes place inside the atom where $\hbar\vec{k}$ is very small compared to $\vec{p}$. 2-96 leads to four energies given by

$$\left(E_p + \frac{\Delta}{3} - E'\right)\left[(E_s - E')(E_p - \frac{\Delta}{3} - E')(E_p - E') - \frac{2\Delta^2}{9}(E_s - E') - \hbar^2 P^2 (E_p - \frac{\Delta}{3} - E')\right] = 0 \qquad 2\text{-}98$$

$$\therefore \quad E_{v_1} = E_p + \frac{\Delta}{3} + \frac{\hbar^2 k^2}{2m} \qquad 2\text{-}99$$

$$E_{v_2} = E_p + \frac{\Delta}{3} + \frac{\hbar^2 k^2}{2m} - \frac{2P^2}{3E_g} h^2 \qquad 2\text{-}100\,(a)$$

$$E_{v_3} = E_p - \frac{2\Delta}{3} + \frac{\hbar^2 k^2}{2m} - \frac{P^2}{3(E_g + \Delta)} h^2 \qquad 2\text{-}100\,(b)$$

$$E_c = E_s + \frac{\hbar^2 k^2}{2m} + \frac{P^2}{3}\left(\frac{2}{E_g} + \frac{1}{E_g + \Delta}\right) h^2 \qquad 2\text{-}100\,(c)$$

where

$$E_g = E_s - \left(E_p + \frac{\Delta}{3}\right) \qquad 2\text{-}101$$

Writing

$$\frac{1}{\hbar^2}\frac{\partial^2 E_c}{\partial k^2} = \frac{1}{m_c}$$

$$P^2 = \frac{\hbar^2}{2}\left(\frac{1}{m_c} - \frac{1}{m}\right)\frac{E_g(E_g + \Delta)}{E_g + \frac{2\Delta}{3}} \qquad 2\text{-}102$$

Returning to 2-87, we can now calculate the absorption coefficient under two assumptions.[4] The first applies for pure materials involving band-to-band transitions. Here the wave-functions may be written as Bloch functions and hence P vanishes unless the initial and final states have the same $\vec{k}$ value (neglecting $\vec{k}_{opt}$). In this case the density of states in 2-87 is the joint density of states connecting the conduction band with the valence bands.

$$P_j(E_m - E_j = \hbar\omega) = \frac{k^2}{2\pi^2} \frac{1}{\left.\frac{d(E_m - E_j)}{dk}\right|_{E_m - E_j = \hbar\omega}} \qquad 2\text{-}103$$

Note that the split-off band cannot be connected in this way for light energy close to the energy gap

$$P_j(E_m - E_j = \hbar\omega) = \frac{1}{4\pi^2}\left(\frac{2}{\hbar^2}\frac{m_c m_{vj}}{m_c + m_{vj}}\right)^{3/2}(\hbar\omega - E_g)^{1/2} \qquad 2\text{-}104$$

averaging the matrix element over polarization of the incident light and noting that spin is unchanged in a dipole transition we find

$$\left[|\langle c|\hat{a}_0 \cdot \vec{p}|v_j\rangle|^2\right]_{av} = \frac{m^2 P^2}{6\hbar^2} \qquad 2\text{-}105$$

and

$$\beta = \frac{1}{12c}\varepsilon_{av}^{\frac{1}{2}}\frac{e^2}{\hbar^2}\left[\frac{1}{m_c} - \frac{1}{m}\right]\frac{E_g}{\hbar\omega}\frac{E_g + \Delta}{E_g + \frac{2\Delta}{3}} m_c^{3/2}\left[\left(\frac{m_{v_1}}{m_c + m_{v_1}}\right)^{\frac{3}{2}} + \left(\frac{m_{v_2}}{m_c + m_{v_2}}\right)^{\frac{3}{2}}\right](\hbar\omega - E_g)^{\frac{1}{2}} \qquad 2\text{-}106$$

in Cgs units. Here it has been assumed $f(E_c)=1$ and $f(E_v)=0$. Taking for GaAs

$$m_c = .075\, m$$

$$E_g = 1.5 \text{ eV}$$

$$\Delta = 0.33 \text{ ev}$$

$$m_{v_1} = m$$

$$m_{v_2} = 0.5\, m$$

$$\beta = \frac{12.6 \times 10^4}{E_{AV}^{1/2}} (\hbar\omega - E_g)^{\frac{1}{2}} \qquad 2\text{-}107$$

$$= 3.57 \times 10^4 (\hbar\omega - E_g)^{\frac{1}{2}} \qquad 2\text{-}108$$

Equation 2-108 assumes that the transitions involved are band-to-band. In junction lasers, however, the impurity concentrations are high so that this assumption is not true. Instead, transitions involve an acceptor and possibly a donor state. In general, calculation of matrix elements for such transitions is very complex. We thus assume that the transitions involved are from a 1s conduction band (applicable for GaAs) to a hydrogenic acceptor level. Since an acceptor level is involved, the k-selection rule no longer applies because the wave-functions involved will be modified. In general the matrix element for a transition is a complicated function of energy and so the assumption is made that the matrix element is the same for all initial and final states. Finally, for large concentrations, such as occur in junction lasers, the impurity levels merge with the band edges. This effect may be approximated by a rigid shift of the bands toward the center of the gap and a change in the effective mass. The wave-function $\Phi_a(\vec{r})$ for an acceptor level may be written in terms of the valence band functions[6] $|V(\vec{k},\vec{r})>$

$$\Phi_a(\vec{r}) = \sum_{\vec{k}} a(\vec{k}) \, |V(\vec{k},\vec{r})> \qquad 2\text{-}109(a)$$

where

$$a(\vec{k}) = 8\pi^{1/2} V^{-\frac{1}{2}} \frac{a^{*\,3/2}}{(1 + a^{*2} k^2)^2}$$

and V is volume of the crystal over which the wave-functions are nomalized,

$a^* = a_o K \frac{m}{m^*}$, where a_o is Bohr radius of a hydrogen atom, K = static dielectric constant and m^* = the effective mass of the perturbed band edge. The matrix element M for the transitions when impurities are present is thus given by

$$\langle |M|^2 \rangle_{av} = |a(\vec{r})|^2 |\langle \psi_c | \hat{a}_o \cdot \vec{p} | \psi_v \rangle|^2_{\substack{pure \\ AV}} \qquad 2\text{-}109(b)$$

Since the direct gap in GaAs is at $\vec{k} = 0$, the value of the matrix element for all initial and final states is assumed to be that at $\vec{k} = 0$ so that

$$\langle |M|^2 \rangle_{av} = 64\pi \kappa^3 \frac{m^3 a_o^3}{m^{*3}} |\langle \psi_c | \hat{a}_o \cdot \vec{p} | \psi_v \rangle|^2_{\substack{pure \\ AV}} \qquad 2\text{-}109(c)$$

Using this in 2-87

$$\beta = \frac{128}{3\pi} \frac{\hbar}{e^4 c} \frac{m_c^{\frac{1}{2}} m_v^{3/2}}{m^{*3}} \frac{\kappa^3}{E_{AV}^{1/2}} \frac{E_g + \Delta}{E_g + \frac{2\Delta}{3}} \int_0^{E-E_g} E'^{\frac{1}{2}} (E - E_g - E')^{\frac{1}{2}} (f_u - f_\ell) dE' \qquad 2\text{-}110$$

Here Eg is the effective energy gap in the material. From the measured acceptor energy of 34 mev, m^* is given by

$$E_a = \frac{m^* e^4}{2\kappa^2 \hbar^2} \qquad 2\text{-}111$$

from which

$$m^* = 0.39\, m \qquad 2\text{-}112$$

where we have used K = 12.5. Using this in 2-110 we find

$$\beta = 24 \times 10^6 \int_0^{E-E_g} E'^{1/2} (E - E_g - E')^{\frac{1}{2}} (f_u - f_\ell)\, dE' \qquad 2\text{-}113$$

where

$$f_n = \left[1 + \exp\left[\frac{E' - (F_n - E_c)}{kT}\right]\right]^{-1} \qquad 2\text{-}114\,(a)$$

$$f_e = \left[1 + \exp\left[\frac{E' - (E - E_g - F_p + E_v)}{kT}\right]\right]^{-1} \qquad 2\text{-}114\,(b)$$

β here is given in cm^{-1} and energies in electron volts. Figure 2-1 shows a graph of equation 2-113 at T = 0°K. The case $(F_p - E_v) = 1.23\,(F_n - E_c)$ is chosen to correspond to the experimental situation and the graph is plotted as a function of $\delta = \frac{E - E_g}{F_n - E_c}$. We may thus write

$$\beta = 24 \times 10^6 \left(\frac{F_n - E_c}{4}\right)^2 F(\delta) \qquad 2\text{-}115$$

at T = 0°K where $F(\delta)$ is given in figure 2-1 and is a universal function for a given ratio of $F_n - E_c$ to $F_p - E_v$. For low energies $E - E_g < (F_n - E_c)$, $(F_p - E_v)$ we have $\beta \sim (E - E_g)^2$. As $(E - E_g)$ increases, however, the assumption of no k-selection rule should becomes less valid and at high energies, where transitions are band-to-band, we should expect $\beta \sim (E - E_g)^{1/2}$ as in 2-106.

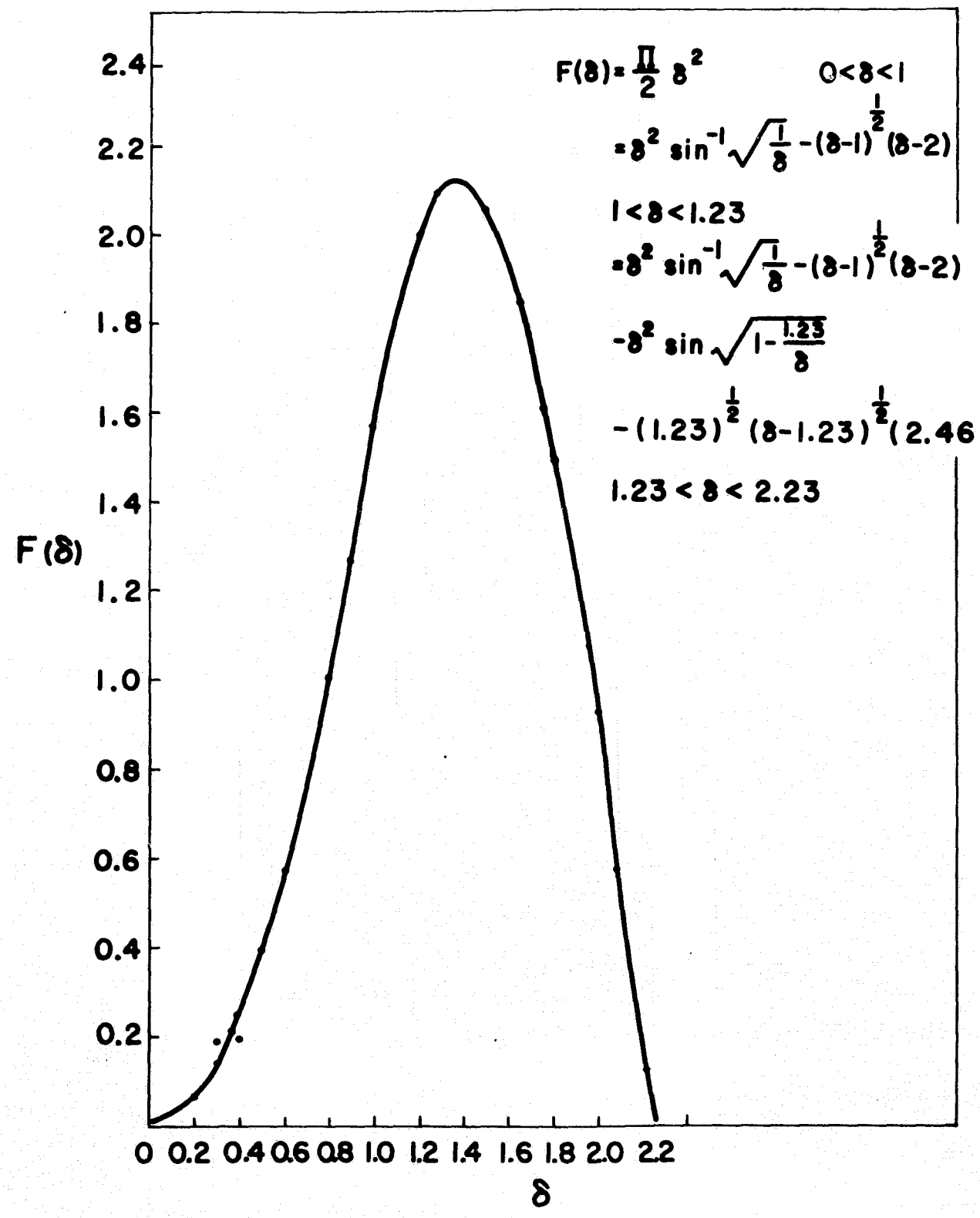

SEMICONDUCTOR LASER GAIN AT T=0°K

FIGURE 2-1

4. Modulation of the Gain

Consider first pressure modulation. The effect of pressure on a semiconductor is firstly to shift the energy gap of the material and secondly to change the dielectric constant which depends on the energy gap. The change in the dielectric constant changes the resonance conditions for the laser modes and hence the mode frequencies must shift in order to maintain resonance. Along with the shift in energy gap is a rigid shift in Fermi levels so that their positions relative to the band edges remain fixed. For pure material the main contribution to the change in the gain arises through the different pressure derivatives of the modes and energy gap as may be seen in 2-106. We thus obtain

$$\frac{d\,\mathcal{C}}{dP} = \frac{1}{2}\,\frac{\mathcal{C}}{(\hbar\omega - E_g)}\,\frac{d\,(\hbar\omega - E_g)}{dP} \qquad 2\text{-}116$$

Using 1-19 and neglecting the change in cavity length with pressure[7]

$$-\frac{1}{\omega}\,\frac{d\omega}{dP} = \frac{1}{\bar{n}}\,\frac{d\bar{n}}{dP} \qquad 2\text{-}117$$

$$\frac{1}{\bar{n}}\,\frac{d\bar{n}}{dP} = \frac{1}{\bar{n}}\left[\frac{\partial\bar{n}}{\partial P} + \frac{\partial\bar{n}}{\partial\omega}\,\frac{d\omega}{dP}\right] \qquad 2\text{-}118$$

thus

$$-\frac{1}{\omega}\,\frac{d\omega}{dP} = \frac{1}{\bar{n} + \omega\frac{d\bar{n}}{\partial\omega}}\,\frac{\partial\bar{n}}{\partial P} \qquad 2\text{-}119$$

In general we can write

$$-\left.\frac{\partial\bar{n}}{\partial P}\right|_{\omega} = \left.\frac{\partial\bar{n}}{\partial\omega}\right|_{P}\left.\frac{\partial\omega}{\partial P}\right|_{\bar{n}} \qquad 2\text{-}120$$

Assuming that the change is entirely due to a shift in the absorption edge

$$\frac{\partial \bar{n}}{\partial p} = -\frac{\partial \bar{n}}{\partial \omega}\frac{1}{h}\frac{dE_g}{dp} \qquad 2\text{-}121$$

$$\frac{d\hbar\omega}{dp} = \frac{\omega\frac{\partial \bar{n}}{\partial \omega}}{\bar{n}+\omega\frac{\partial \bar{n}}{\partial \omega}}\frac{dE_g}{dp} \qquad 2\text{-}122$$

$$\therefore \quad \frac{d\alpha}{dp} = \frac{1}{2}\frac{\alpha}{(\hbar\omega - E_g)}\frac{\bar{n}}{\bar{n}+\omega\frac{\partial \bar{n}}{\partial \omega}}\frac{dE_g}{dp} \qquad 2\text{-}123$$

using $\bar{n}=3.59$ and $\frac{\omega\partial \bar{n}}{\partial \omega} = 1.93$[5]

$$\frac{d\alpha}{dp} = \frac{0.32\,\alpha}{(\hbar\omega - E_g)}\frac{dE_g}{dp} \qquad 2\text{-}124$$

Further using the valve $\frac{dEg}{dp} = 11\times10^{-6}$ ev/atm, and 2-108

$$\frac{d\alpha}{dp} = \frac{4.5\times10^{3}}{\alpha} \quad cm^{-1}/atm \qquad 2\text{-}125$$

For diodes, however, from 2-113 and 2-115 it can be seen that pressure acts on the gain only through the term $E-E_g$, the quasi-Fermi levels remaining fixed. Since the laser modes will be located at the maximum of the gain, the change in $F(\delta)$ will be negligible and hence β will be unaffected by pressure. Thus, while for pure material pressure will give a measurable modulation to the gain, for diodes no such modulation should be observable.

Secondly we consider the case of modulation of the injection a diode. Increasing the bias has no effect on the energy gap but serves to increase the distance of the quasi-Fermi levels from the band edges. The corresponding case for pure material would be to increase the pumping intensity in an optically pumped laser. From 2-106 and 2-108 for pure material

$$\frac{d\alpha}{dV} = \frac{1}{2}\frac{\alpha}{(\hbar\omega - E_g)}\frac{d\hbar\omega}{dV} \qquad 2\text{-}126$$

while for diodes, assuming the the applied voltage does not change the ratio $(F_n-E_c)/(E_n-F_p)$,

$$\frac{d\beta}{dV} = 2\frac{\beta}{(F_n-E_c)}\frac{d(F_n-E_c)}{dV} \qquad 2\text{-}127$$

Verification of equations 2-124 through 2-126 for pure material was not performed. However, both pressure and injection modulation were performed on diodes. The results of these experiments are reported in Chapter III and Chapter IV.

5. Free Carrier Absorption

One of the main losses in a semiconductor laser, particularly at high doping levels, is that due to free carrier absorption. Unlike the other losses mentioned in section three, namely, (i) scattering by optical inhomogeneities; (ii) diffraction losses; and (iii) loss of light from the end mirrors, the free carrier absorption will be modulated by modulating the injection although not by ultrasonic waves.

The transitions involved are those from hole states in the valence band to electron states higher in the valence band and similarly from electron states in the conduction band to hole states higher in the conduction band. The absorption coefficient for these types of transitions may be approximated by the Drude-Zener formula[3]

$$\beta_{fc} = \tau_{avg}(\tau^{-1})_{avg}\, 5.26\times10^{-17}\frac{\lambda^2}{\bar{n}\,\epsilon_0}\left[\frac{N_e}{\mu_e}\left(\frac{m_c^*}{m}\right)^{-2}+\frac{N_p}{\mu_p}\left(\frac{m_v^*}{m}\right)^{-2}\right] \qquad 2\text{-}128$$

where τ is the scattering time, λ is the wavelength in mirrors, Ne and Np are the number of electrons and holes, μ is the mobility in cms/sec, m_c^* is the conduction band mass at the Fermi level and m_v^* the valence band effective mass averaged over valence bands. While 2-128 gives a value for

β_{fc} which is lower than the observed free carrier absorption, it illustrates the dependence on carrier concentration. Hence, modulation of the injection will change this absorption coefficient by changing the number of free carriers in the active region of the laser. Since the observed free carrier absorption is very approximately given by[8] $\beta^{\circ}_{fc} \approx 3\times10^{-18}$ times the number of carriers, most of the absortpion in the lasers used is due to holes and thus

$$\frac{d\,\beta^{\circ}_{fc}}{dV} \approx \frac{3}{2}\,\frac{\beta^{\circ}_{fc}}{(F_p - E_v)}\,\frac{d(F_p - E_v)}{dV} \qquad 2\text{-}129$$

Assuming that the ratio $(F_p-E_v)/(F_n-E_c)$ is not changed by the applied voltage

$$\frac{d\,\beta^{\circ}_{fc}}{dV} \approx \frac{3}{2}\,\frac{\beta^{\circ}_{fc}}{(F_n - E_c)}\,\frac{d(F_n - E_c)}{dV} \qquad 2\text{-}130$$

This value must be subtracted from 2-127 to obtain the net modulation to be used in 2-49.

6. The Modulated Electric Field

Returning to 2-49, the results of sections 2-2 to 2-5 may be used to obtain the mode electric fields. The quantity

$$-\frac{\alpha}{2\bar{n}^2\epsilon_0} = \frac{\beta c}{2\omega\bar{n}\epsilon_0^{\frac{1}{2}}} \qquad 2\text{-}131$$

Since we may expect $\beta < 1000\ cm^{-1}$

$$\frac{\alpha}{2\bar{n}^2\epsilon_0} < .02 \quad \text{for GaAs} \qquad 2\text{-}132$$

and we neglect it. Thus

$$C_b = e^{-i\omega_b t + \left[i\omega_b \int \frac{\epsilon_2}{2\bar{n}^2\epsilon_0}dt - \int \frac{\omega_b \alpha_2 + \sigma_i}{2\bar{n}^2\epsilon_0}dt - (\epsilon_2 + i\alpha_2)\right]} \qquad 2\text{-}133$$

for the case of sinusoidal modulation and remembering the phase difference between the real and imaginary parts of the modulated dielectric constant, we write

$$\varepsilon_2 = \Delta\varepsilon \cos\omega_s t \qquad 2\text{-}134$$

$$\alpha_2 = \Delta\alpha \sin\omega_s t \qquad 2\text{-}135(a)$$

$$\sigma_1 = \Delta\sigma \sin\omega_s t \qquad 2\text{-}135(b)$$

$$C_b = e^{-i(\omega_b t - m_f \sin\omega_s t) + m_a \cos\omega_s t - \frac{\Delta\varepsilon}{2\varepsilon_{AV}}\cos\omega_s t - \frac{i\Delta\alpha}{2\varepsilon_{AV}}\sin\omega_s t}$$

where

2-136

$$m_f = \frac{\Delta\varepsilon}{2\varepsilon_{AV}} \frac{\omega_b}{\omega_s} \qquad 2\text{-}137$$

$$m_a = -\left[\frac{\omega_b \Delta\alpha + \Delta\sigma}{2\varepsilon_{AV}\omega_s}\right] \qquad 2\text{-}138$$

The last two terms in the exponential in 2-136 represent a very small amplitude modulation due to the real part of the dielectric constant and a very small frequency modulation due to the imaginary part of ε. Since $\frac{\Delta\varepsilon}{2\varepsilon_{AV}}, \frac{\Delta\alpha}{2\varepsilon_{AV}} \approx 10^{-5}$ for injection modulation and pressure modulation, via ultrasonic waves, we can neglect these two terms and using 2-16 write

$$\vec{E} = \sum_{nmq} \sqrt{\frac{\omega_{nmq}}{2\varepsilon_{AV}}}\, \vec{E}_{nmq}(\vec{r})\, e^{m_a \cos\omega_s t} \sin\left[\omega_{nmq} t - m_f \sin\omega_s t\right] \qquad 2\text{-}139$$

where $\vec{E}_{nmq}(\vec{r})$ is given by the spatial part of 1-20. Equation 2-139 thus shows that the mode electric field are frequency modulated by the real part of the dielectric constant and amplitude modulated by the imaginary part. Using the results of section 2-4 and 2-5 we may relate m_a to measurable quantities thus

$$m_a = \frac{c}{\varepsilon_{AV}^{1/2}} \frac{\Delta\beta - \Delta\beta_{sc}}{2\omega_s} \qquad 2\text{-}140$$

For pressure modulation in diode lasers $m_a = 0$ while,

For pressure modulation in diode lasers $m_a = 0$ while,

$$m_f = \frac{\omega_o}{\omega_s} \frac{1}{2\bar{n}^2\epsilon_o} \frac{\partial \epsilon}{\partial P} \Delta P \qquad 2\text{-}141$$

Since for GaAs no reliable measurements of $\frac{\partial \epsilon}{\partial p}$ for uni-axial stress have been made, we assume it is one-third of the hydrostatic value.[9,10] Then

$$m_f = \frac{330}{f_s} \Delta P \qquad \begin{matrix} f_s \text{ is in MHz} \\ P \text{ is in Atm} \end{matrix} \qquad 2\text{-}142$$

When modulation is performed via the injection, the value of m_a will depend on the biasing point, as will that of m_f.

7. Conclusions

The effect of an arbitrary time-dependent modulation of both the real and imaginary parts of the dielectric constant on a semiconductor laser has been considered. It has been shown that modulation of the real part of the dielectric constant gives rise to frequency modulation while modulation of the imaginary part results in amplitude modulation. Furthermore, it has been shown, quite generally, that the modulations of the real and imaginary parts of the dielectric constant are out of phase by $\Pi/2$. The use of pressure as a modulator has been shown to give rise to pure frequency modulation (i.e. pressure has no effect in the gain) for diode lasers while for pure crystals the change in the gain is sufficient to give measureable amplitude modulation as well. Under modulation of the injection for a diode laser or modulation of the pumping power intensity for an optically pumped crystal. Both frequency and amplitude modulation will be present.

References

1. See for example A. Yariv, "Quantum Electronics" John Wiley and Sons, Inc., New York, P. 79 (1967).
2. L. Landau and E. Lifshitz, "Statistical Physics," Pergamon Press, P. 391 (1958).
3. F. Stern, "Solid State Physics. Advances in Research and Applications." Edited by F. Seitz and D. Turnbull, Academic Press, Vol. 15, P. 300 (1963).
4. G. Lasher and F. Stern, Phys. Rev. 133, A553 (1964).
5. E. O. Kane, Journal of Physics and Chemistry of Solids 1, 249 (1957).
6. D. M. Eages, Journal of Physics and Chemistry of Solids 16, 76 (1960).
7. W. E. Engeler and M. Garfinkel, Journal of Applied Physics 34, 2746 (1963).
8. W. J. Turner and W. E. Reese, Journal of Applied Physics 35, 350 (1964).
9. G. E. Fenner, Journal of Applied Physics 34, 2955 (1963).
10. J. Feinlab, S. Groves, W. Paul, R. Zallen, Physical Review 131, 2070 (1963).

CHAPTER III

Pressure Modulation

1. Introduction

In Chapter II the effects of a time dependent modulation of the complex dielectric constant on the laser modes were deduced. It was seen that this lead, in general, to both an amplitude and frequency modulation -- the amplitude modulation arising from changes in the gain, while frequency modulation arose from perturbations in the real part of the dielectric constant. In this chapter, the finite wavelength of the ultrasonic waves used to modulate the laser is taken into account. Since it was deduced in Chapter II that for diode lasers, the change in gain with pressure was negligible only variations in the real part of the dielectric constant are considered here.

Following the treatment of Ripper[1] we solve for the laser mode frequencies using a quasistatic approximation. Starting with the unperturbed laser mode frequencies and amplitudes given by equations 1-19 and 1-20 respectively, we use first order perturbation theory to solve for the laser frequencies. A quasistatic approximation is valid providing the lifetime τ_p of the photon in the cavity is short compared to the period $\tau_m = \frac{1}{\nu_m}$ of the perturbation. Since, typically, $\tau_p \simeq 10^{-12}$ secs and, for the modulating frequencies used, $\nu_m < 10^9$ cps, $\tau_m > 10^{-9}$ secs. Thus this condition was satisfied and a quasistatic approximation justified.

It is assumed that the dielectric constant in the presence of ultrasonic waves may be written

$$\varepsilon = \bar{n}^2 \varepsilon_0 \left[1 - \left(\frac{x}{x_e}\right)^2 - \left(\frac{y}{y_e}\right)^2\right] + \Delta\varepsilon \cos(\omega_s t + q_s x) \quad 3\text{-}1$$

where ω_s and q_s are the modulating angular frequency and wave number. The

first term is just the unperturbed dielectric constant which was used in Chapter I to calculate the laser mode frequencies and amplitudes. The second term is the modulation produced by the ultrasonic waves. The direction of propagation of the waves x is perpendicular to the direction of propagation of the laser electric field. Solving for the new mode frequencies we find

$$\nu'_{nmq} = \nu_{nmq} + \frac{\partial \nu}{\partial \varepsilon} \frac{\int_V E^2_{nmq}(\vec{r},r)\, \Delta\varepsilon \cos(\omega_s t + q_s x)\, d^3\vec{r}}{\int_V E^2_{nmq}(\vec{r},r)\, d^3\vec{r}} \qquad 3\text{-}2$$

where V is the volume of the cavity. The result, given in reference 1 is

$$\nu'_{nmq} = \nu_{nmq} - \frac{\nu_{nmq}}{2\bar{n}^2\varepsilon_0} L_n(k_u^2)\, e^{-\frac{k_u^2}{4}}\, \Delta\varepsilon \cos\omega_s t \qquad 3\text{-}3$$

where $L_n(k_u^2)$ is the Laguerre polynominal of order n and $k_u^2 = \frac{q_s^2 x_e c}{2\pi \bar{n}\, \nu_{nmq}}$.

Writing

$$m_f = \frac{\nu_{nmq}}{\nu_s} \frac{\Delta\varepsilon}{2\bar{n}^2\varepsilon_0} L_n(k_u^2)\, e^{-k_u^2/4} \qquad 3\text{-}4$$

$$\nu'_{nmq} = \nu_{nmq} - \nu_s m_f \cos\omega_s t \qquad 3\text{-}5$$

and the electric field is given by

$$\vec{E}'_{nmq}(\vec{r},t) = \vec{E}_{nmq}(\vec{r}) \cos\left[\int^t dt' 2\pi (\nu_{nmq} - \nu_s m_f \cos\omega_s t)\right] \qquad 3\text{-}6$$

$$= \vec{E}_{nmq}(\vec{r}) \cos\left[2\pi \nu_{nmq} t - m_f \sin\omega_s t\right] \qquad 3\text{-}7$$

where $\vec{E}_{nmq}(\vec{r})$ is given from 1-20 by

$$\vec{E}_{nmq}(\vec{r},t) = \vec{E}_{nmq}(\vec{r}) \cos 2\pi \nu_{nmq} t \qquad 3\text{-}8$$

and

$$\nu_s = \frac{\omega_s}{2\pi} \qquad 3\text{-}9$$

Using the well-known bessel function expansion 3-7 may be written

$$E_{nmq}(\vec{r},t) = \vec{E}_{nmq}(\vec{r}) \sum_{p=-\infty}^{\infty} J_p(m_f) \cos 2\pi(\nu_{nmq} - p\nu_s)t \qquad 3\text{-}10$$

Thus we see, from 3-10, that the effect of modulating the real part of the dielectric constant is to produce a set of sidebands on either side of the carrier frequency which are separated from each other by the modulating frequency ν_s and which have amplitudes governed by the bessel functions $J_p(m_f)$. Note that in the limit of low frequency $k_u \to 0$, 3-10 agrees with 2- 137 and the modulation index is given by

$$m_f = \frac{\Delta\varepsilon}{2\bar{n}^2\varepsilon_0} \frac{\omega_{nmq}}{\omega_s} \qquad 3\text{-}11$$

Assuming that $\frac{d\varepsilon}{dp}$ for uniaxial pressure is one third of the hydrostatic pressure[2,3] value we find

$$m_f = \frac{330}{\nu_s} \Delta P \qquad \begin{array}{l}\nu_s \text{ is in MHz} \\ P \text{ is in Atm}\end{array} \qquad 3\text{-}12$$

where P is the ultrasonic pressure in atmospheres and ν_s is in MHz.

The perturbation in the dielectric constant also introduces some mode mixing from modes of different n. However, provided $\Delta\varepsilon << \bar{n}^2\varepsilon_0$ this is shown in reference 1 to be very small. For ultrasonic waves $\frac{\Delta\varepsilon}{\bar{n}^2\varepsilon_0} \sim 10^{-5}$ so that no mode mixing could be observed.

2. Experiment

A gallium arsenide laser of the "stripe" geometry* was bonded with indium onto one end of a sapphire rod which was one quarter of an inch in diameter and one quarter of an inch long. The top surface of the rod, to which the laser was bonded, had a thin gold layer evaporated onto it so that the indium solder would adhere to it. The laser was mounted p-side down on the sapphire and the junction depth from the top of the p-side was 2.5μ. The p-side was gold coated so that the laser could be soldered. On the bottom surface of the sapphire, a 10MHz or 30MHz quartz transducer with coaxial plating was bonded using non-aq solution to ensure efficient transmission of the ultrasonic waves across the quartz-sapphire interface. The sapphire rod was clamped around its circumference by two pieces of OFHC copper as shown in figure 3-1. The top contact of the laser was made via a 3 mil gold wire indium soldered to the n side of the laser and running to a stand-off mounted on the copper block and thence to a microvolt connector. The p-side of the laser was grounded to the copper block by applying conducting silver paint between the gold layer on the sapphire and the block itself. A coaxially shielded connection was made to the transducer via a modified BNC connector as shown in figure 3-1. The transducer was cemented in place using silver paint which also served to ensure a common ground between the transducer and copper block. A teflon sleeve whose inside diameter was equal to that of the center contact of the transducer and whose outside diameter was equal to that of the sapphire rod, was placed ontop of the transducer and acted as a guide for a spring contact which was pressure bonded to the center of the transducer. The outside shield of the transducer ground connection could slide in a trombone fashion so that the spring connection could be made

*Kindly supplied by Dr. Ripper at Bell Telephone Labs., Murray Hill, NJ. (see fig. 1-1)

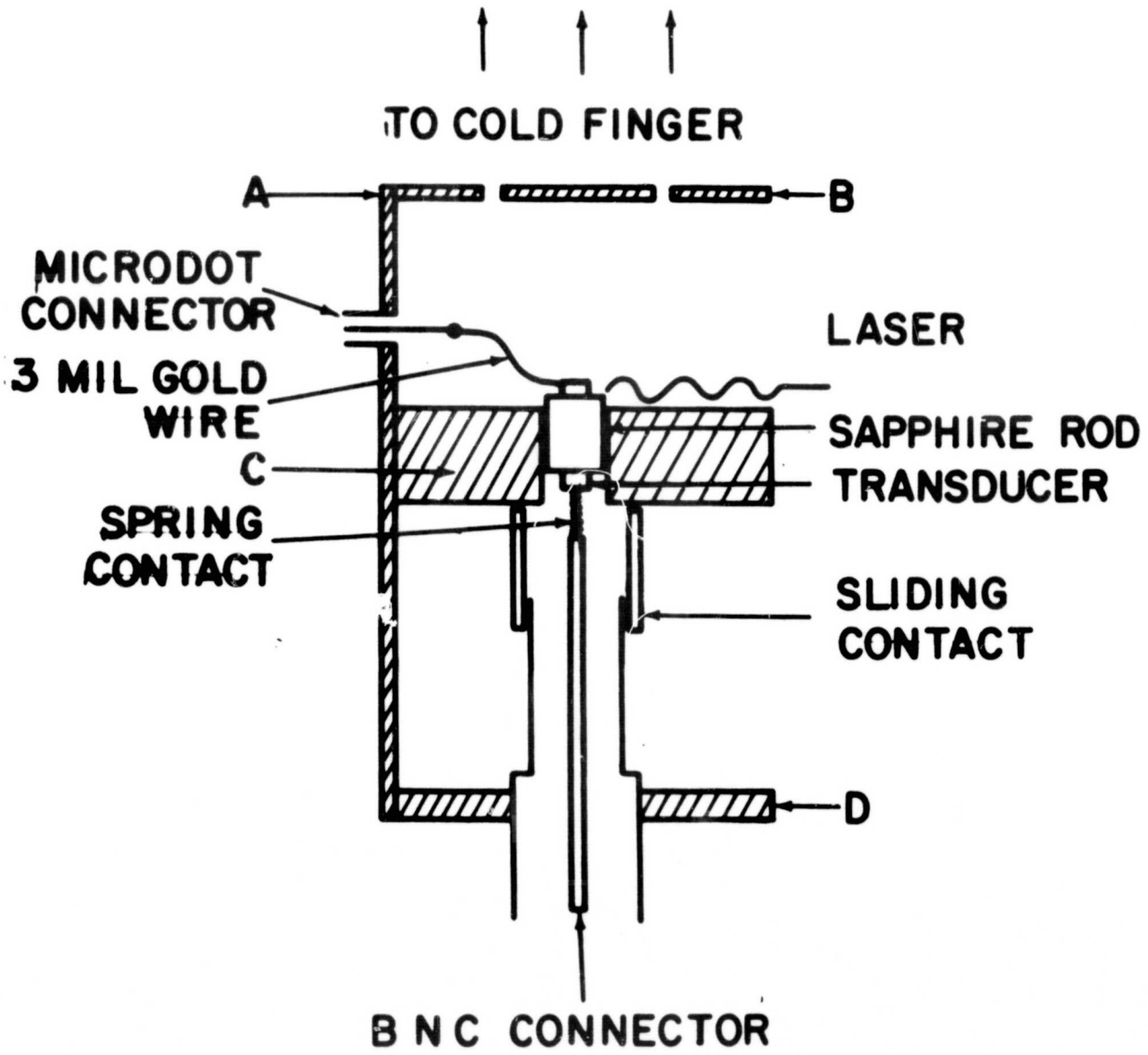

SAMPLE HOLDER CONSISTS OF A CYLINDER CUT IN HALF ALONG ITS AXIS (PIECE A) INTO WHICH THREE DISCS (PIECES B,C,D) ARE SCREWED

SAMPLE HOLDER CROSS-SECTION

FIGURE 3-1

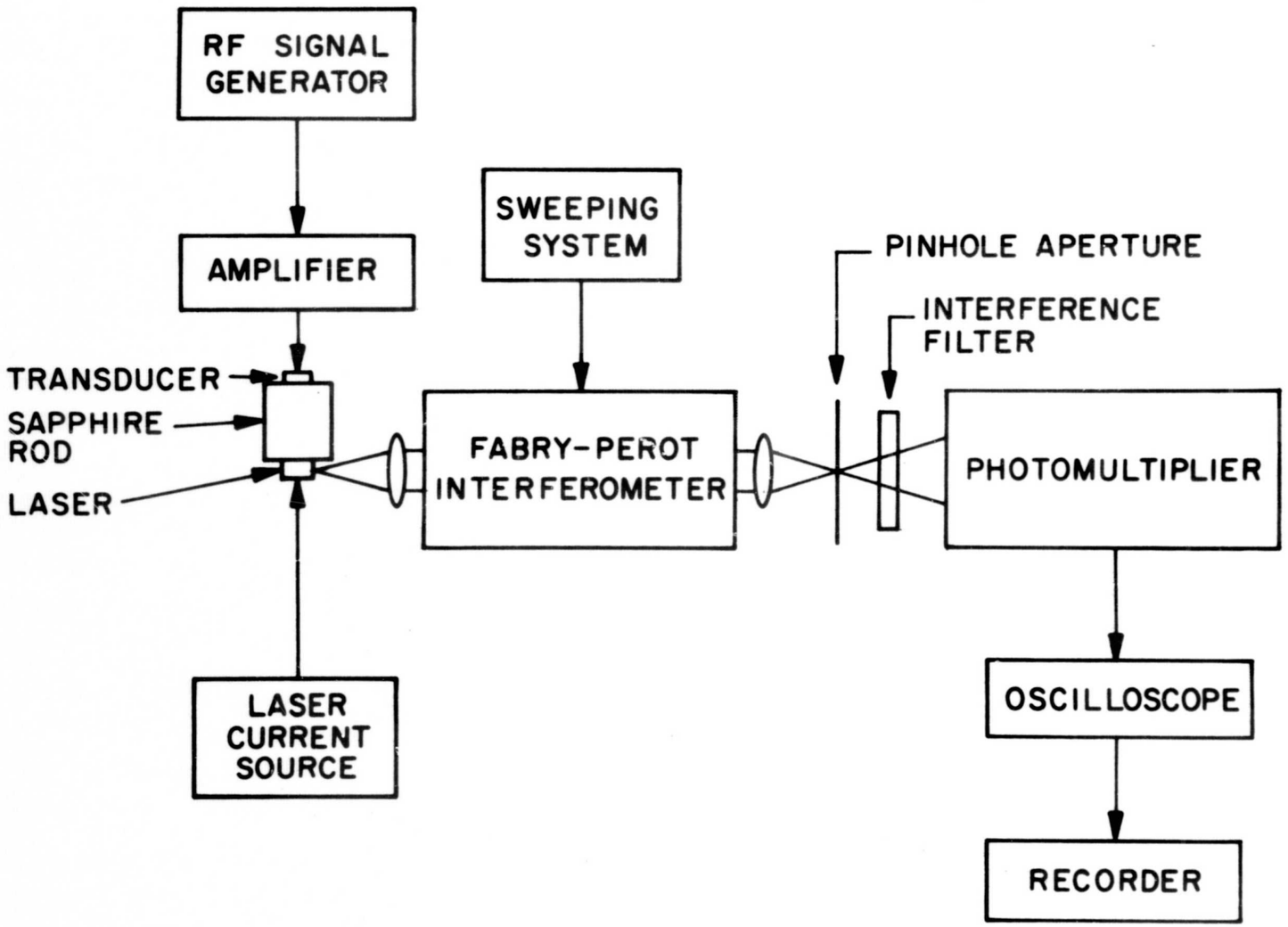

EXPERIMENTAL APPARATUS

FIGURE 3-2

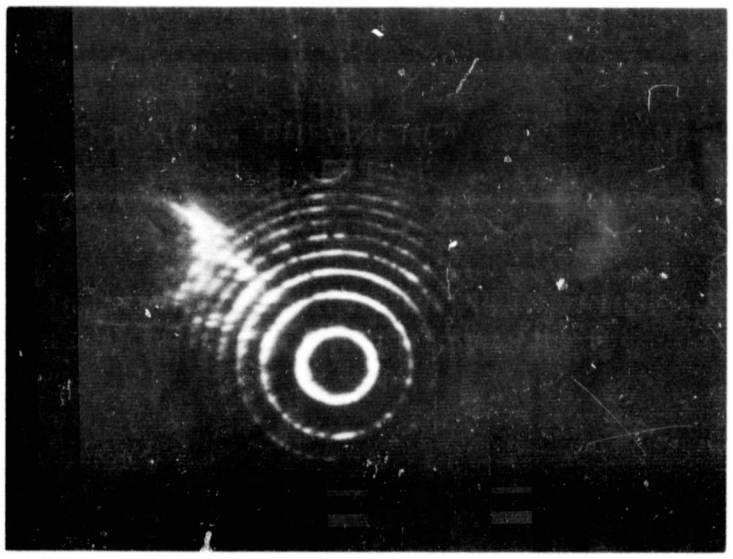

(a)
NO SOUND

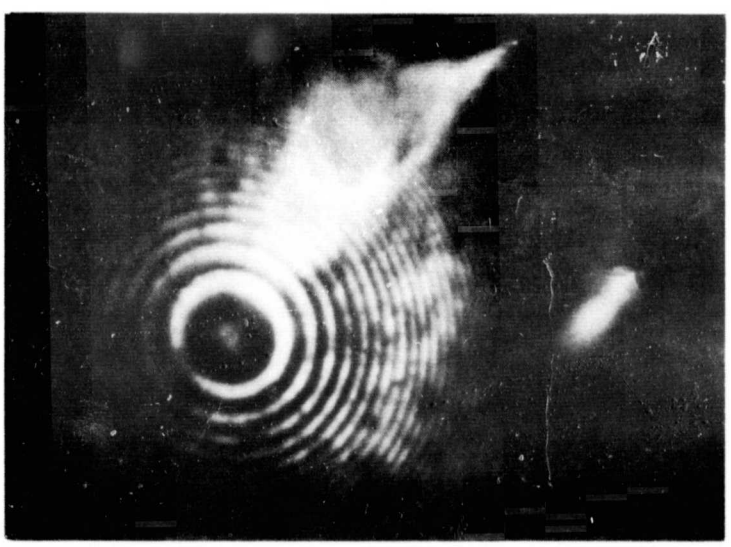

(b)
MAXIMUM SOUND APPLIED

LASER L-5
MODULATING FREQUENCY ν_s = 30 MHz
LASER CURRENT = 40 mA

FIG. 3-3 BLURRING OF RING PATTERN PRODUCED BY FABRY-PEROT INTERFEROMETER

and then the ground connection slid over it and soldered to the copper block. The block was then screwed and soldered to another piece of copper designed, as shown in figure 3-1, so that the whole assembly could be brought in contact with a copper cold finger for operation at liquid nitrogen or liquid helium temperatures.

Figure 3-2 shows a diagram of the experimental apparatus. The laser was operated cw using a Trygon Model T50-2 power supply. The transducer was excited using either a Hewlett Packard Model 608C signal generator and a Boonton Radio Model 230A power amplifier or an Airborne Instruments Laboratories Model 125 power signal source. The sound waves generated in the transducer travelled through the sapphire rod to the laser mounted on the other side. Sapphire was chosen because (i) it is a good heat sink for the laser and (ii) it has good acoustic conduction properties. The frequency modulated output from the GaAs laser was passed through a confocal lens and through a Fabry-Perot interferometer. Two interferometers were used; One, which had flat mirrors and could be pressure scanned, had a free spectral range of 1GHz while the other, Tropel Model 7600 with spherical mirror, was piezoelectrically scanned and had a free spectral range of 7.5 GHz. Light leaving the flat Fabry-Perot interferometer was focussed using a 50 cms lens. A pinhole was placed at the focal point of the lens and a photomultiplier placed behind the pinhole, used to detect the light. Single frequency coherent light passing through the flat Fabry-Perot interferometer, produces rings in the focal plane of the 50 cms lens corresponding to the discrete transmission angles of the interferometer. The interferometer was scanned by evacuating it and slowly filling it with nitrogen gas. This changes the refractive index between the interferometer mirrors and hence the transmission angles. Light parallel to the axis of the interferometer will be transmitted only when the optical distance between mirrors is an integral number of half

wavelengths. Thus, the light detected by the photomultiplier, for a single frequency when the interferometer was scanned, consisted of a series of peaks spaced by a distance corresponding to the free spectral range (1 GHz 2). When the laser was modulated, additional peaks appeared which corresponded to the sideband frequencies. When the spherical Fabry-Perot interferometer was used, the light was detected using a silicon photodiode placed on axis behind the rear mirror, since interference of the light in the interferometer takes place at the mirrors. The signal from the detectors was fed directly to a 1A7 plug-in on a 547 oscilloscope. The output of the scanned interferometer could be seen on the oscilloscope. For the pressure scanned interferometer, the oscilloscope trace was free run, while for the piezoelectrically scanned interferometer, the mirror was driven from the sawtooth output of the oscilloscope which was synchronized to the x-axis. Graphs of the Fabry-Perot output could be obtained on a Moseley 7035B X-Y recorder by applying the output of the plug-in to the Y-axis and the sawtooth to the X-axis.

Operation at 4.2°K or 77°K was achieved by using a Janis helium dewar with an optical tail. The cold finger cooling method was used. Whenever possible, the laser was kept continuously at 77°K except when operation at liquid helium temperature was desired. This prevented unnecessary cycling between roon temperature and nitrogen temperature which adversely affects the operation of the lasers. Operation at 77°K could also be achieved by using a wide-mouth dewar flask. The laser assembly was mounted on a big copper rod which was partially immersed in the liquid nitrogen. Frosting of the laser was prevented by placing an inverted, optical dewar flask over the laser assembly and rod.

3. Results

Equation 3-10 shows that when a semiconductor laser is modulated via ultra-

LASER L-5
LASER CURRENT=43 mA
TRANSDUCER VOLTAGE=0 VOLTS

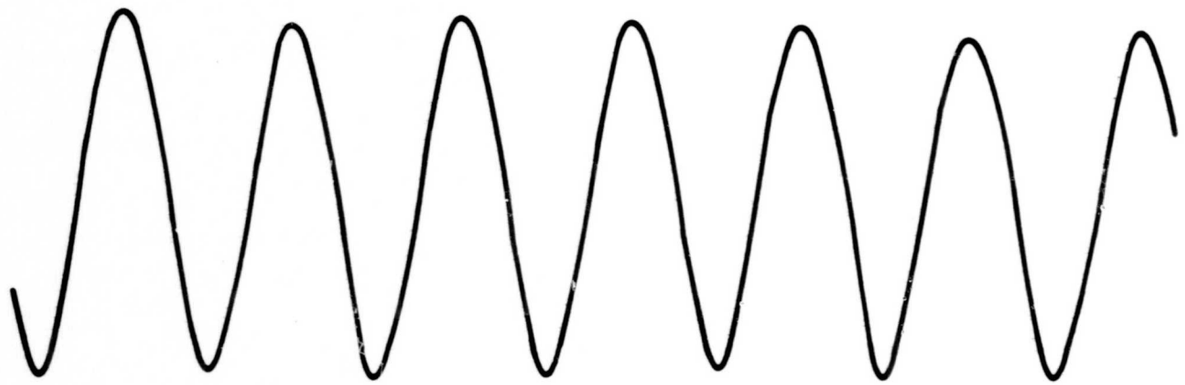

←1GHz→

FABRY-PEROT INTERFEROMETER TRACE
OF A LASER MODULATED AT 10 MHz

FIGURE 3-4 (a)

LASER CURRENT= 43 mA
TRANSDUCER VOLTAGE=0 VOLTS

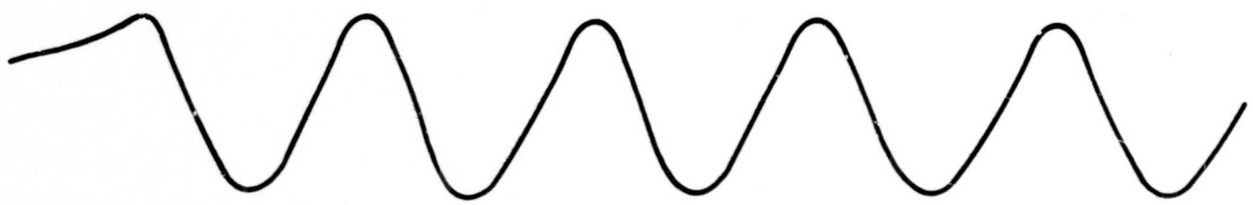

←1GHz→

FABRY-PEROT INTERFEROMETER TRACE
OF A LASER MODULATED AT 10 MHz
FIGURE 3-4(b)

LASER CURRENT = 43 mA
TRANSDUCER VOLTAGE = 75 VOLTS

FREQUENCY DEVIATION = 1 GHz

FABRY-PEROT INTERFEROMETER
OF A LASER MODULATER AT 10 MHz

FIGURE 3-4 (c)

sonic waves, a set of sidebands appear. The amplitudes of the sidebands are governed by Bessel functions while their spacing in frequency is equal to the modulating frequency ν_s. Thus for a single mode laser, the output of the scanned Fabry-Perot interferometer should consist of a series of peaks spaced a distance ν_s from each other. If the instrumental width of the interferometer is greater than the modulating frequency, then only the envelope of the sidebands will be observed. Figure 3-3 shows a picture of the ring pattern produced after passing a single mode GaAs laser beam through a Fabry-Perot interferometer. In figure 3-3(a), where no sound modulation is applied, each ring corresponds to the discrete transmission angle of the interferometer for a particular frequency. When sound is applied, the rings broaden as shown in figure 3-3(b). For these pictures, a modulating frequency of 30 MHz was used and the experimental arrangement of the sample holder was different from that described in section 3-2. Instead of the sound waves travelling through sapphire to the laser, they were passed through copper. It was noticed that whereas at 10 MHz the rings could be broadened so that they overlapped, at 30 MHz the maximum broadening attained was that shown in figure 3-3(b). The decrease in the frequency deviation may be attributed to the increased acoustic attenuation in copper between 10 MHz and 30 MHz which resulted in a smaller acoustic pressure reaching the laser crystal. The maximum frequency deviation attained at 10 MHz was of the order of 1 GHz corresponding to a modulation index of 100 and an acoustic pressure of 3 atmospheres. Figure 3-4 shows an interferometer scan when modulation at 10 MHz was applied. Figure 3-4(a) shows the scan when no sound was applied, figure 3-4(b) when 42 volts was applied to the transducer and figure 3-4(c) when the applied voltage was 75 volts. In figure 3-4(b) some broadening of the rings can be seen while in figure

LASER L-5
LASER CURRENT = 52 mA
TRANSDUCER VOLTAGE = 0
MODULATION INDEX = 0

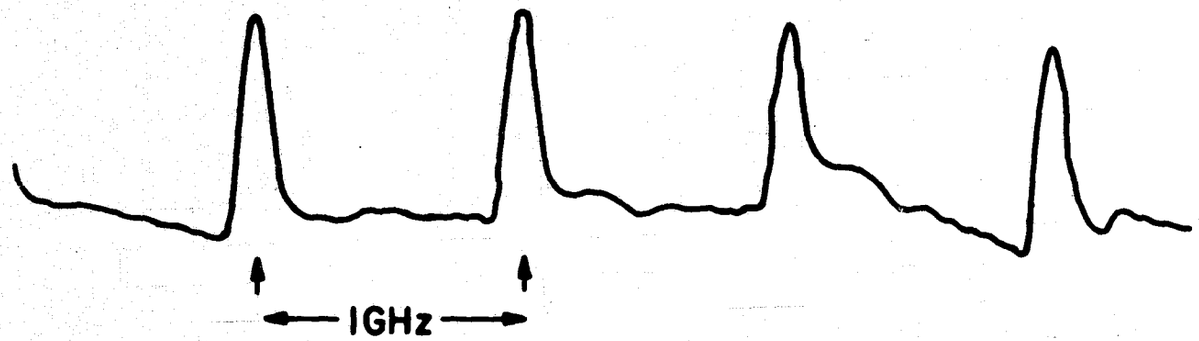

FABRY-PEROT INTERFEROMETER TRACE
OF A GALLIUM ARSENIDE LASER
FREQUENCY MODULATED AT 150 MHz

FIGURE 3-5(a)

LASER CURRENT = 52 mA
TRANSDUCER VOLTAGE = 1.2 V
MODULATION INDEX = 1.9

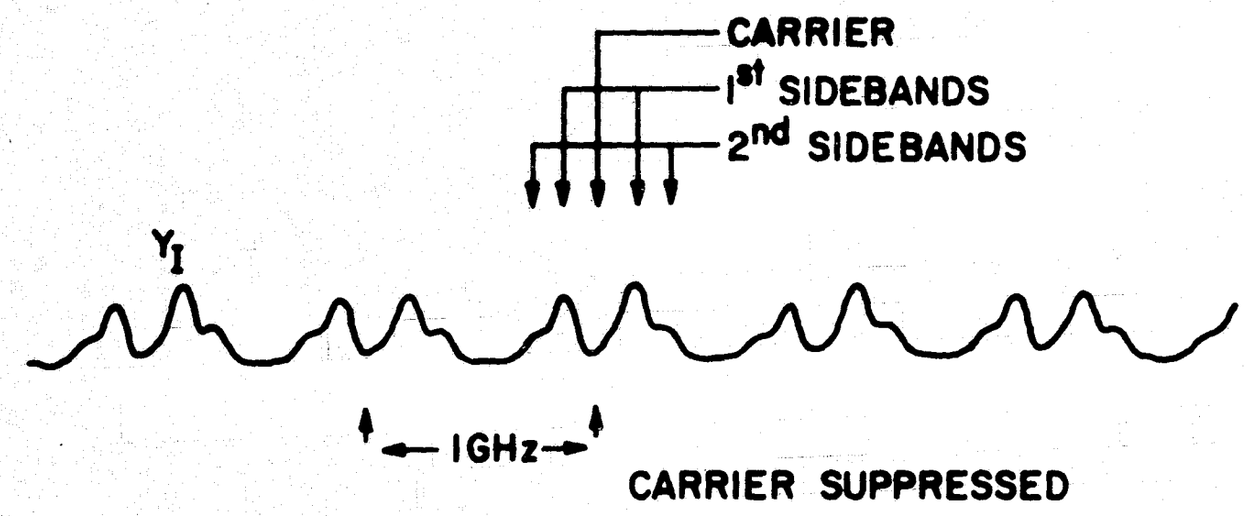

FREQUENCY MODULATION OF A GALLIUM ARSENIDE LASER AT 150 MM_2 FABRY PEROT INTERFEROMETER TRACE

FIGURE 3-5 (b)

09

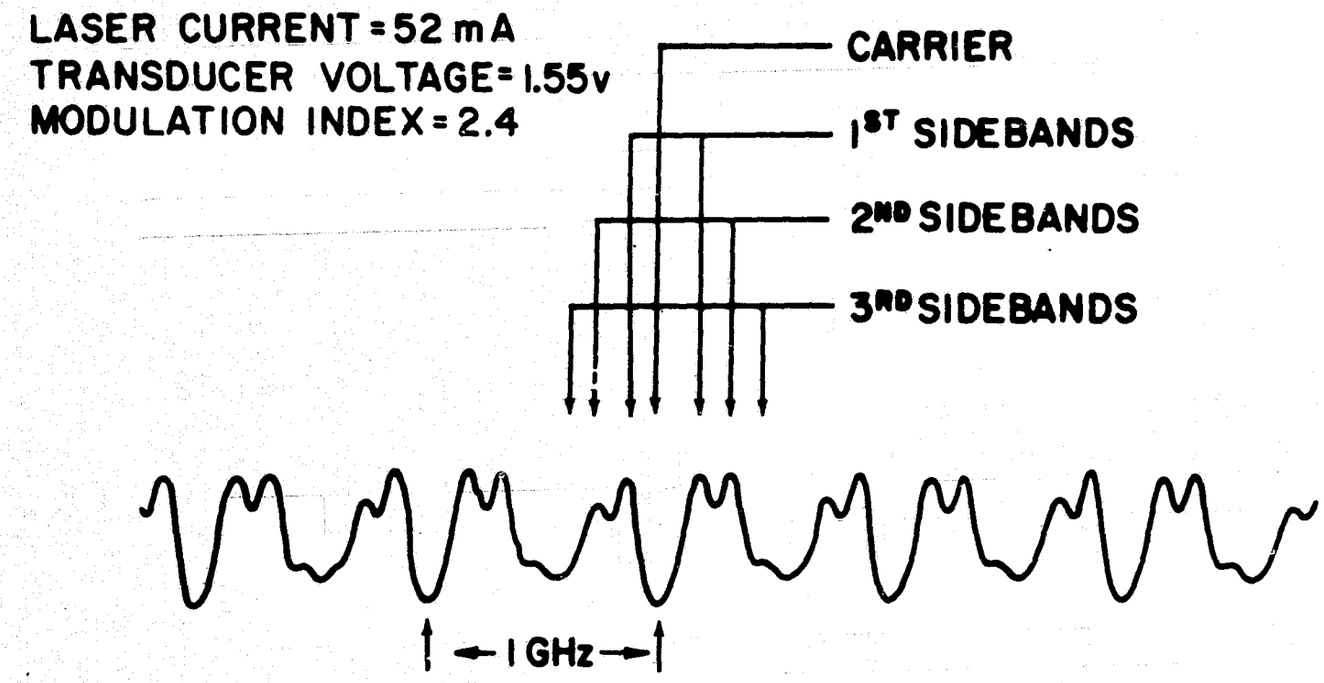

FABRY-PEROT INTERFEROMETER TRACE
OF A GALLIUM ARSENIDE LASER
FREQUENCY MODULATED AT 150 MHz

FIGURE 3-5(c)

LASER CURRENT = 52 mA
TRANSDUCER VOLTAGE = 2.5 V
MODULATION INDEX = 3.9

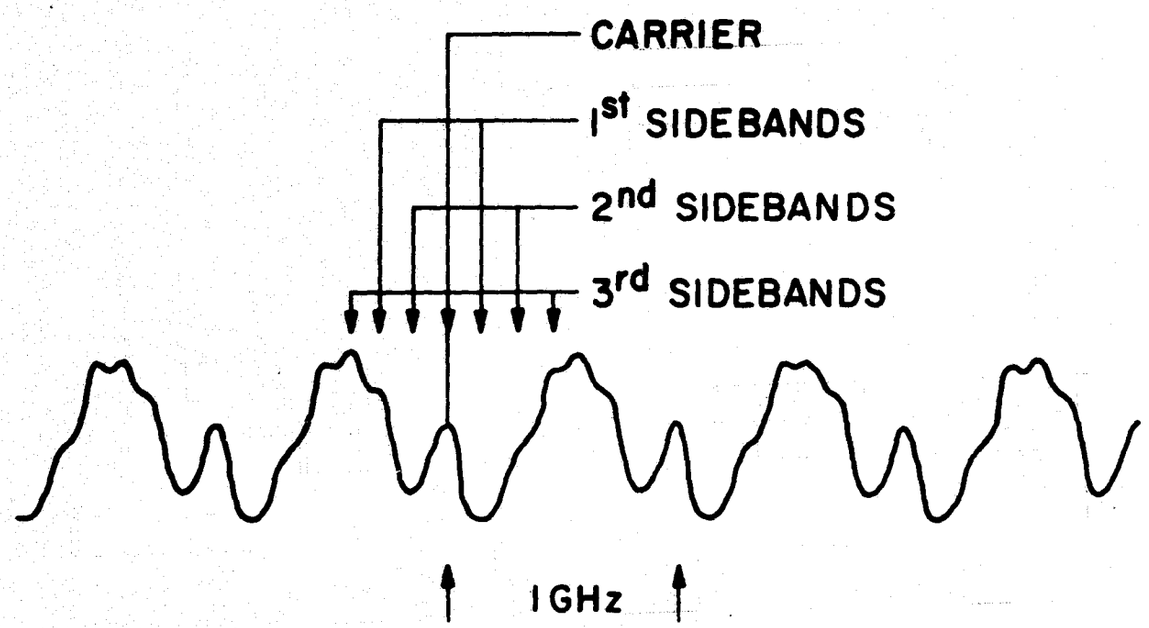

FABRY-PEROT INTERFEROMETER TRACE
OF A GALLIUM ARSENIDE LASER
FREQUENCY MODULATED AT 150MHz

FIGURE 3-5(d)

3-4(c) the rings are broadened so much that they almost cross and hence the intensity is fairly uniform. In order to observe the individual sidebands, the modulating frequency was raised to 150 MHz and the sample holder was changed so that the sound waves did not travel through copper and hence become attenuated. Figure 3-5 shows interferometer scans at ν_s = 150 MHz and various transducer voltages V. Figure 3-5(a) shows the scan for the unmodulated laser i.e. V=0. Figure 3-5(b) corresponds to a modulation index m_f=1.9. Here the carrier frequency is almost zero and the first sidebands are nearing a maximum and the second are clearly visible. In figure 3-5(c) at m_f=2.4, the carrier is completely suppressed and the first sidebands are a maximum. The second sidebands are now approaching their maximum while the third sidebands have appeared. The first sidebands are completely suppressed at a modulation index m_f=3.9 as can be seen in figure 3-5(d).

A picture of the theoretical behavior of the sidebands is given in figure 4-2(a). One point of difference in the observed spectra, between pressure modulation and injection modulation is that for pressure modulation (pure frequency modulation), there is symmetry about the carrier frequency while for injection modulation, the inherent amplitude modulation causes an asymmetry in the sideband pattern. This will be seen in Chapter IV. Sideband patterns for modulation indices up to 6 were obtained. However, at these high frequency deviations, considerable overlap occurred between the high frequency sidebands of one interferometer ring and the low frequency sidebands of the adjacent one. Figure 3-6(a) shows a plot of carrier intensity versus transducer voltage compared with the theoretical variation J_o^2. Figures 3-6(b), (c), and (d) show similar plots for the first, second, and third sidebands. As can be seen, the fit is very close to the theoretical variations J_1^2, J_2^2, and J_3^2 respectively indicating that very little distortion is present. Particularly for the second and third sidebands, corrections were

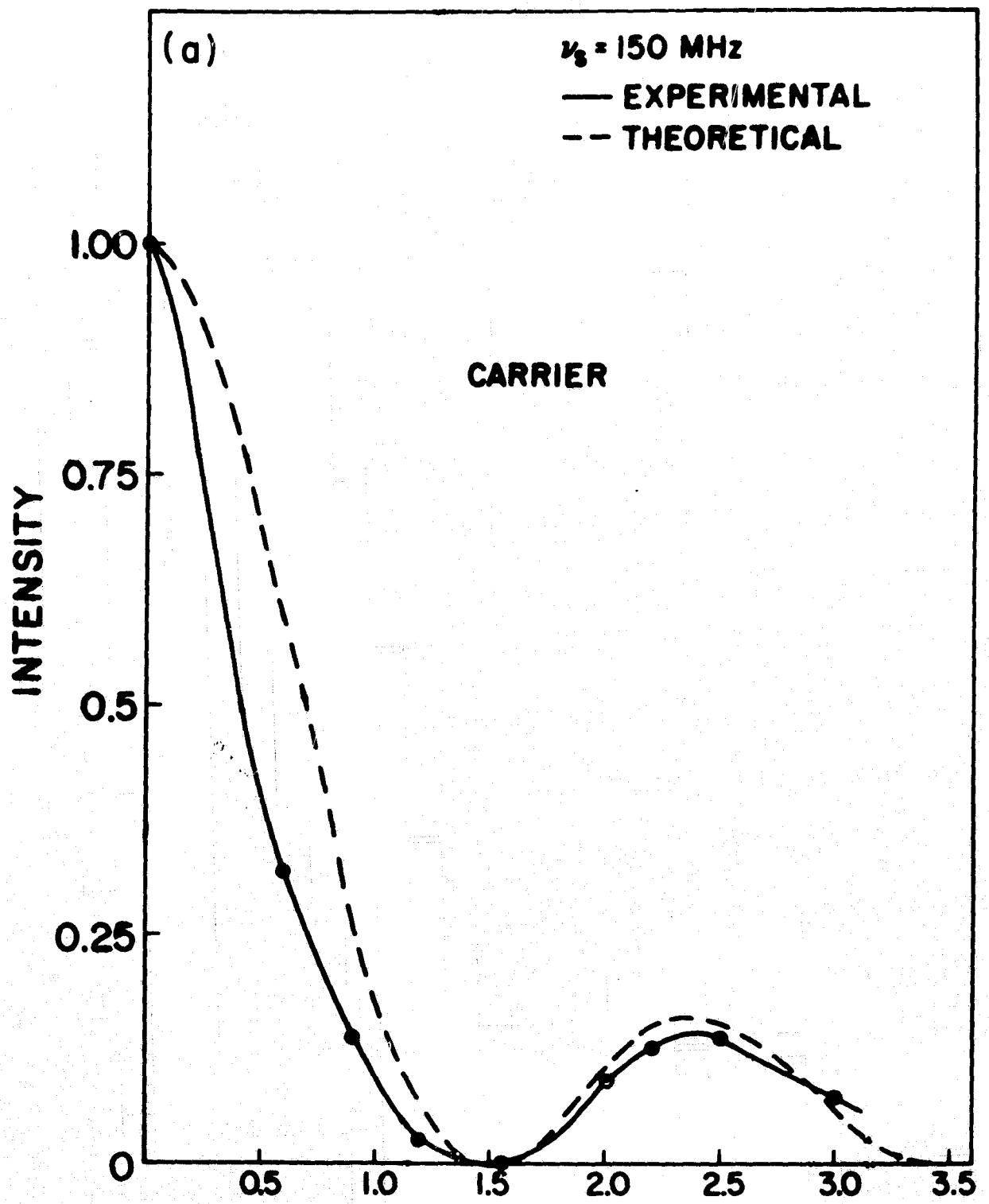

SIDEBAND INTENSITY
Vs TRANSDUCER VOLTAGE

FIGURE 3-6(a)

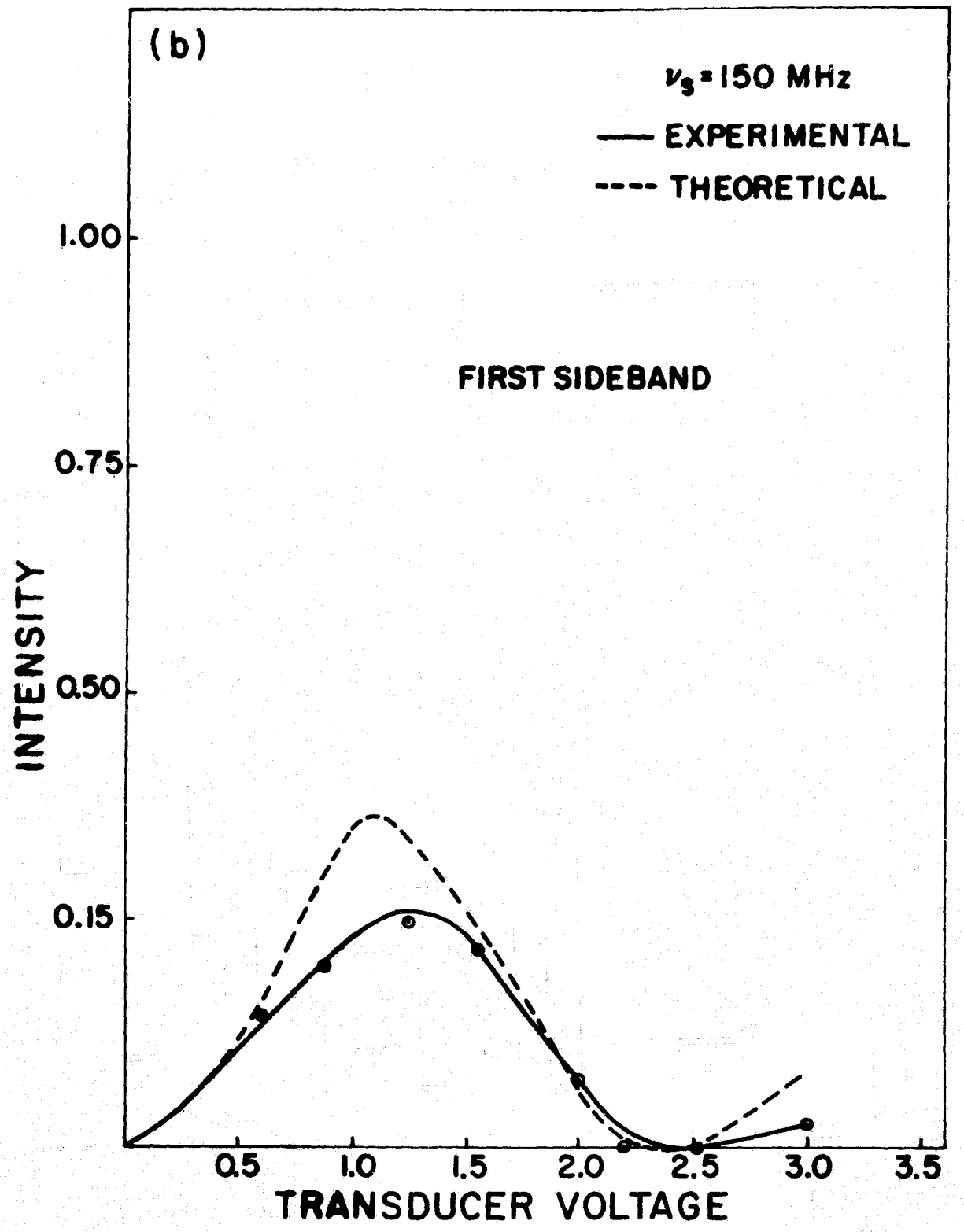

SIDEBAND INTENSITY VS
TRANSDUCER VOLTAGE
FIGURE 3-6(b)

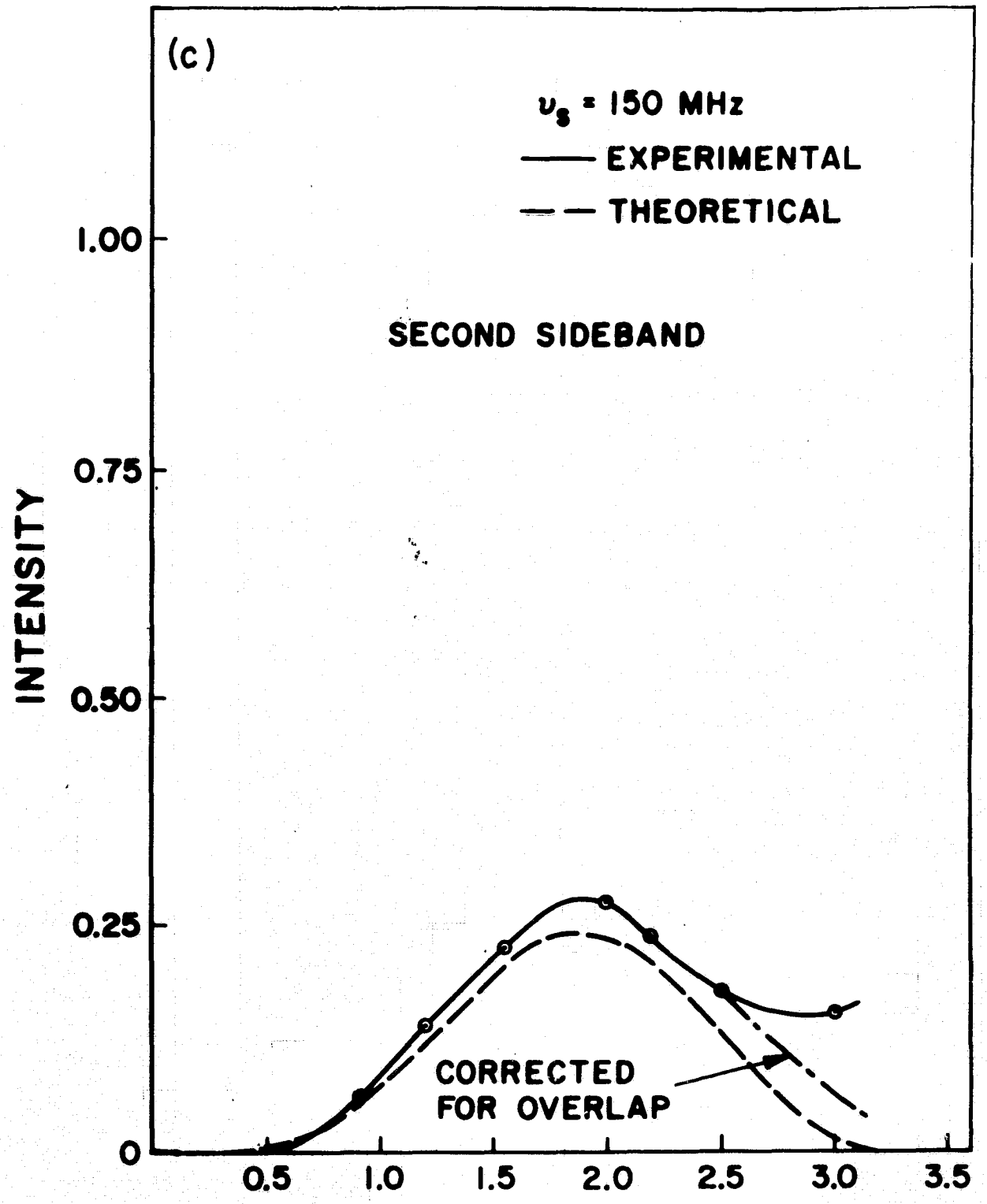

SIDEBAND INTENSITY
Vs TRANSDUCER VOLTAGE
FIGURE 3-6(c)

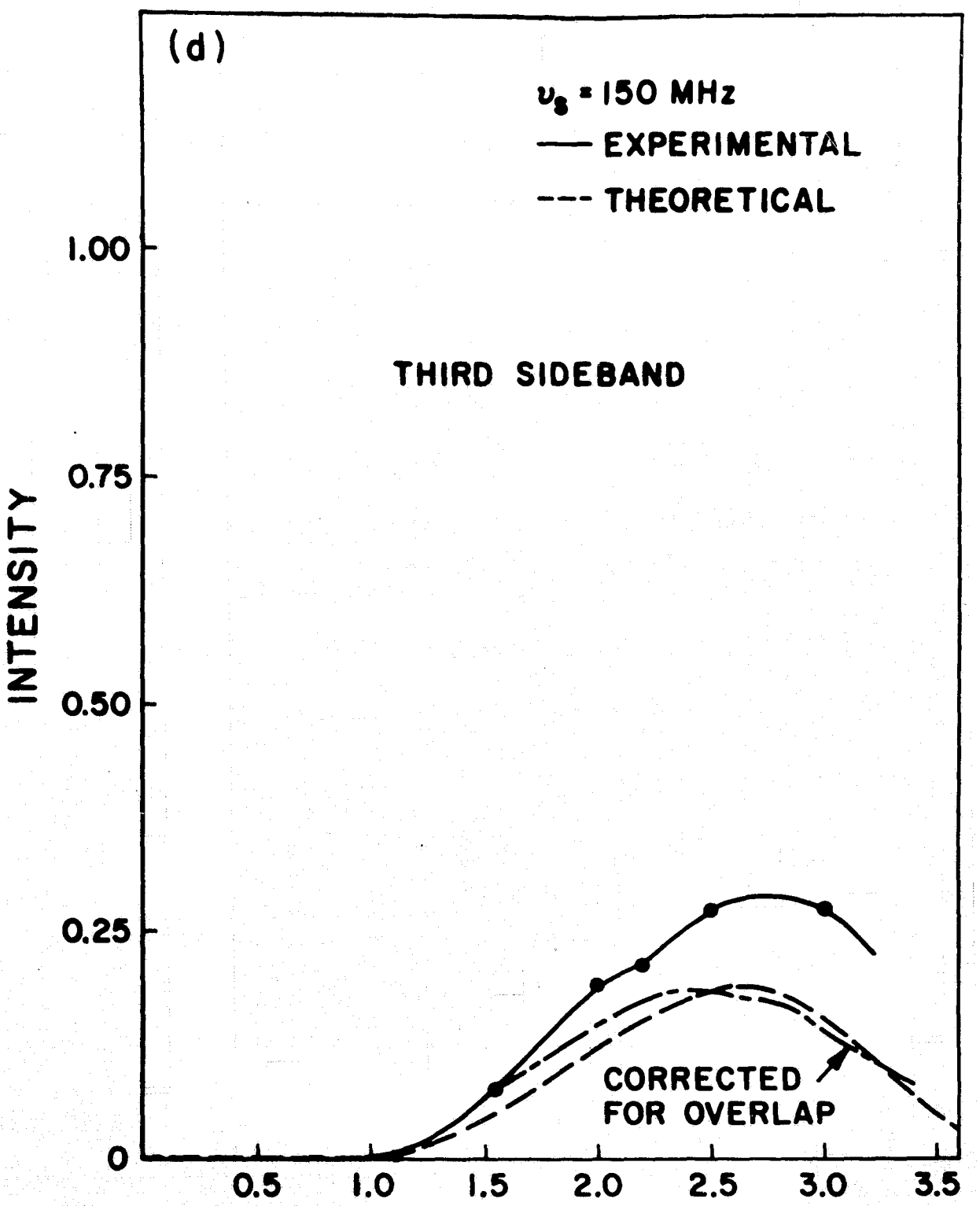
(d)
υ_s = 150 MHz
EXPERIMENTAL
THEORETICAL
THIRD SIDEBAND
CORRECTED FOR OVERLAP
INTENSITY
1.00
0.75
0.50
0.25
0
0.5
1.0
1.5
2.0
2.5
3.0
3.5
TRANSDUCER VOLTAGE
SIDEBAND INTENSITY
Vs TRANSDUCER VOLTAGE

FIGURE 3-6(d)

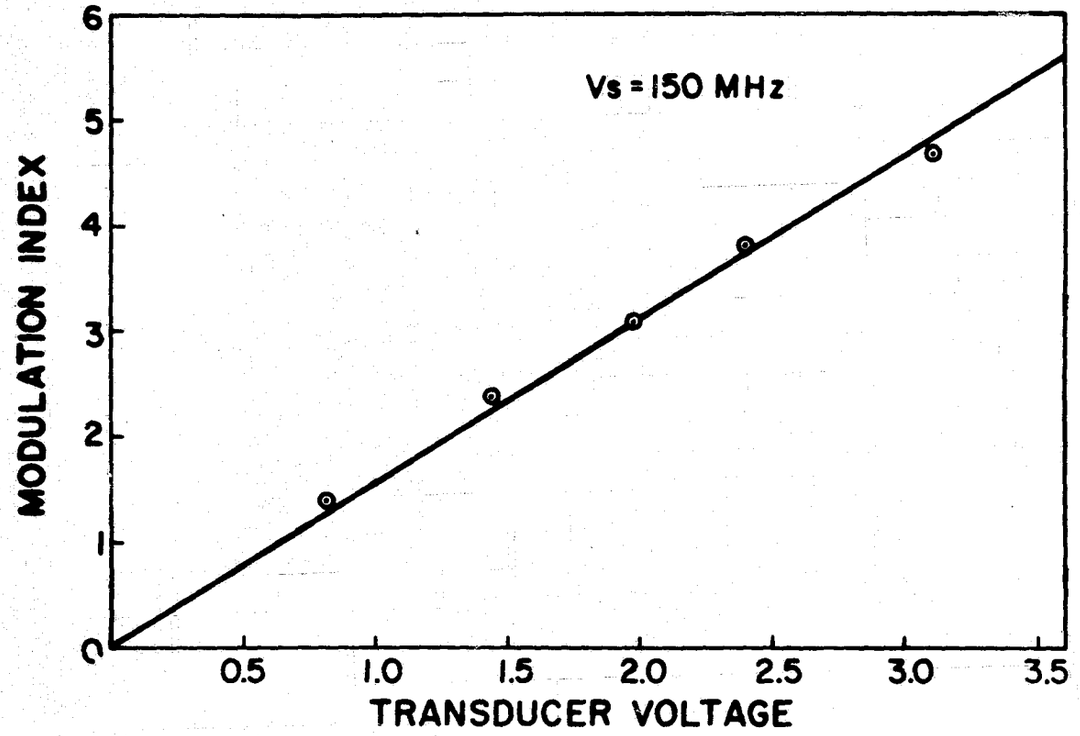

MODULATION INDEX VS TRANSDUCER VOLTAGE

FIGURE 3-7

made to allow for the overlap mentioned at the higher modulation indices.

The modulation index was measured as follows: The variation of the sidebands with transducer voltage was noted as shown in figures 3-6. In particular, the voltage at which the maxima and minima of the n^{th} sideband occurred was noted. The value of m_f at which J_n^2 has its maxima and minima is known and was plotted against the measured voltage. Figure 3-7 shows such a plot. The relationship between m_f and transducer voltage is linear since both are proportional to the acoustic pressure. The highest modulation index attained was 6 corresponding to a frequency deviation of 900 MHz and an acoustic pressure of 2.7 atmospheres.

In order to be certain that modulation was occurring via pressure rather than via injection modulation due to pickup from the transducer lead onto the laser bias lead, the following measurements were made: firstly, the sideband pattern was observed and found to contain little or no asymmetry about the carrier frequency. As discussed in Chapter IV, when modulation was applied via the injection, considerable asymmetry was detectable. Secondly, the voltage in the laser bias lead could be monitored using a spectrum analyzer tuned to the modulating frequency. Either no voltage was measurable down to a few microvolts which would be insufficient to produce the noted modulation, or the voltage measured was too small. That this was so was checked by purposely introducing modulation onto the bias lead and noting the observed modulation for a given voltage. Thirdly, by measuring the total laser intensity with a photodetector, as described in Chapter IV, no amplitude modulation was measurable on the spectrum analyzer at frequency deviations where it could easily be observed when the injection was modulated. Co-axial cabling and shielding was used on the transducer lead so that it was completely shielded. On the laser lead, co-axial cabling

was used up to the microdot connector mentioned in section 3-2. Considerable care was taken in properly grounding all equipment and where necessary, double shielding was used. Fifthly, a laser was operated cw using the arrangement described in section 3-2. In order for ultrasonic waves generated in the transducer to reach the laser, they had to travel through the sapphire rod. Modulation was observed in the interferometer when a voltage was applied across the transducer. Next, a thin piece of cardboard was placed between the transducer and the sapphire rod to prevent any ultrasonic waves from reaching the laser. The transducer was cemented in place with silver paint and the sample holder assembled as before. No modulation was observed when the same voltage was applied to the transducer. Also, when the active area of the transducer was not exactly under the laser, no modulation was observed.

4. Conclusions

The experiment described above shows that when an injection laser is modulated via ultrasonic waves, sidebands are generated at multiples of the modulating frequency from the carrier. These sidebands closely follow the behavior expected from a laser which is frequency modulated but contains no amplitude modulation. The modulation index showed the expected linear relationship with the transducer voltage. Experiments were performed to show that it was, in fact, pressure from the ultrasonic waves which caused the observed modulation.

Since pressure does provide a means for obtaining pure frequency modulation, an injection laser modulated via ultrasonic waves could be used in an optical FM communications system. The maximum useable center frequency has a limitation imposed by equation 3-4 which arises when the sound wavelength becomes comparable to the width of the laser beam in the active region.

With current semiconductor laser this means a maximum frequency of about 2 GHz. This is attractive for many applications so that a useful semiconductor laser FM communications transmitter is a possibility.

An interesting experiment which could be performed would be one designed to probe the frequency limitation predicted by 3-4. In order to do this, the input power necessary to cause a fixed frequency deviation would be measured as a function of modulating frequency. This would give directly the variation of modulation index m_f with frequency or wavelength of the ultrasonic waves. Considerable care would have to be exercised in such an experiment. Over the frequency range of interest, say 500 MHz to 3 GHz, the voltage reaching the transducer from the signal generator would have to be measured at each frequency; the performance of the transducer at each frequency would have to be known. Probably more than one transducer would be required for a bandwidth this large. Furthermore, the acoustic properties of any material in between the transducer and the laser would have to be accounted for. A possible way of avoiding some of these problems would be to use a GaAs depletion layer transducer in the same laser crystal as proposed by Ripper.[4]

Another experiment which could be performed, is one designed to verify the prediction of equation 2-116 and 2-125 that an optically pumped semiconductor laser when modulated via ultrasonic waves, will contain amplitude modulation. For this, a pure GaAs laser crystal, with opposite faces cleaved to form an optical cavity, would be bonded to a sapphire rod. On the other end of the rod, a transducer would be placed so that acoustic waves generated in the transducer could be transmitted to the laser. The GaAs crystal could be pumped with a GaAsP laser operated either cw or, as the results of Chapter V show, it would be possible to operate pulsed. Both lasers would be cooled to 77°K or 4.2°K. Amplitude modulation could be detected simply by allowing the pressure modulated GaAs laser beam to fall on a photodetector connected to a spectrum analyzer.

References

1. J. E. Ripper, IEEE Journal of Quantum Electrons QE-6, 129 (1970).

2. G. E. Fenner, Journal of Applied Physics 34, 2955 (1963).

3. J. Feinlab, S. Groves, W. Paul, R. Zallen, Physical Review 131, 2070 (1963).

4. J. E. Ripper, MIT Ph.D. Thesis, Department of Electrical Engineering (1966).

CHAPTER IV

Injection Modulation

1. Introduction

In Chapter II, the effect on a laser mode of a simultaneous modulation of the real and imaginary parts of the dielectric constant was considered. There it was shown that the major effect was a modulation of the frequency by the real part of the dielectric constant while the imaginary gave rise to modulation of the amplitude. In Chapter III, it was shown that for injection lasers, pressure modulation induces a freqeuncy spectrum which closely follows that produced by pure frequency modulation and that hence modulation of the gain or imaginary part of the dielectric constant, is negligible. In this chapter, the experimental results of modulating the injection will be presented. It will be seen that both the frequency and amplitude modulations are appreciable and that the effect of the amplitude modulation on the spectrum of the laser is pronounced.

2. Experiment

The experimental arrangement used to modulate the injection was similar to that used for the pressure modulation experiment. However, instead of applying a modulating signal to a transducer, it was capacitively coupled to the laser bias lead so that the signal generator output fed a 50 ohm load in series with the biased laser. The modulated laser beam was passed through a Fabry-Perot interferometer, as before, but this time one which had a free spectral range of 7.5 GHz and which could be piezoelectrically scanned. The beam emergent from the interferometer was detected using a silicon photodiode on axis, and the diode signal amplified using a Tektronix 1A7 plug-in amplifier. The output from the amplifier was fed to the Y axis of an X-Y

recorder whose X-axis was driven by the scanning voltage applied to the interferometer mirror. A beam splitter was placed between the laser and the interferometer so that a portion of the beam could be allowed to fall directly on another photodiode which was connected to a Tektronix 491 Spectrum Analyzer. This was used to measure the amplitude modulation on the laser beam. Since the detector responds only to amplitude changes in the light beam and not to frequency changes, any frequency modulation on the beam will not be measured and thus the amplitude modulated component could be separated out. All measurements of the injection modulation were performed at 77°K on a cw GaAs laser. The modulating frequencies used ranged from 30 MHz to 1 GHz.

3. Results

Equation 2-139 gives the effect of a time dependent modulation of the complex dielectric constant on the total electric field of the laser modes. For each mode we have

$$\vec{E}_{nmq}(\vec{r},t) = \vec{E}_{nmq}(\vec{r})\, e^{m_a \cos\omega_s t} \sin\left[\omega_{nmq} t - m_f \sin\omega_s t\right] \qquad 4-1$$

Using the well-known Bessel function expansions, this may be written

$$\vec{E}_{nmq}(\vec{r},t) = \mathrm{Im}\,\vec{E}_{nmq}(\vec{r})\left[\sum_{k=-\infty}^{\infty} I_k(m_a)\, e^{ik\omega_s t}\right]\left[\sum_{p=-\infty}^{\infty} J_p(m_f)\, e^{i(\omega_{nmq} - p\omega_s)t}\right] \qquad 4-2$$

putting p - k = l

$$\vec{E}_{nmq}(\vec{r},t) = \mathrm{Im}\,\vec{E}_{nmq}(\vec{r}) \sum_{k,l=-\infty}^{\infty} I_k(m_a)\, J_{k+l}(m_f)\, e^{i(\omega_{nmq} - l\omega_s)t} \qquad 4-3$$

The coefficient of the 1^{th} sideband is thus

$$\vec{E}_{n,m,q,l}(\vec{r},t) = I_m \vec{E}_{nmq}(\vec{r}) \sum_{k=-\infty}^{\infty} I_k(m_a) J_{k+l}(m_f) e^{i(\omega_{nmq} - l\omega_s)t} \qquad 4-4$$

while

$$\vec{E}_{n,m,q,-l}(\vec{r},t) = I_m \vec{E}_{nmq}(\vec{r})(-1)^l \sum_{k=-\infty}^{\infty} (-1)^k I_k(m_a) J_{k+l}(m_f) e^{i(\omega_{nmq} + l\omega_s)t} \qquad 4-5$$

Thus there is an asymmetry about the center frequency, in the sideband pattern. Had the modulation of the amplitude and frequency been in phase, then no assymmetry would result. Furthermore, putting $m_a \rightarrow -m_a$ or $m_f \rightarrow -m_f$ changes the side on which the assymmetry is higher. Thus by observing on which side the sidebands are higher, the relative signs of m_a and m_f may be determined.

Since the signal produced by the photodiode is proportional to the intensity of light falling upon it, the photocurrent produced by the 1^{th} sideband is proportional to

$$I_{n,m,q,l} = \frac{E^2_{nmq}(\vec{r})}{2} \left[\sum_{k=-\infty}^{\infty} I_k(m_a) J_{k+l}(m_f) \right]^2 \qquad 4-6$$

while that produced by the detector in front of the interferometer is proportional to

$$I_{nmq} = \frac{E^2_{nmq}(\vec{r})}{2} e^{2 m_a \cos \omega_s t} \qquad 4-7$$

The signal displayed on the screen of the spectrum analyzer was the component of the intensity at the modulating frequency

$$[I_{nmq}]_{obs} = \frac{E^2_{nmq}(\vec{r})}{2} 2 I_1(2 m_a) \qquad 4-8$$

Measurement of harmonics could not be performed because their signal levels were below, or about equal to, that of the noise and the signal generator output contained harmonics larger than those to be measured.

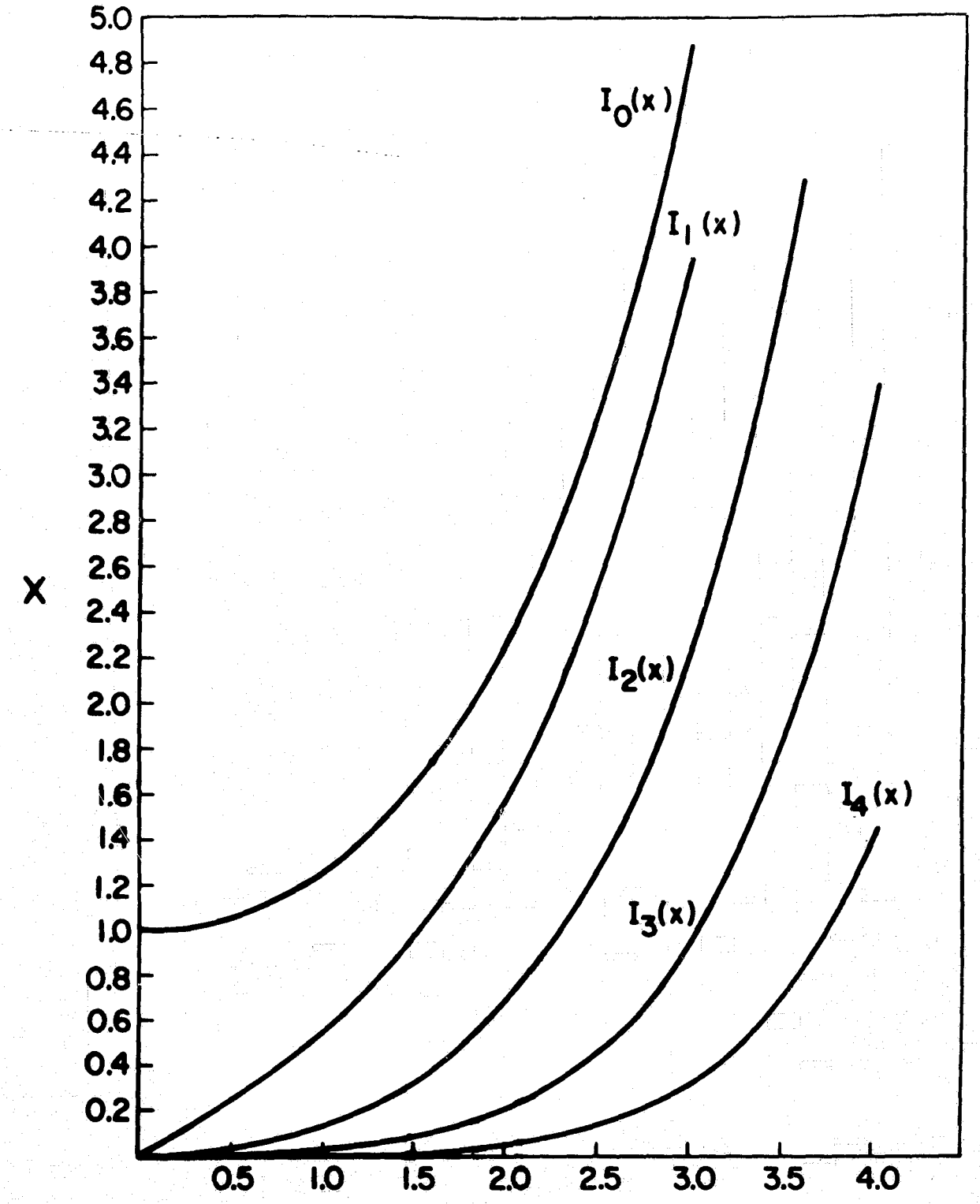

MODIFIED BESSEL FUNCTIONS

$I_n(x) = i^{-n} J_n(ix)$

FIGURE 4-1

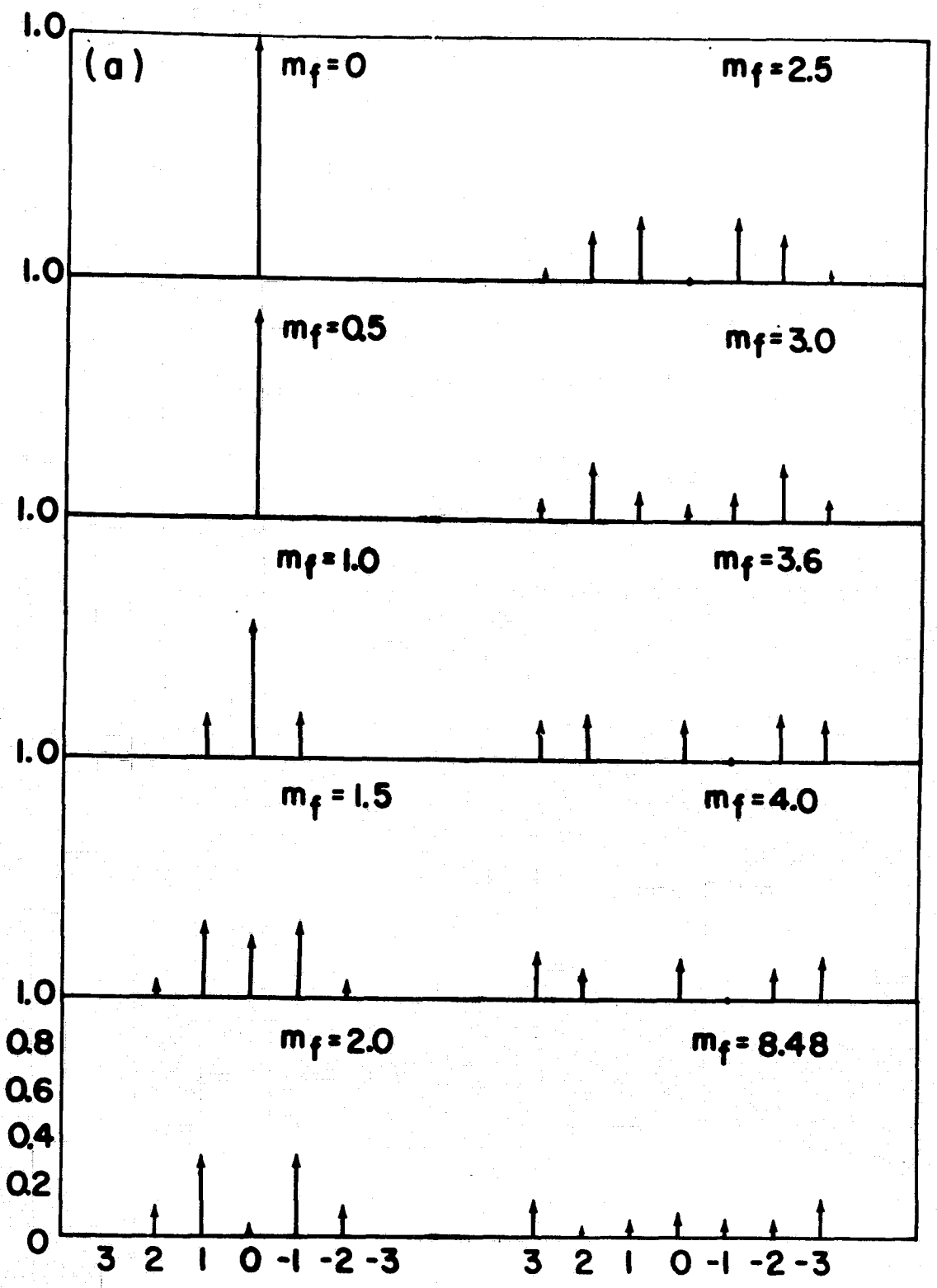

THEORETICAL CURVES FOR MODULATION OF THE COMPLEX DILECTRIC CONSTANT

PURE FREQUENCY MODULATION

$\lambda = 0$

FIGURE 4-2 (a)

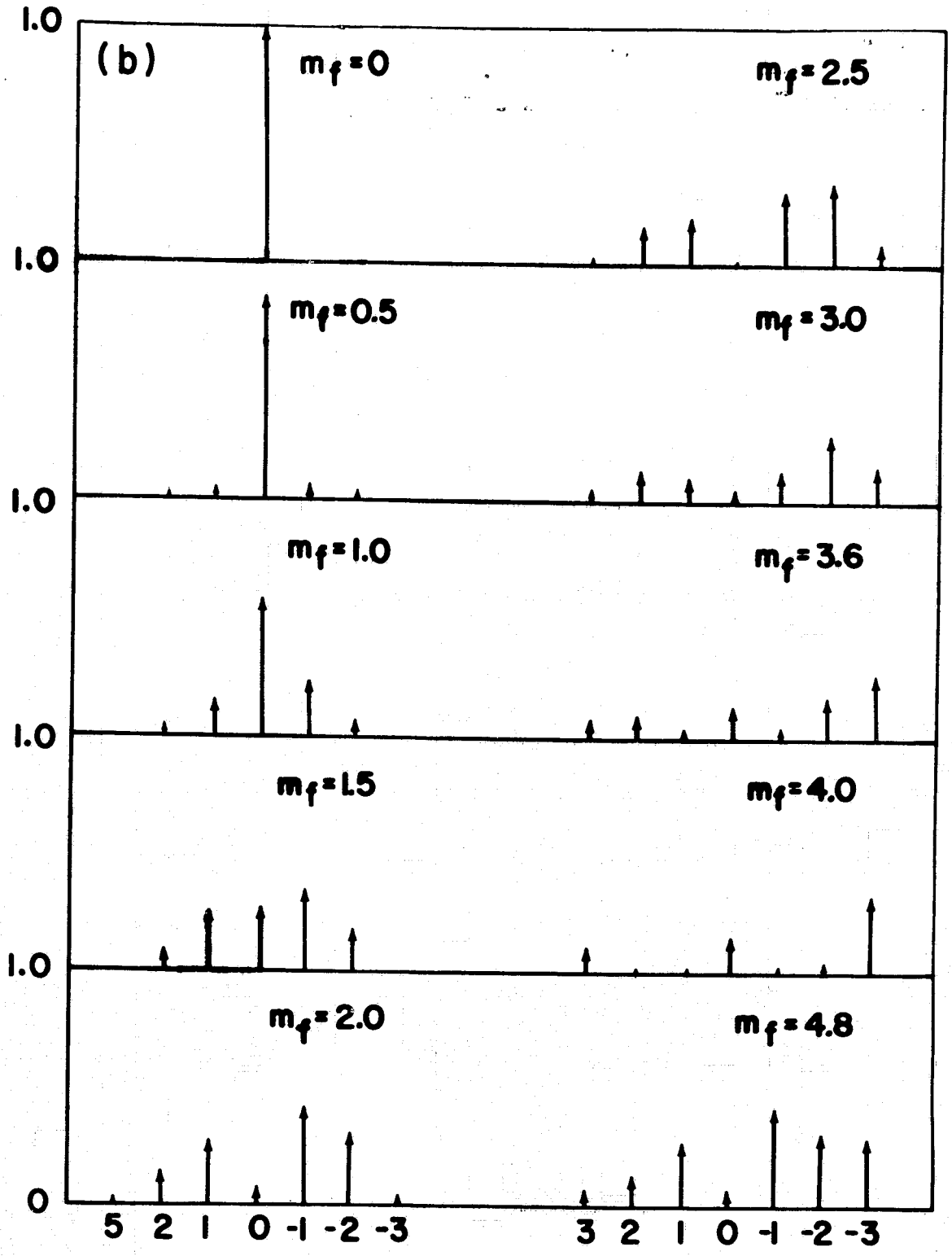

THEORETICAL CURVES FOR MODULATION OF THE COMPLEX DILECTRIC CONSTANT
$\lambda = 0.1$

FIGURE 4-2(b)

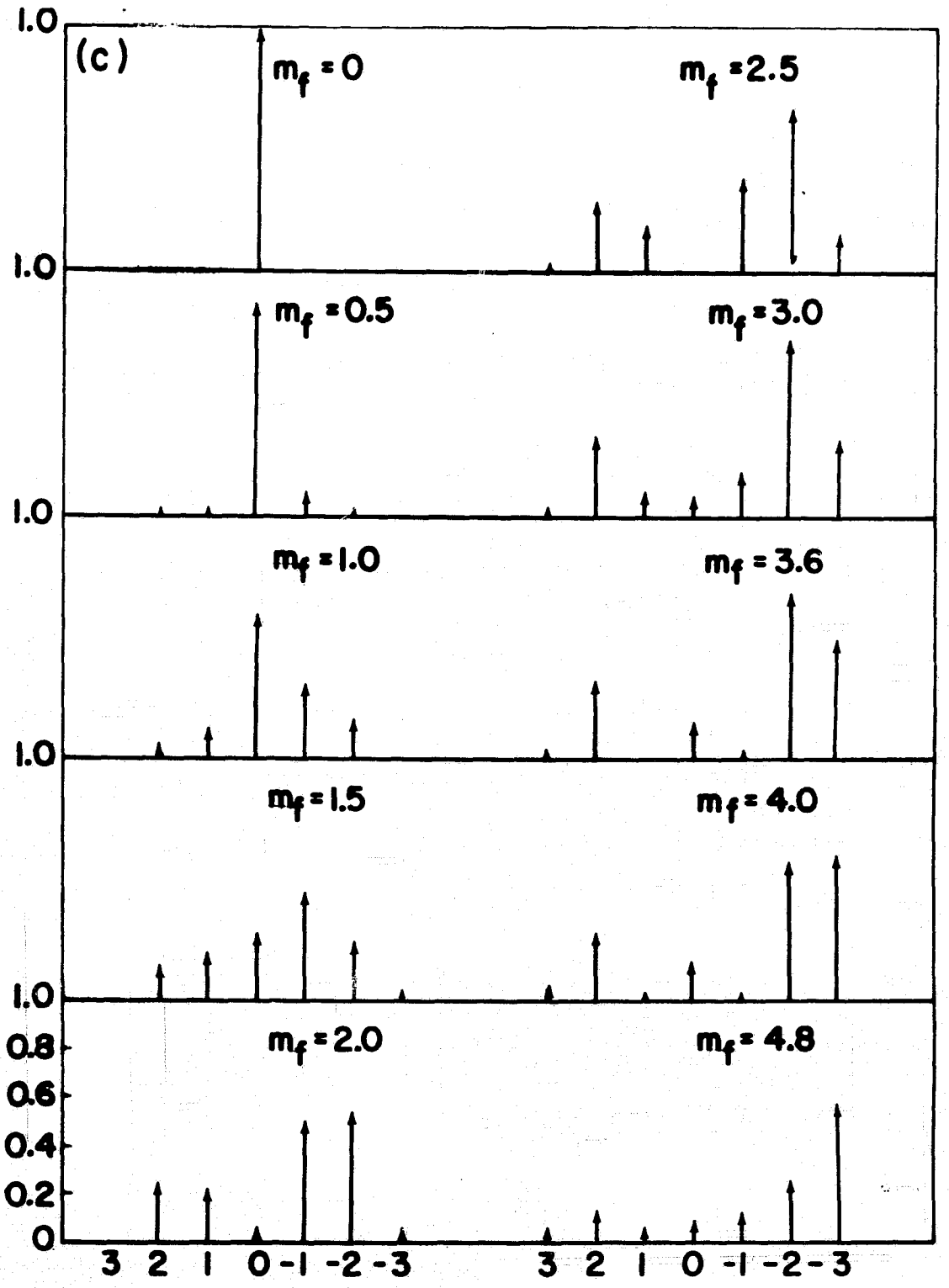

THEORETICAL CURVES FOR MODULATION OF THE COMPLEX DILECTRIC CONSTANT

$\lambda = 0.2$

FIGURE 4-2 (c)

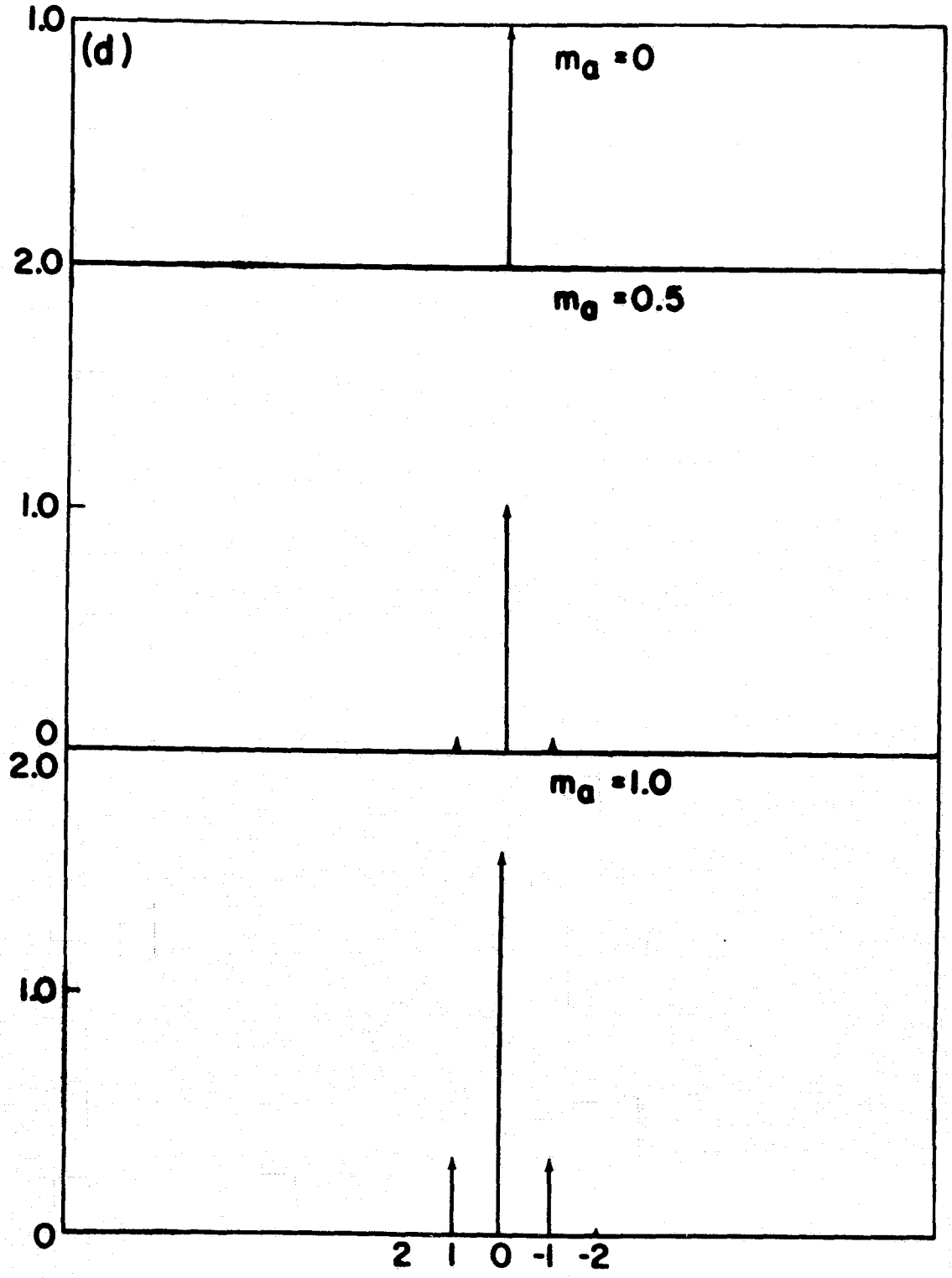

THEORETICAL CURVES FOR MODULATION OF THE COMPLEX DIELECTRIC CONSTANT $\lambda = \infty$ PURE AMPLITUDE MODULATION

FIGURE 4-2 (d)

Figure 4-1 shows the behavior of the modified Bessel functions $I_o(x)$ through $I_4(x)$ for values of x up to 4. In particular, it can be seen that $I_1(x)$ is linear with x to within 1% for $x=2m_a$ less than 0.28. Thus for m_a less than 0.14 little distortion would be present in a laser AM communications system where the injection laser was amplitude modulated by applying modulation to the bias. Harmonic distortion at this point is about 5%. Note also that for square law detection, the frequency modulation simultaneously produced on the laser beam, would have no effect on the photodetector. Thus, an AM communications system using an injection laser is possible and for small signals, little distortion would be present.

The sideband pattern observed from an injection modulated laser, as given by equation 4-6, will depend on the relative magnitudes of m_a and m_f. Figure 4-2 shows some results for the first few sidebands. The spectra are shown at different values of m_f for fixed values of λ where λ is defined by

$$m_a = \lambda m_f \qquad 4-9$$

the case $\lambda = 0$ is the case for pure frequency modulation. In this case, the electric field of the modes is given by

$$\vec{E}_{nmq}(\vec{r},t) = \vec{E}_{nmq}(\vec{r}) \sum_{p=-\infty}^{\infty} J_p(m_f) \sin(\omega_{nmq} - p\omega_s)t \qquad 4-10$$

while the case denoted $\lambda = \infty$ is that for pure amplitude modulation

$$\vec{E}_{nmq}(\vec{r},t) = \vec{E}_{nmq}(\vec{r}) \sum_{k=-\infty}^{\infty} I_k(m_a) \sin(\omega_{nmq} + k\omega_s)t \qquad 4-11$$

When individual sidebands cannot be resolved because the modulation frequency is less than the instrumental width of the interferometer, the envelope of the sidebands is observed at the output of the photodetector. Figure 4-3 shows an interferometer scan at a modulating frequency of 30 MHz for various modulating voltages. The free spectral range of the interferometer

(a)

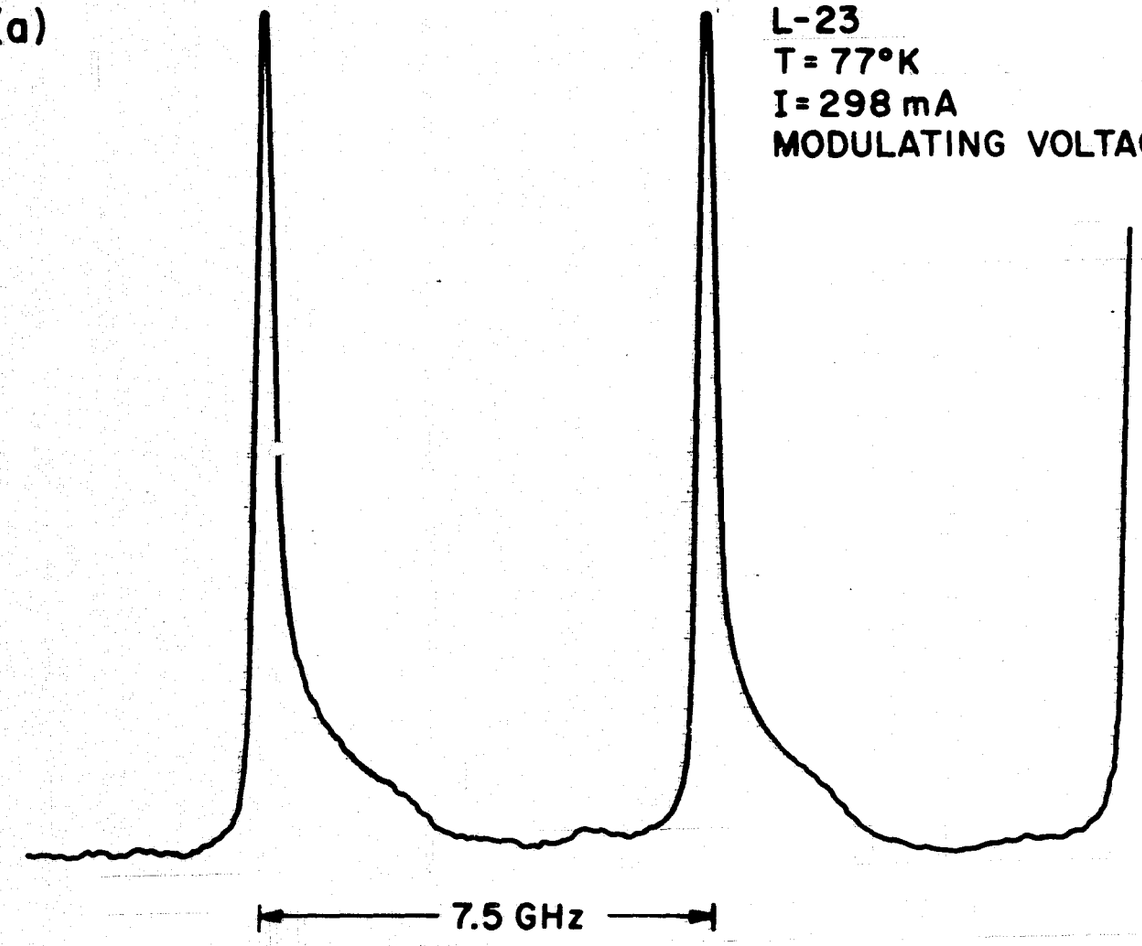

INJECTION MODULATION AT 30 MHz

FIGURE 4-3 (a)

(b)

L-23
T = 77° K
I = 298 mA
MODULATING VOLTAGE = 3 mV

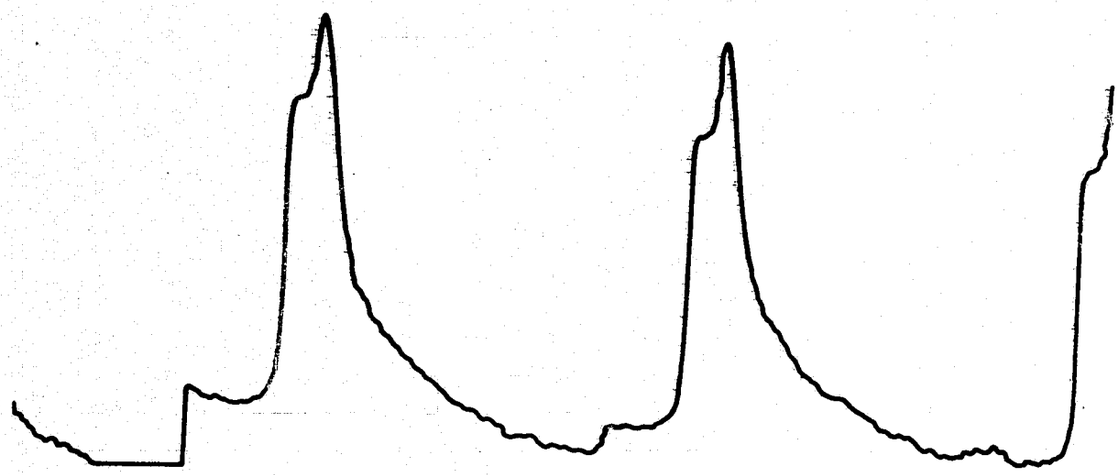

INJECTION MODULATION AT 30 MHz

FIGURE 4-3(b)

T=77°K
I=298 mA
MODULATING VOLTAGE 9 mV

INJECTION MODULATION AT 30 MHz
FIGURE 4-3 (c)

(d)

L-23
T = 77° K
I = 298 mK
MODULATING VOLTAGE = 15 mV

INJECTION MODULATION AT 30 MHz

FIGURE 4-3 (d)

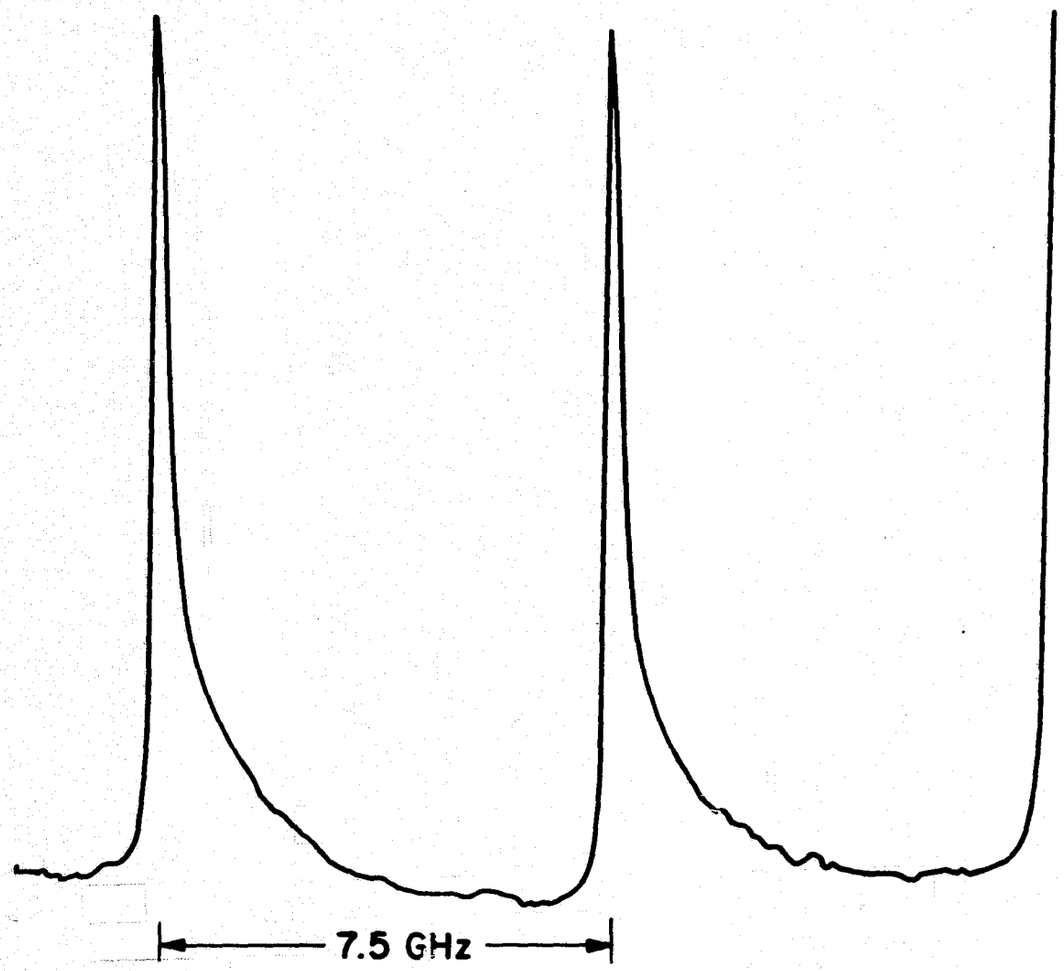

L-23
T = 77° K
I = 248 mA
MODULATING VOLTAGE = 0

INJECTION MODULATION AT 150 MHz
FIGURE 4-4 (a)

(b)

L-23
T = 77° K
I = 298 mA
MODULATING VOLTAGE = 3mV

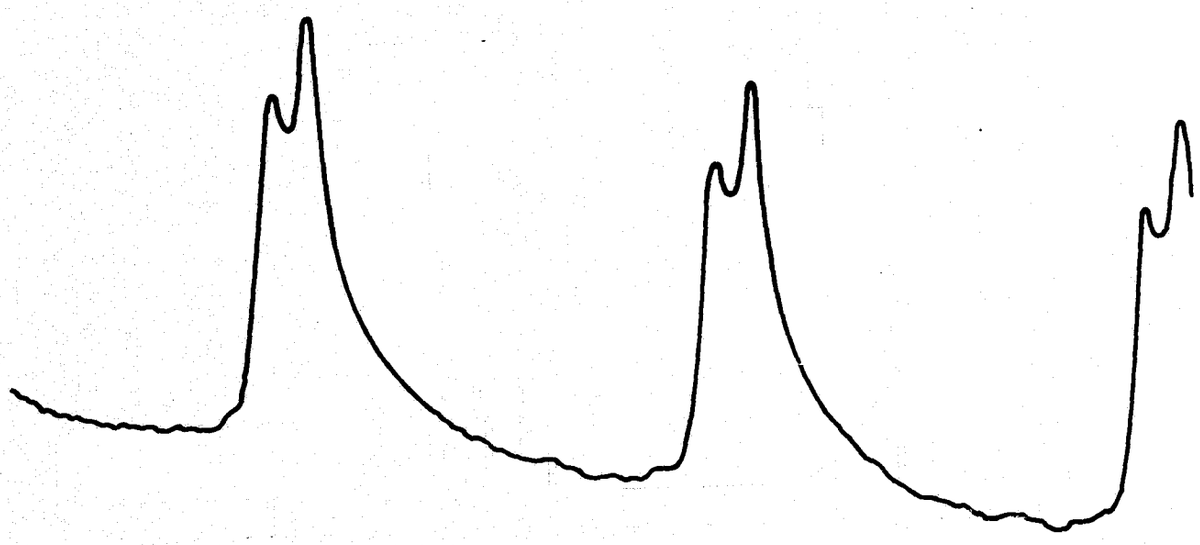

INJECTION MODULATION AT 150 MHz
FIGURE 4-4 (b)

(c)

L-23
T = 77° K
I = 298 mA
MODULATING VOLTAGE = 9mV

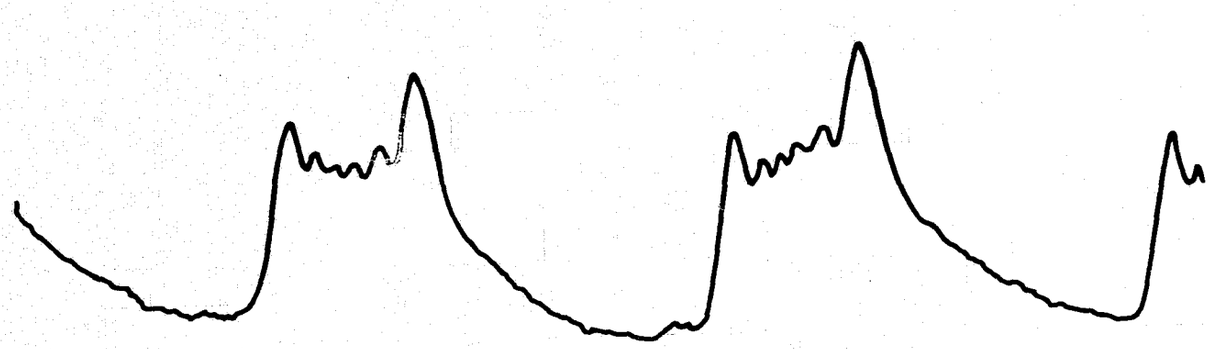

INJECTION MODULATION AT 150 MHz
FIGURE 4-4 (c)

(d)

L-23
T=77°K
I=298 mA
MODULATING VOLTAGE=15 mV

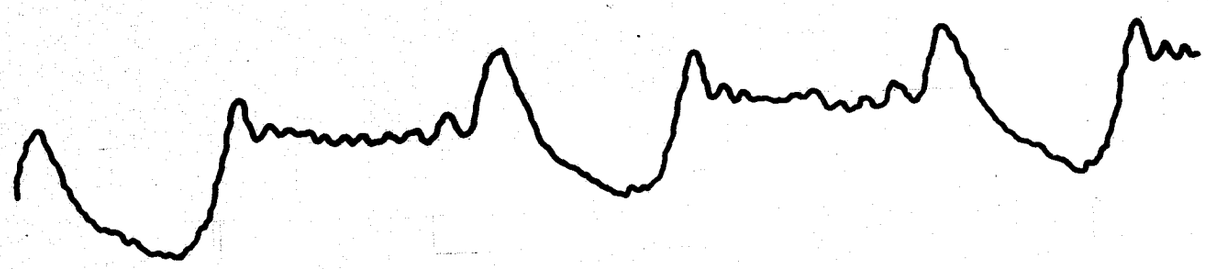

INJECTION MODULATION AT 150 MHz

FIGURE 4-4(d)

(a)

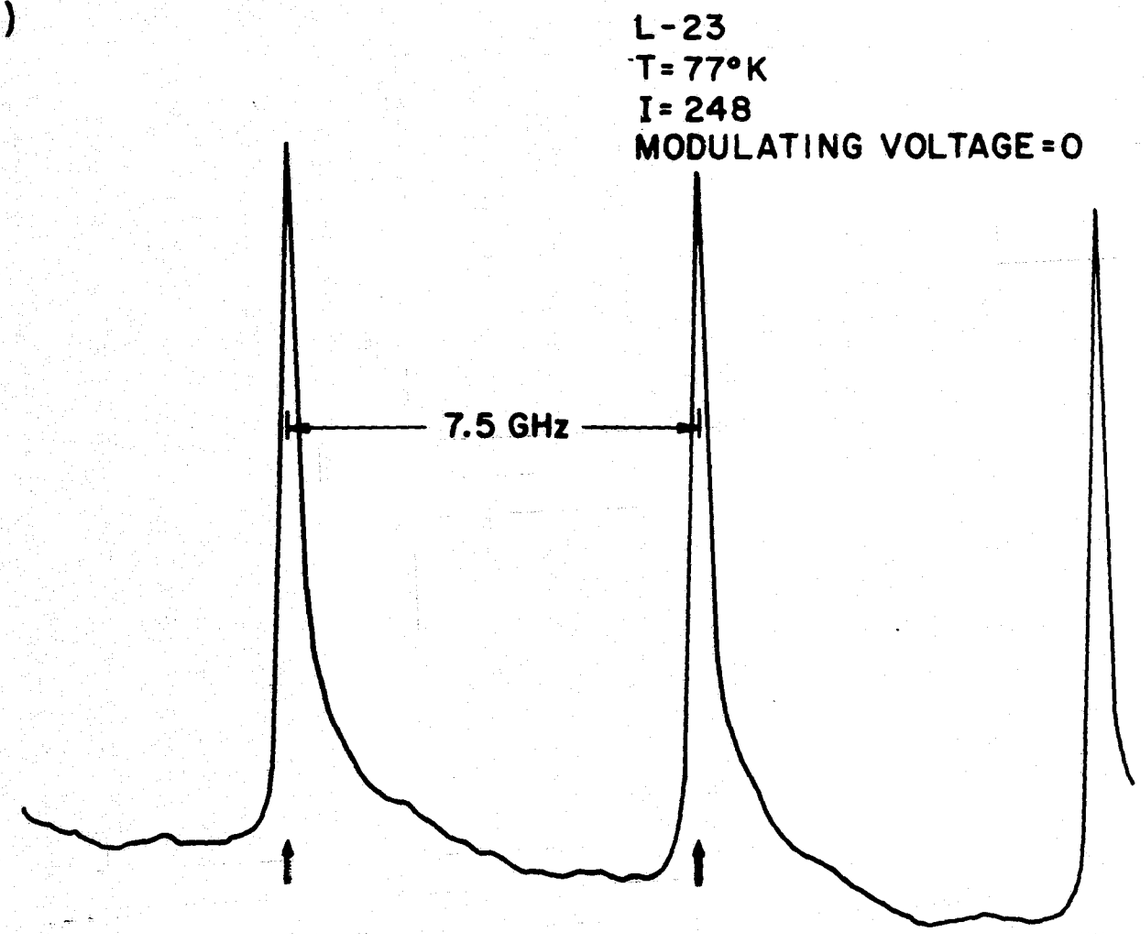

INJECTION MODULATION AT 330 MHz

FIGURE 4-5(a)

(b)

L=23
T=77°K
I=298 mA
MODULATING VOLTAGE=6mV

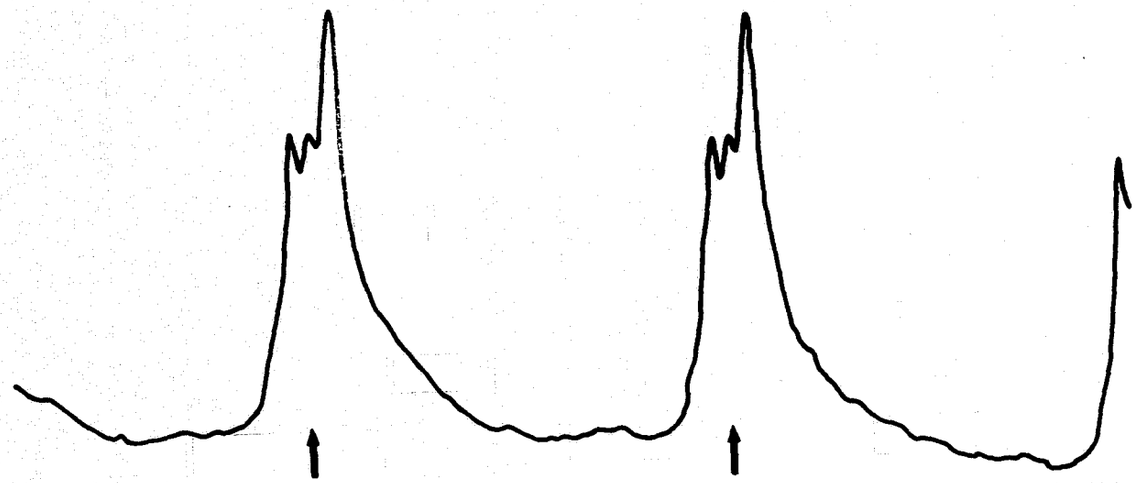

INJECTION MODULATION AT 330 MHz

FIGURE 4-5(b)

(c)

L-23
T= 77°K
I= 298mA
MODULATING VOLTAGE = 8 mV
SUPPRESSION OF CARRIER

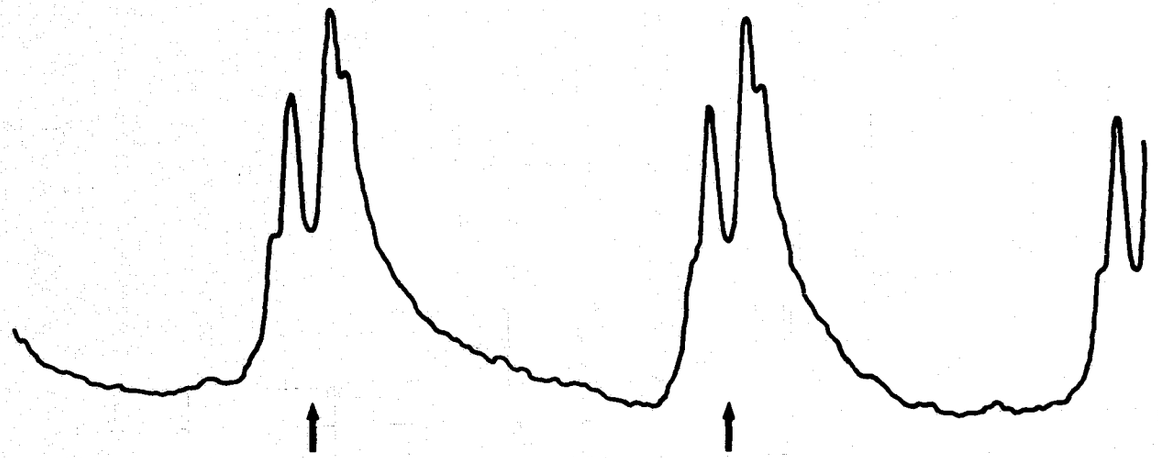

INJECTION MODULATION AT 330 MHz

FIGURE 4-5 (c)

(d)

L-23
T=77°K
I=298 mA
MODULATING VOLTAGE = 12 mV
SUPPRESSION OF FIRST SIDEBANDS

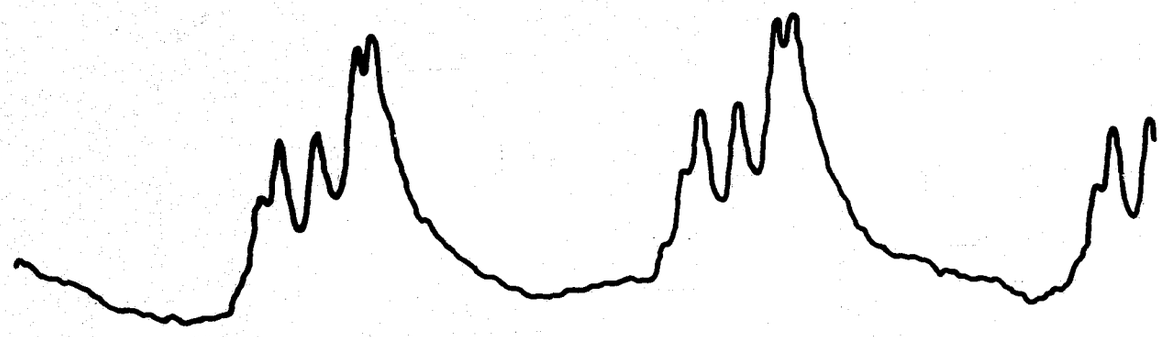

INJECTION MODULATION AT 330 MHz

FIGURE 4-5(d)

(e)

L-23
T = 77° K
I = 298 mA
MODULATING VOLTAGE = 16 mV

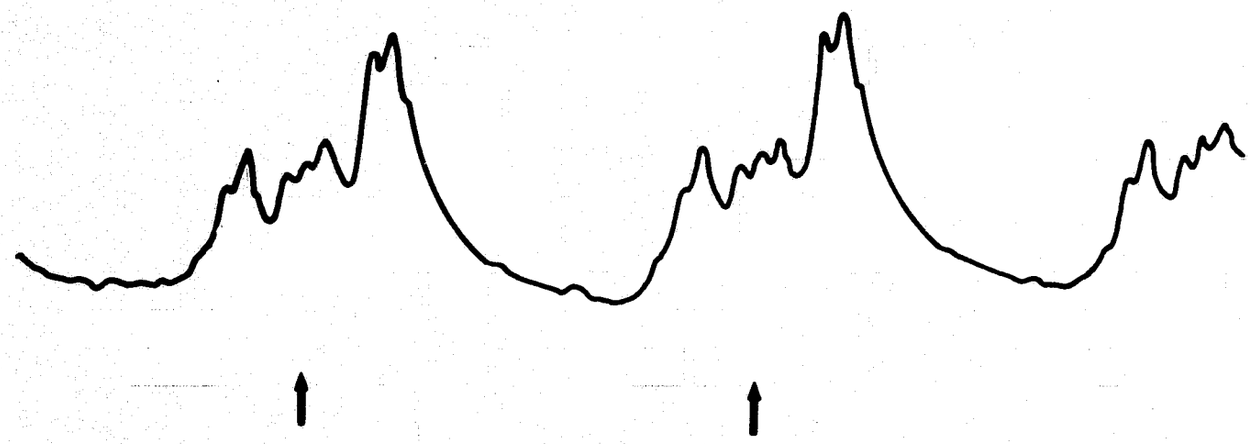

INJECTION MODULATION AT 330 MHz

FIGURE 4-5 (e)

(a)

L-23
T = 77° K
I = 298 mA
MODULATING VOLTAGE = 0

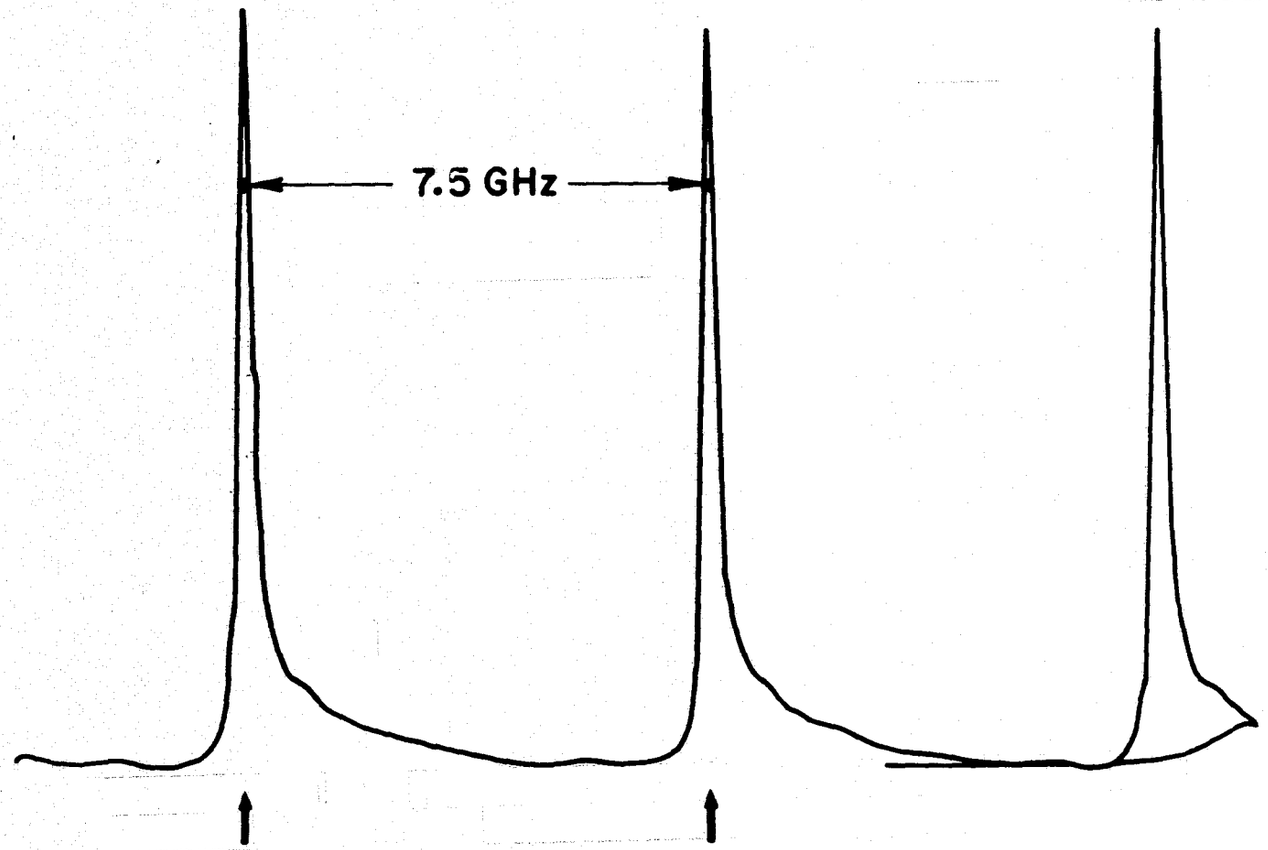

INJECTION MODULATION AT 660 MHz
FIGURE 4-6 (a)

(b)

L-23
T = 77° K
I = 298 mA
MODULATING VOLTAGE = 6mV

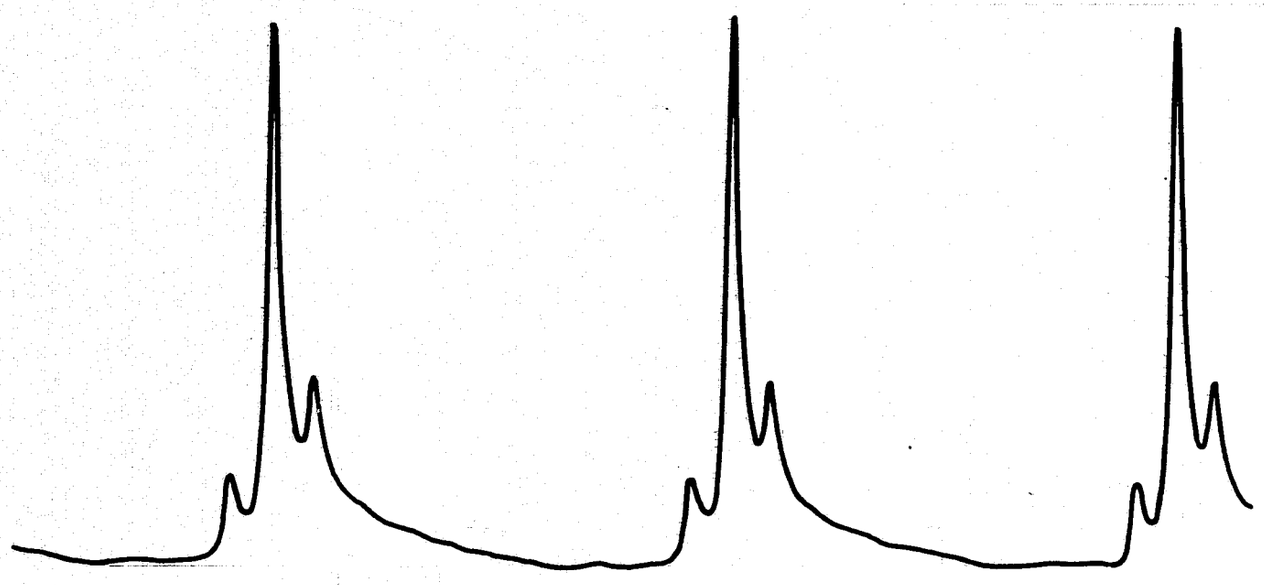

INJECTION MODULATION AT 660 MHz

FIGURE 4-6 (b)

(c)

L-23
T= 77°K
I= 248 mA
MODULATING VOLTAGE = 10mV

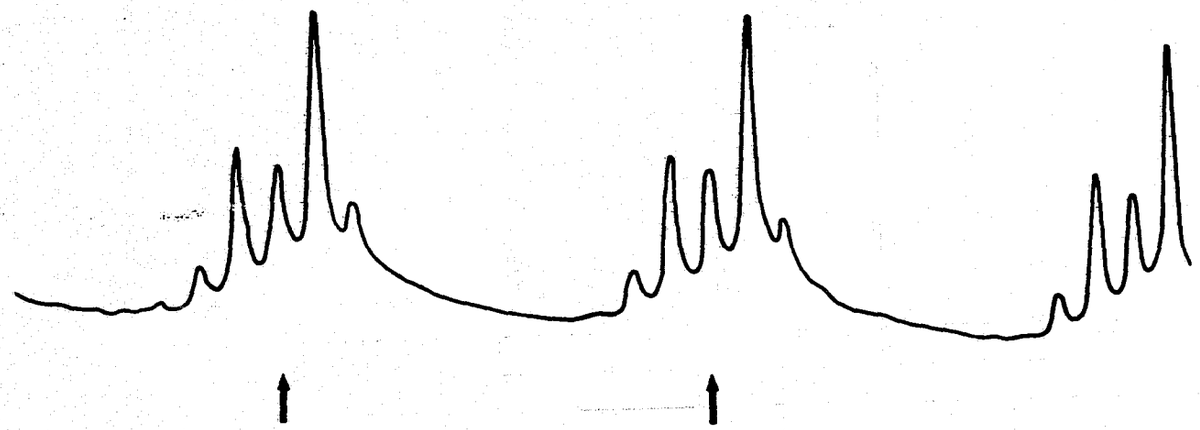

INJECTION MODULATION AT 660 MHz
FIGURE 4-6 (c)

(d)

L-23
T=77°K
I=298mA
MODULATING VOLTAGE = 14 mV

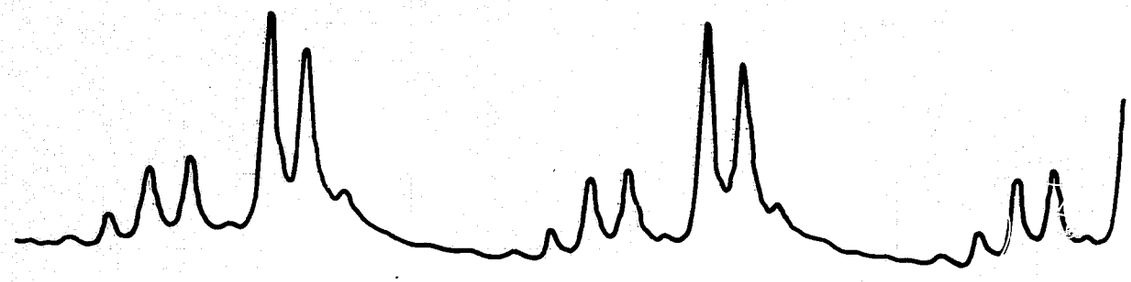

INJECTION MODULATION AT 660 MHz

FIGURE 4-6 (d)

(e)

L-2
T=77°K
I=298mA
MODULATING VOLTAGE=18mV

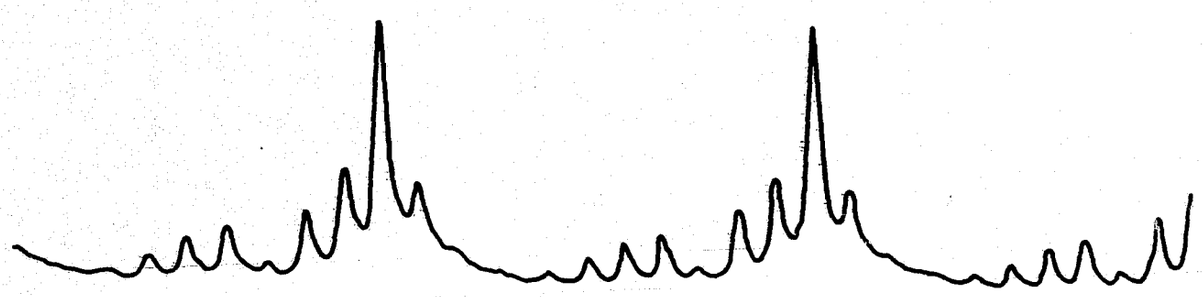

INJECTION MODULATION AT 660 MHz

FIGURE 4-6(e)

(a)

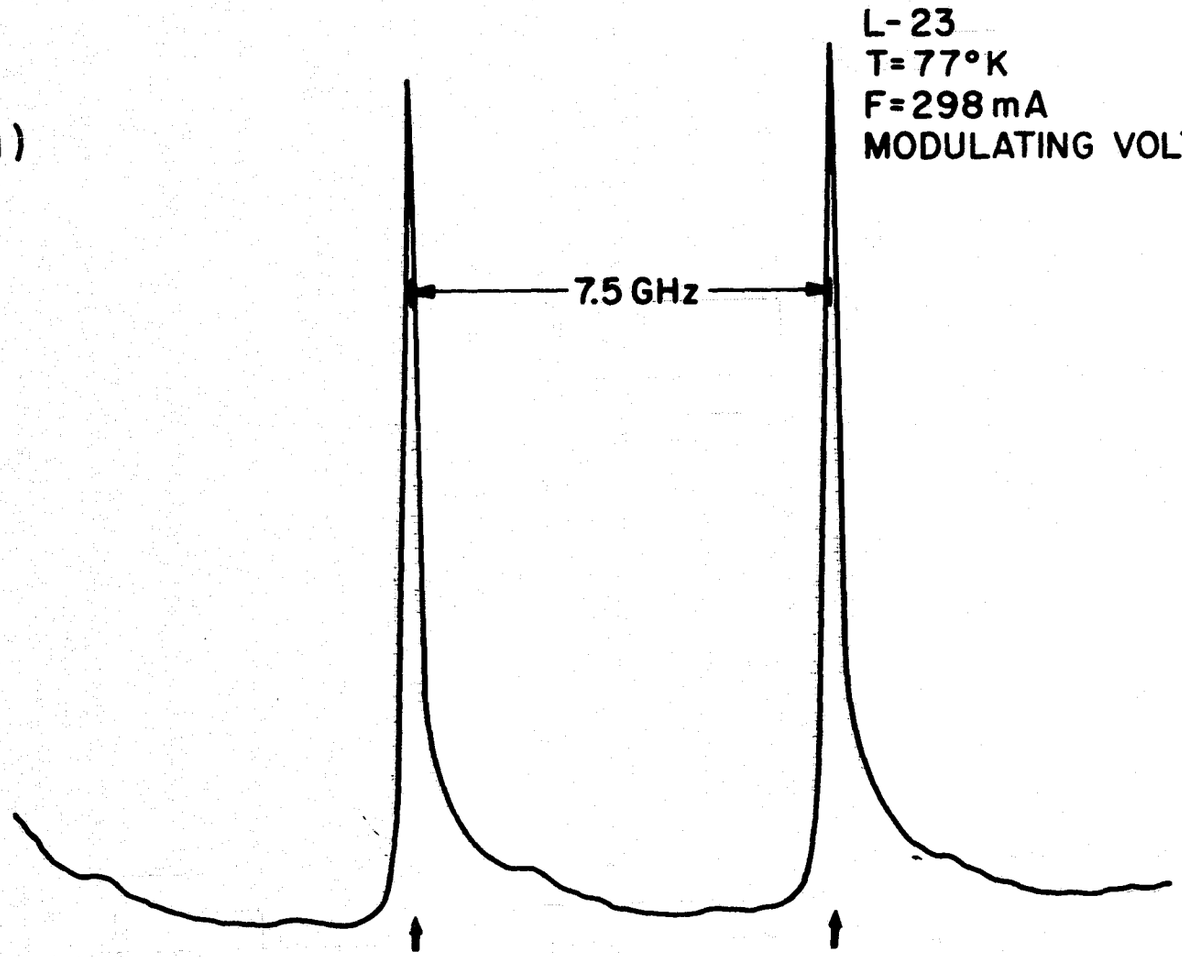

INJECTION MODULATION AT 990 MHz
FIGURE 4-7 (a)

(b)

L-23
T=77° K
I=298 mA
MODULATING VOLTAGE=15mV

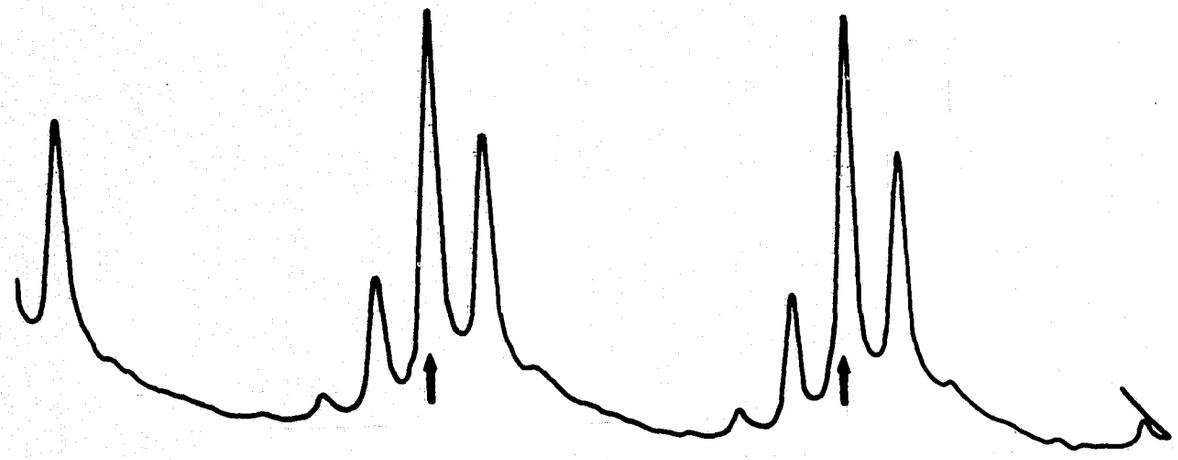

INJECTION MODULATION AT 990 MHz
FIGURE 4-7 (b)

L-2
T=77°K
F=298 mA
MODULATING VOLTAGE=20 mV

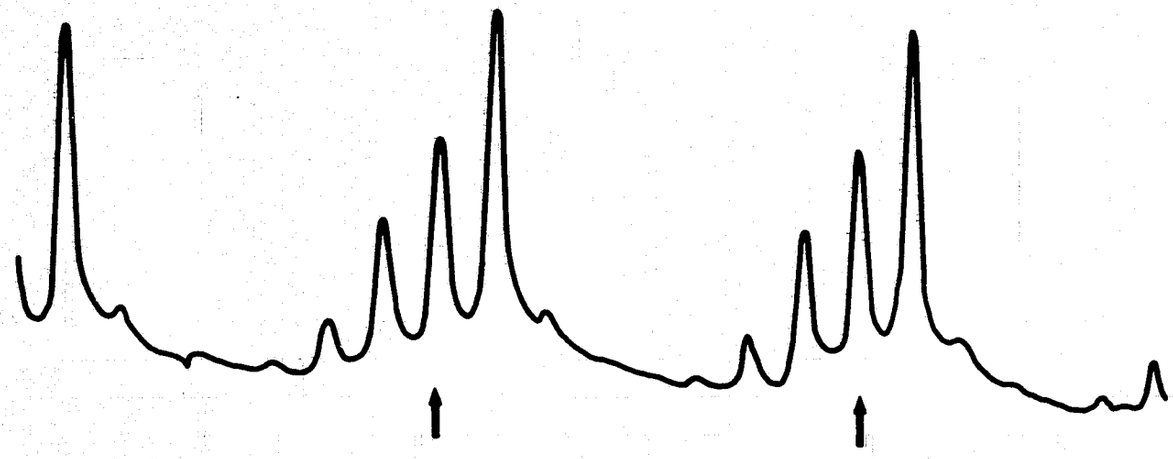

INJECTION MODULATION AT 990 MHz
FIGURE 4-7 (c)

(d)

L-23
T=77°K
I=298 mA
MODULATING VOLTAGE=30mV

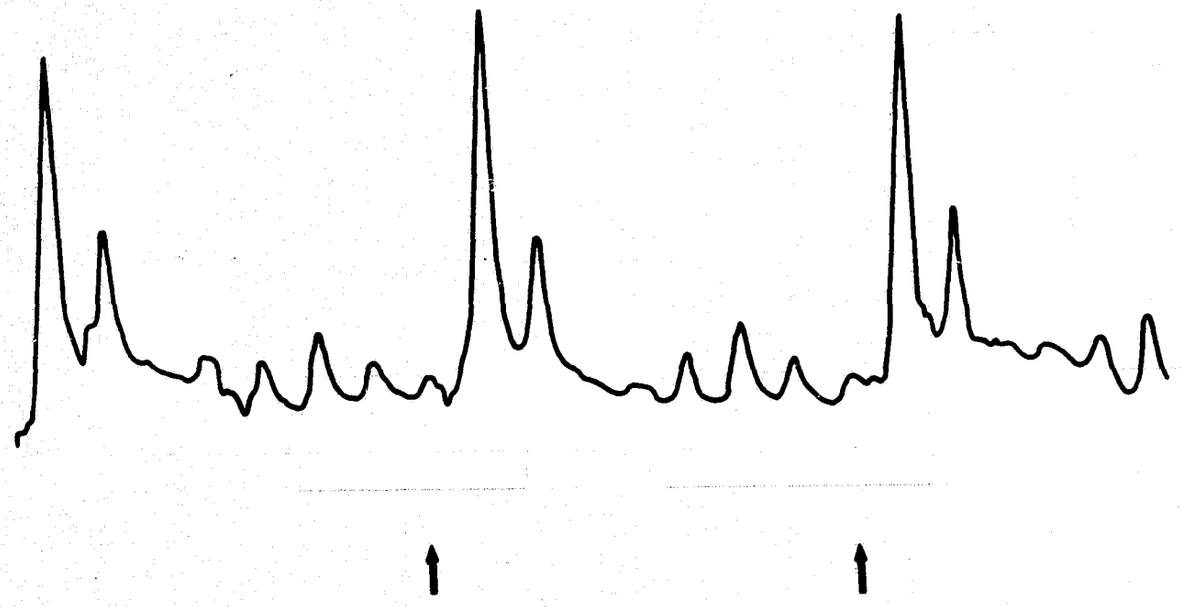

INJECTION MODULATION AT 990 MHz
FIGURE 4-7 (d)

is 7.5 GHz and frequency is decreasing to the right. Figures 4-3 through 4-7 are taken at the same injection current of 298 ma. The threshold current at 77°K was 250 ma. In figure 4-3, as in the others, it will be noticed that the low frequency sidebands are higher than the high frequency ones. This indicates that m_a and m_f, as written in 4-1, have the same sign. In these pictures, the modulation index varies from zero to about 150. Figures 4-4 represents similar scans as those of figure 4-3. The modulating voltages are the same as those in figure 4-3 but the frequency has been changed to 150 MHz. It can be seen that the frequency broadening is the same as that produced at 30 MHz at the same modulating voltage indicating that the modulating power in the sidebands is the same in both cases. However, in figure 4-4, some detail of the sideband pattern begins to appear. At a modulating frequency of 330 MHz, as shown in figure 4-5, the individual sidebands are fairly well resolved. The suppression of the carrier frequency can be seen in figure 4-5(c), while that of the first sidebands can be seen in figure 4-5(d). Figures 4-6 and 4-7 are similar traces taken at modulating frequencies of 660 MHz and 990 MHz respectively. All are at the same injection current. Figure 4-8 shows a plot of sideband intensity versus modulating voltage at 330 MHz. These sidebands correspond to $\lambda = 0.1$. Figures 4-9 and 4-10show similar graphs at 660 MHz and 990 MHz respectively. Agreement, at the higher power levels, between 4-6 and figs. 4-9 and 4-10 diverge. It is thought that the reason for this lies in the mode-locking phenomena reported in reference 1 at frequencies from 500 MHz to 3 GHz. This conclusion is substantiated by the observation that the sidebands broadened, as the modulating power level was increased, and eventually disappeared. The disappearance of the sidebands is caused by the coherence time of the mode-locked laser becoming shorter than the lifetime of a photon in the Fabry-Perot interferometer. Furthermore, this phenomena was observed at 660 MHz and 1 GHz whereas

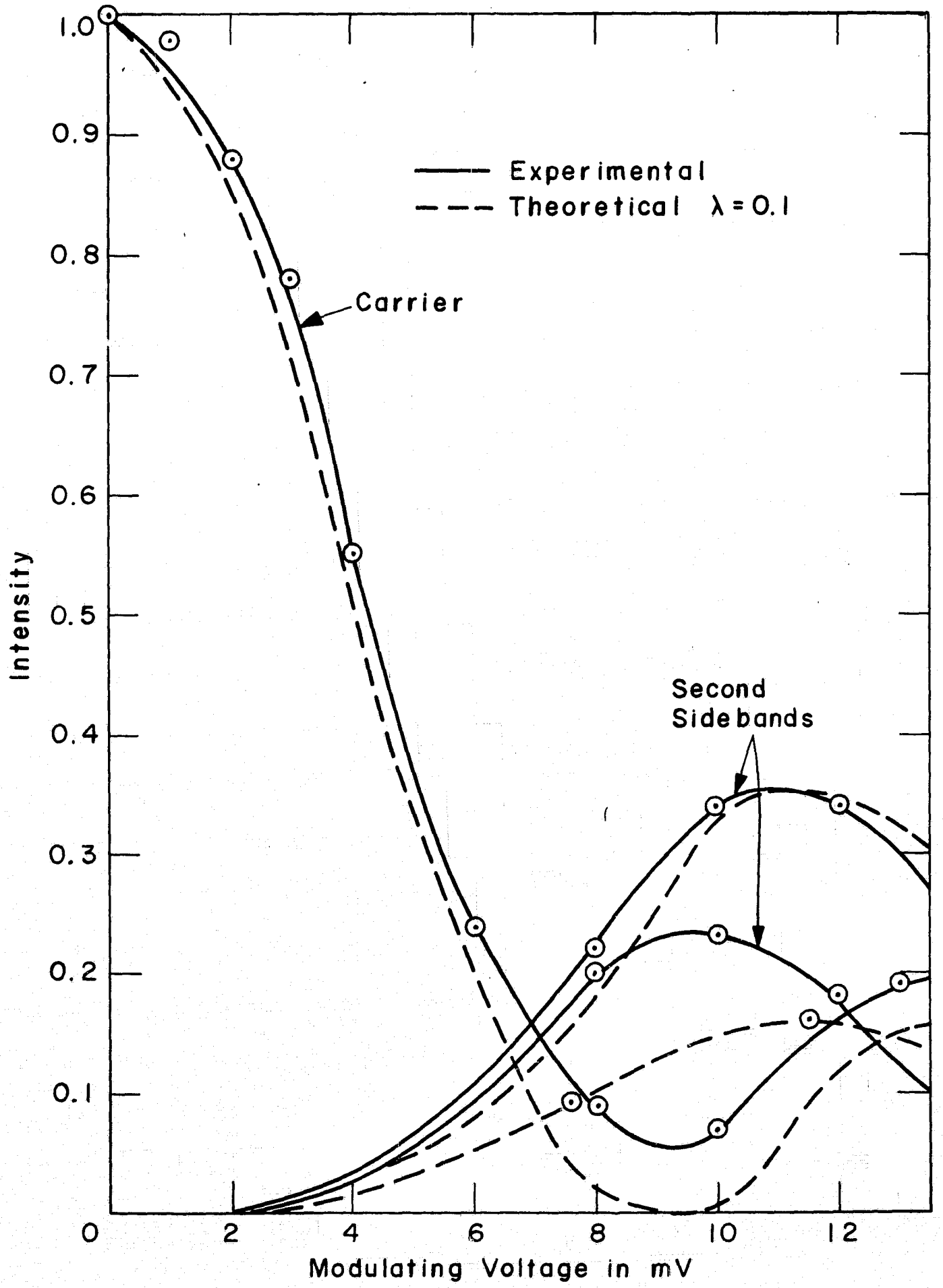

Figure 4-8 (a) Sideband Intensity vs Modulating Voltage at 330 MH_z

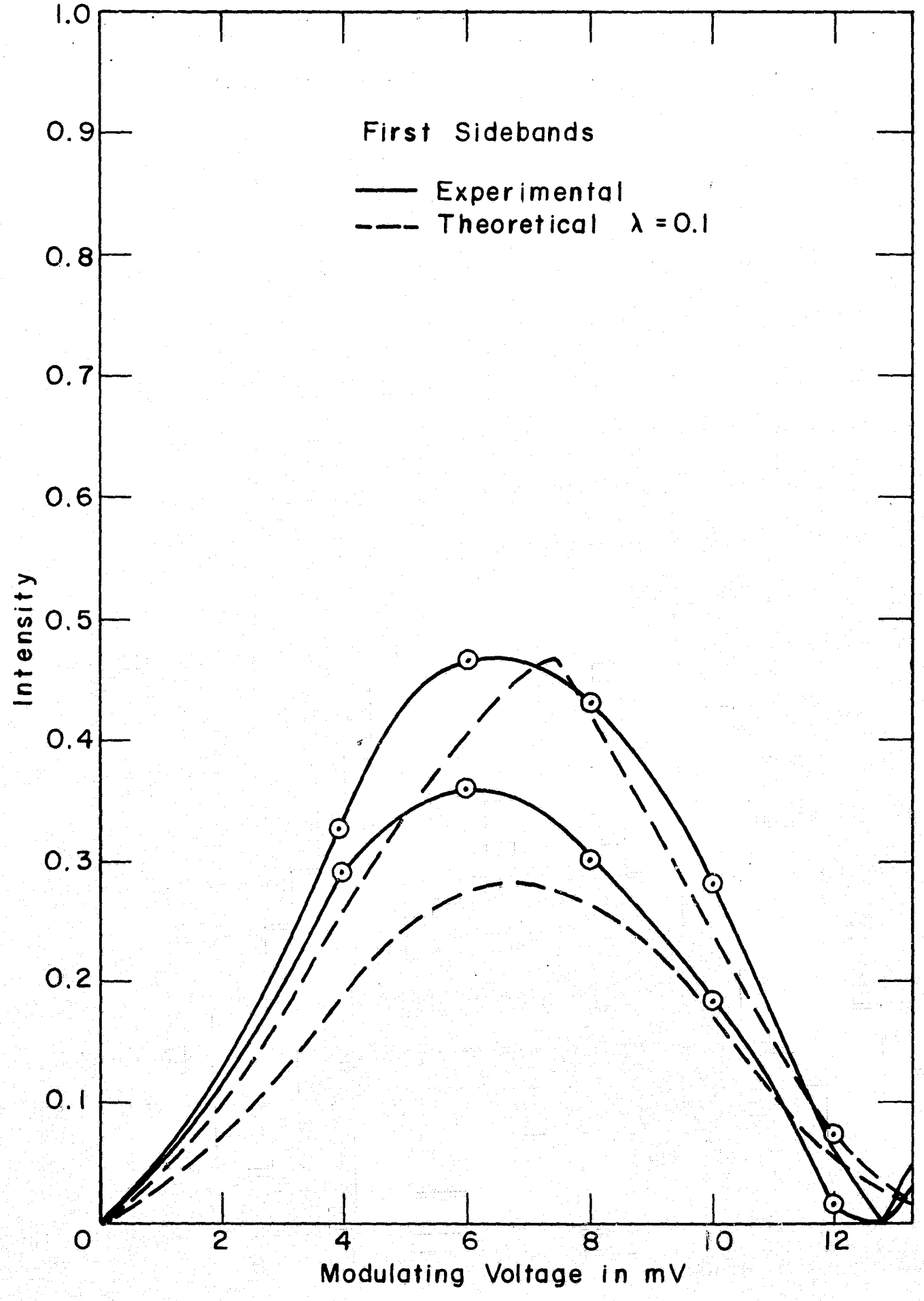

Figure 4-8(b) Sideband Intensity vs Modulating Voltage at 330 MHz

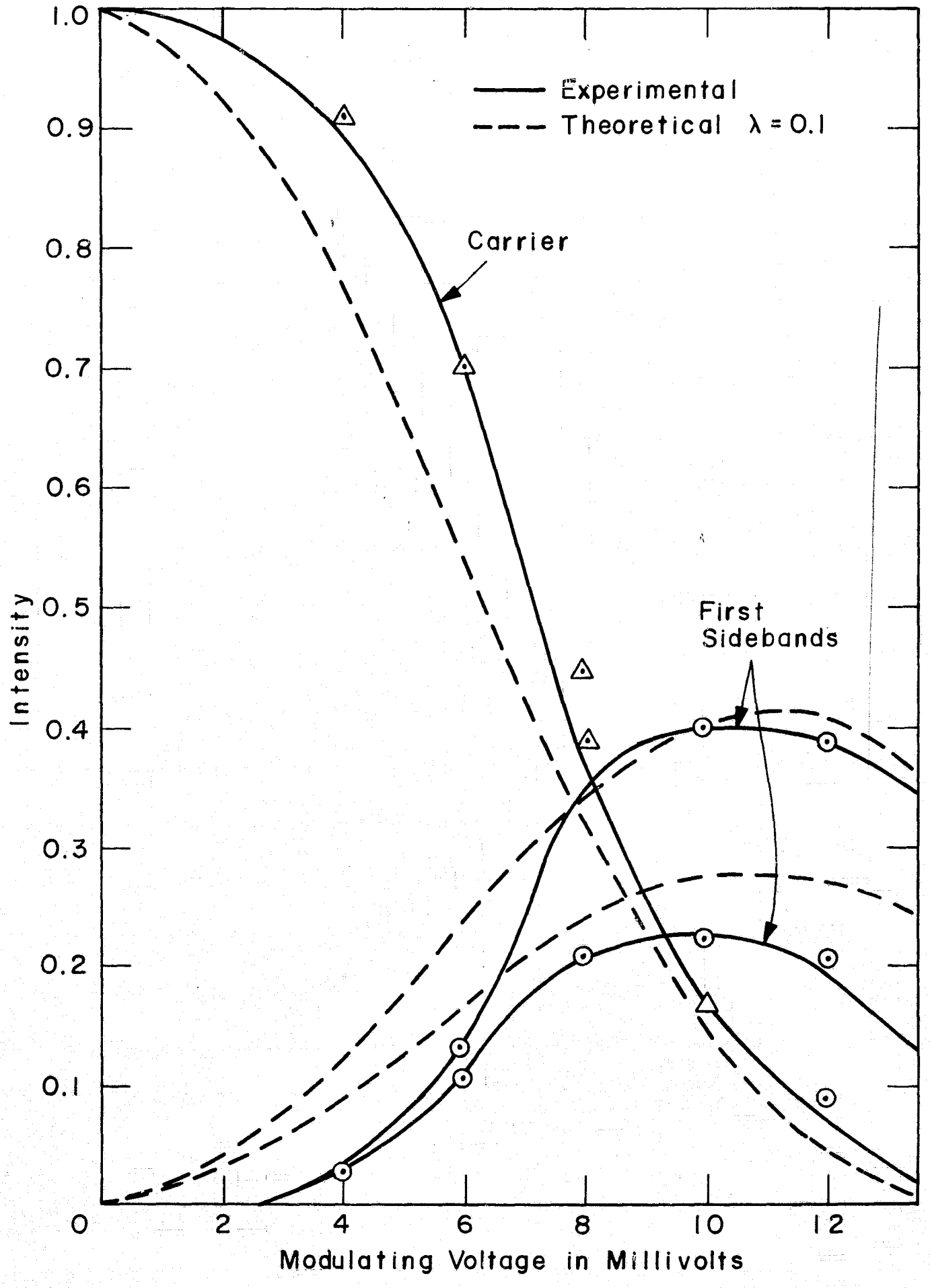

Figure 4-9 (a) Sideband Intensity vs Modulating Voltage at 660 MHz

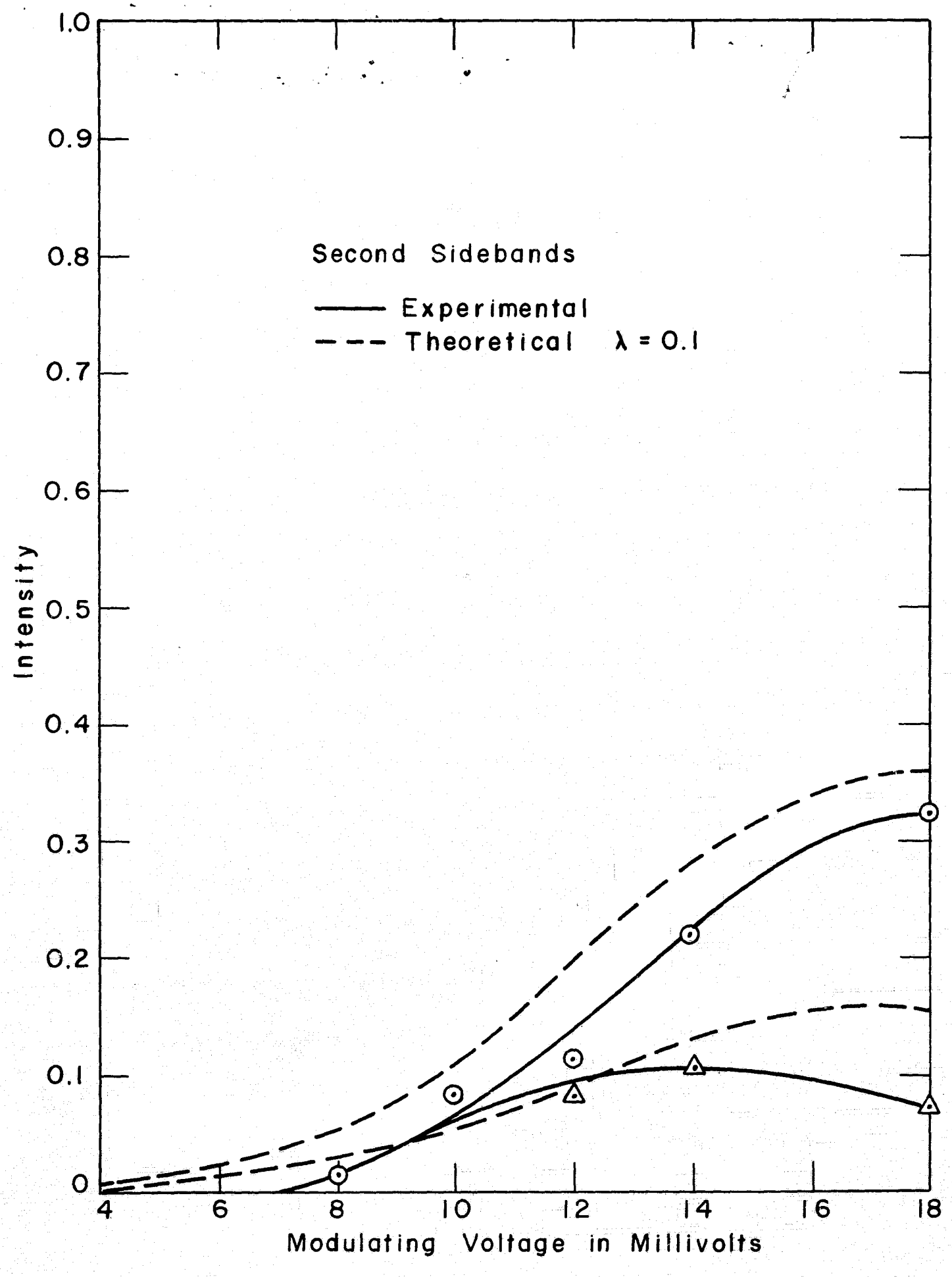

Figure 4-9(b) Sideband Intensity vs Modulating Voltage at 660 MH_z

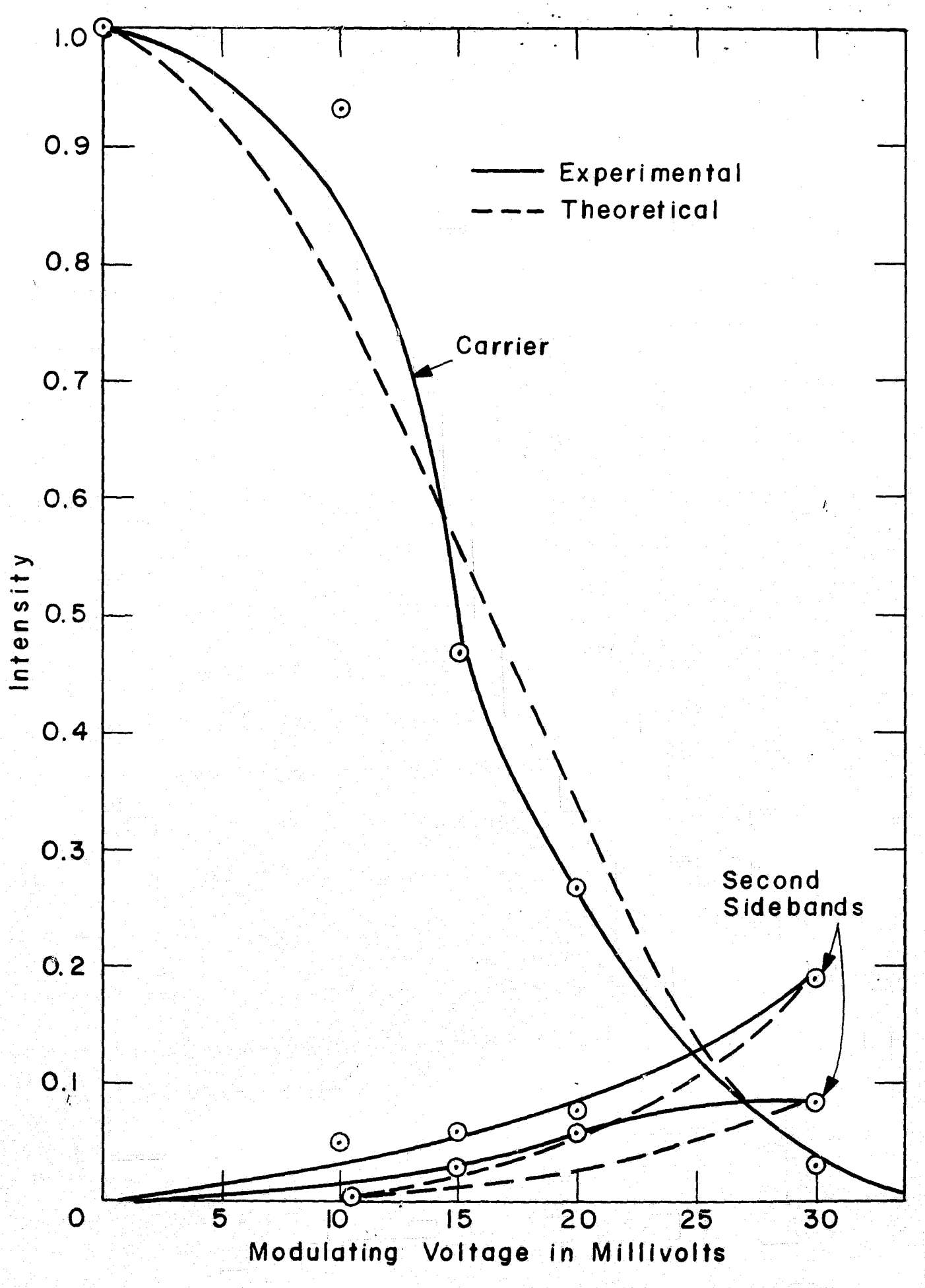

Figure 4-10(a) Sideband Intensity vs Modulating Voltage at 990 MM_z

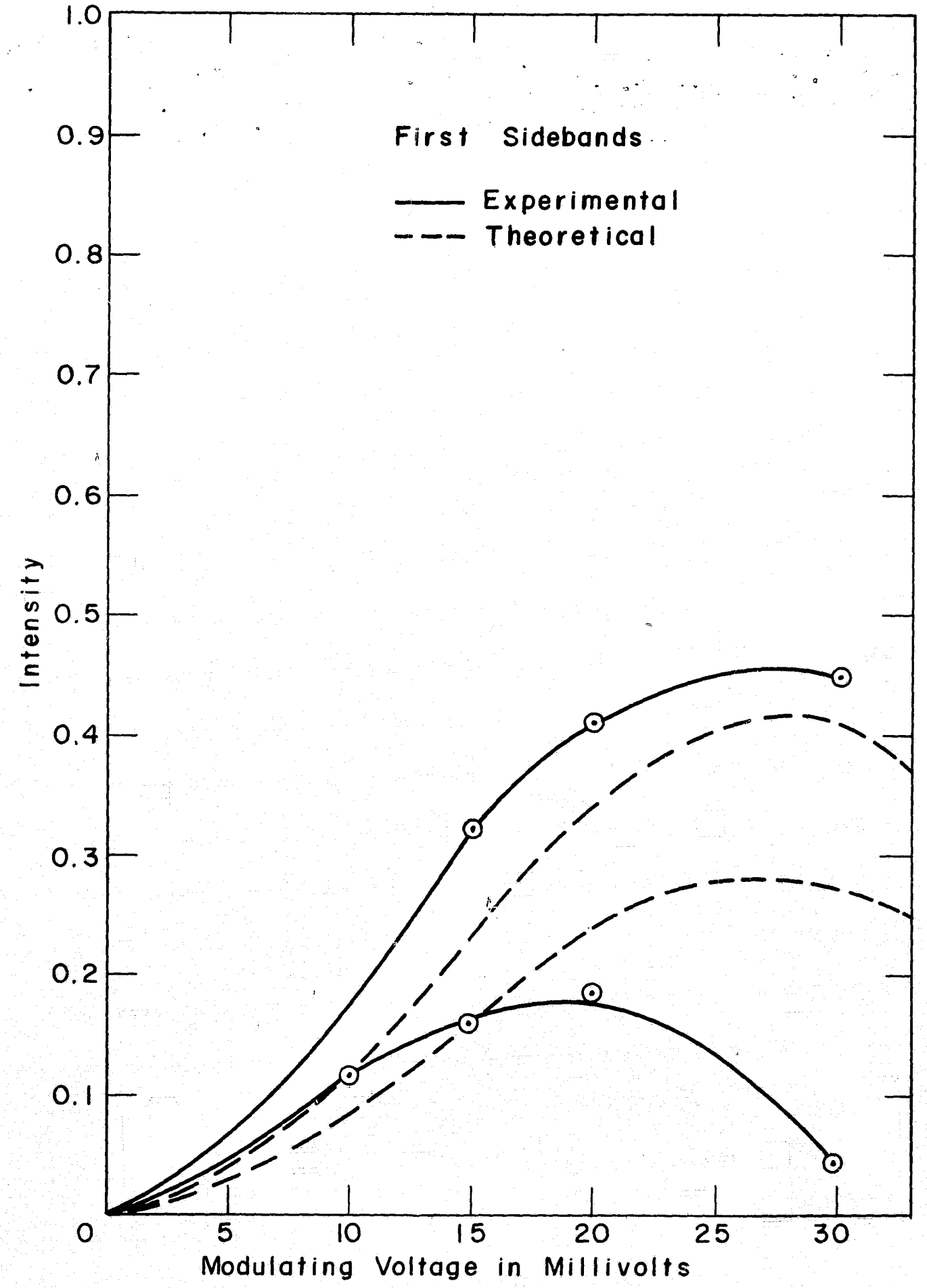

Figure 4-10 (b) Sideband Intensity vs Modulating Voltage at 990 MH_z

at 330 MHz and frequencies below, it was not. Figure 4-11 shows the manner in which the sidebands disappear at 660 MHz. In contrast, at 150 MHz, frequency deviations of 80 GHz were obtained without signs of mode-locking. In general, agreement was better for the low frequency sidebands than for the high frequency.

The deviation of 150 MHz was found to vary linearly with modulating voltage as shown in figure 4-12. Simultaneous measurement was made of the amplitude modulation, as described above, and a plot is shown in figure 4-13 of the photodiode voltage measured on a spectrum analyzer versus frequency deviation. It is seen to be super linear with frequency deviation. An exact measurement could not be made of the percentage of modulation to determine m_a since the photodiode also measured the modulation of the spontaneous emission and this could not be separated out from the laser mode without a spectrometer. Thus figure 4-13 shows a plot of the total light modulation, spontaneous and stimulated modulation, versus frequency deviation. Results obtained at 725 MHz show similar behavior.

Since $\frac{\partial \varepsilon}{\partial J} = -\frac{\varepsilon}{\nu}\frac{\partial \nu}{\partial J}$ and considering equation 2-127, m_a and m_f are expected to vary with bias point. Some experiments were thus performed to examine their behavior. First, the frequency of the unmodulated laser was plotted as a function of current. This was achieved by measuring the peak shift in the Fabry-Perot interferometer as the laser current was changed. Figure 4-14 shows the results of this observation. The breaks in the curve show where the laser jumped from one mode to another. The actual frequency shift at this point was an integral number of free spectral ranges (7.5 GHz) plus the apparent shift in the interferometer. Only the apparent shift is recorded here. In all, the laser passed through four modes as the current was changed from 280 ma to 420 ma. The initial decrease in laser frequency between 280 ma and 300 ma is not fully understood although the behavior was common to all lasers used. One explanation is that it is due to many-body

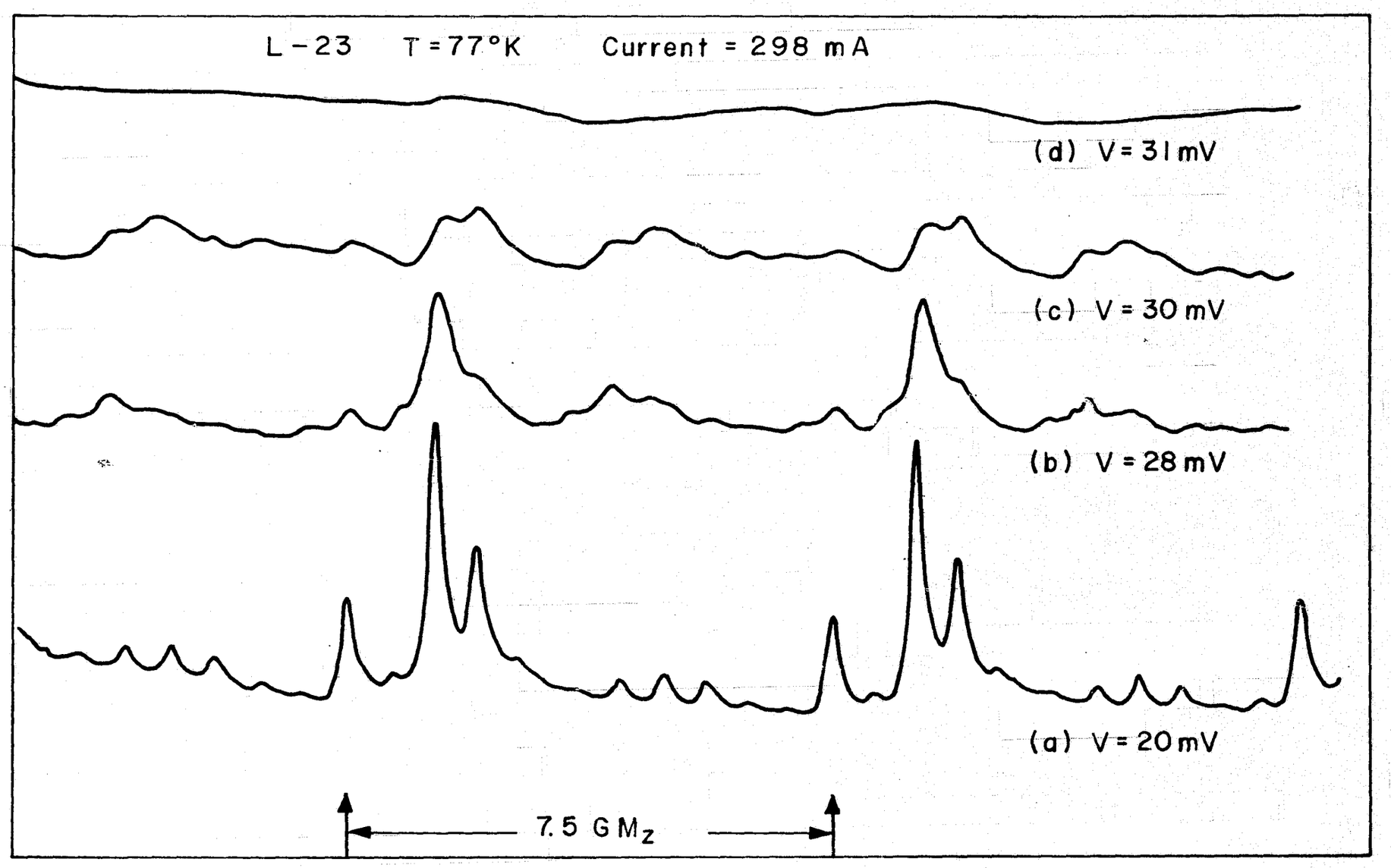

Figure 4-11 Disappearance of Interferometer Trace with Increasing Modulating Voltage at 660 MH_z

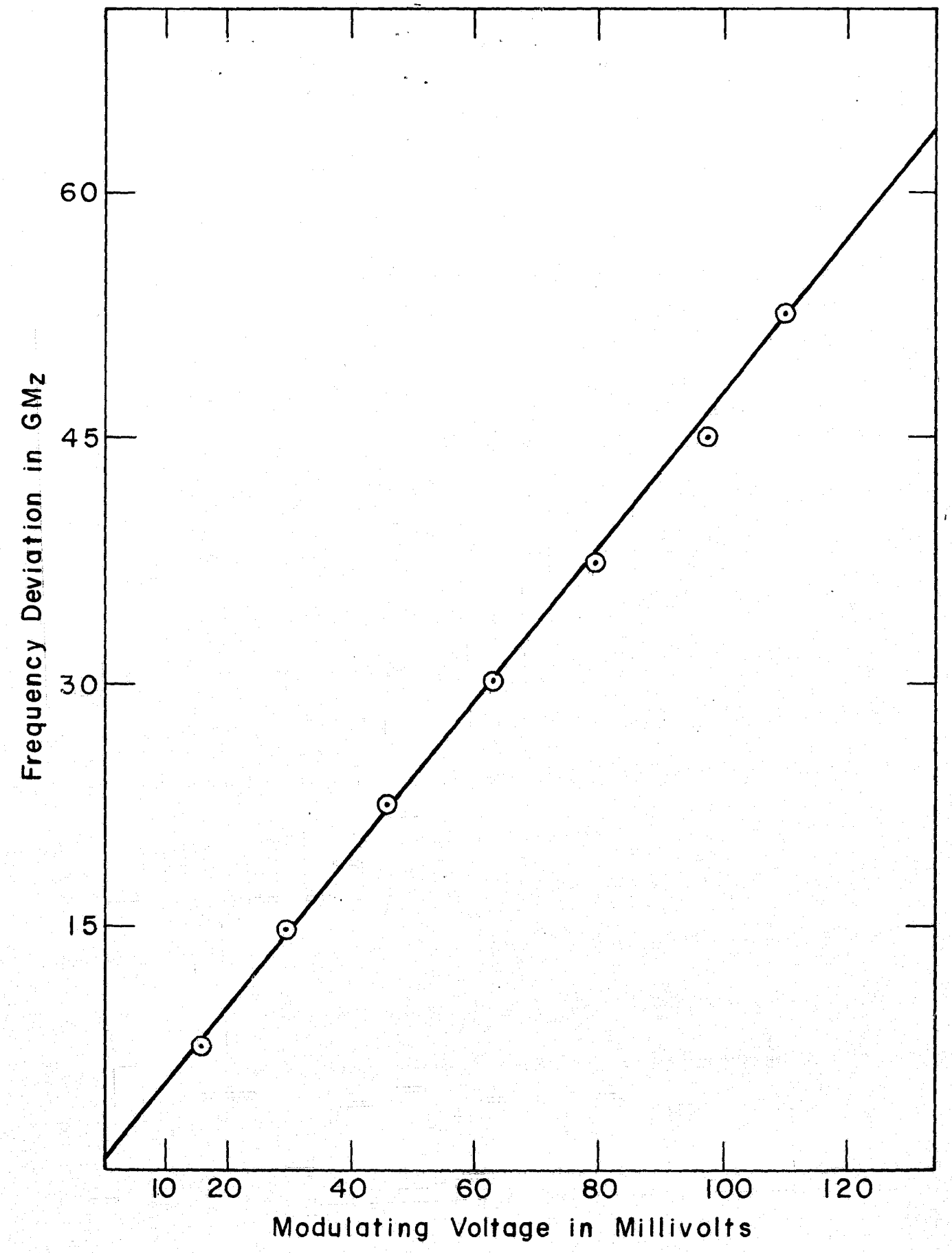

Figure 4-12 Frequency Deviation vs Modulating Voltage at 150 MM_Z.

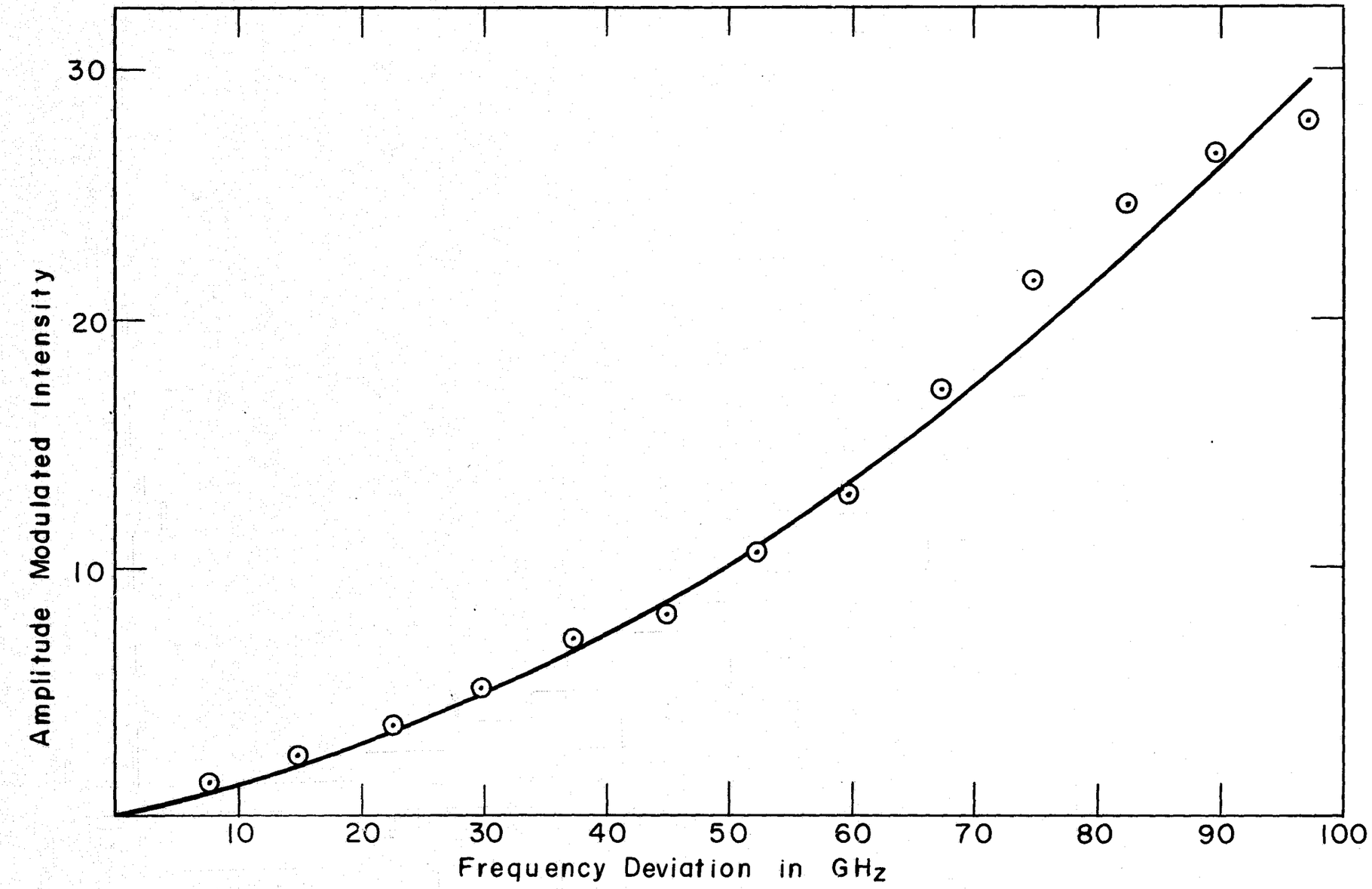

Figure 4-13 Component of the Amplitude Modulated Intensity at the Modulating Frequency vs Frequency Deviation

interactions as observed in reference 2. Basov et.al.[3] have proposed that screening of the crystal field by free carriers and interactions between the carriers reduce the effective energy gap. As the number of carriers is increased with injection, the reduction in the energy gap continues so that the total energy gap shift is excitation dependent. However, in Reference 1, no quenching of the short wavelength modes was noticed as the modes shifted to longer wavelength. In our case, however, the laser changed modes as the wavelength was increasing. Unfortunately, no means were available to measure whether the new mode was on the long or short wavelength side of the original mode.

Between 300 ma and 400 ma the laser frequency increased with current. This is to be expected from the change in gain with Fermi energy calculated in equation 2-127. The frequency decrease above 400 ma may be attributed to dominance of heating effects which tend to decrease the energy gap and hence the laser frequency.

Having obtained the plot shown in figure 4-14 for the unmodulated laser; the laser was operated at various currents from 280 ma to 400 ma and at each current position, fixed modulating voltages at 600 MHz applied to the laser. Spectral traces were then taken with the Fabry-Perot interferometer. These traces are shown in figure 4-15. An attempt was made to correlate this with the data of figure 4-14. However, since the decrease in frequency with current initially indicates that mechanisms were present which had not been accounted for in Chapter II, quantitative agreement was not expected. The qualitative effects were as follows: Mode #1 (see figure 4-15(a)), where the frequency decreased with injection, was easily modulated, with the modulation, for a given modulating power input, increasing with current. Mode #2 was harder to modulate than Mode #1 and near the termination point (about 315 ma) on Mode #3 the modulation produced was least. From there, on Mode #3

and Mode #4, the modulation increased roughly as the slope of the curve on figure 4-14 increased.

4. Conclusions

Modulation of the injection of a semiconductor laser was seen to produce both amplitude and frequency modulation as predicted in Chapter II. Furthermore, the asymmetry in the sideband pattern showed that m_a and m_f have the same sign and that the behavior of the sidebands may be explained with $m_a \approx 0.1\ m_f$. At frequencies above 660 MHz deviations in the behavior of the sidebands from that expected was attributed to a mode-locking phenomenon. Observations were also made of the change in the spectrum with bias point.

The initial decrease in laser frequency with laser current was tentatively attributed to many-body interactions. Further examination of this effect with a spectrometer and Fabry-Perot interferometer in tandem should help to elucidate the mechanism involved.

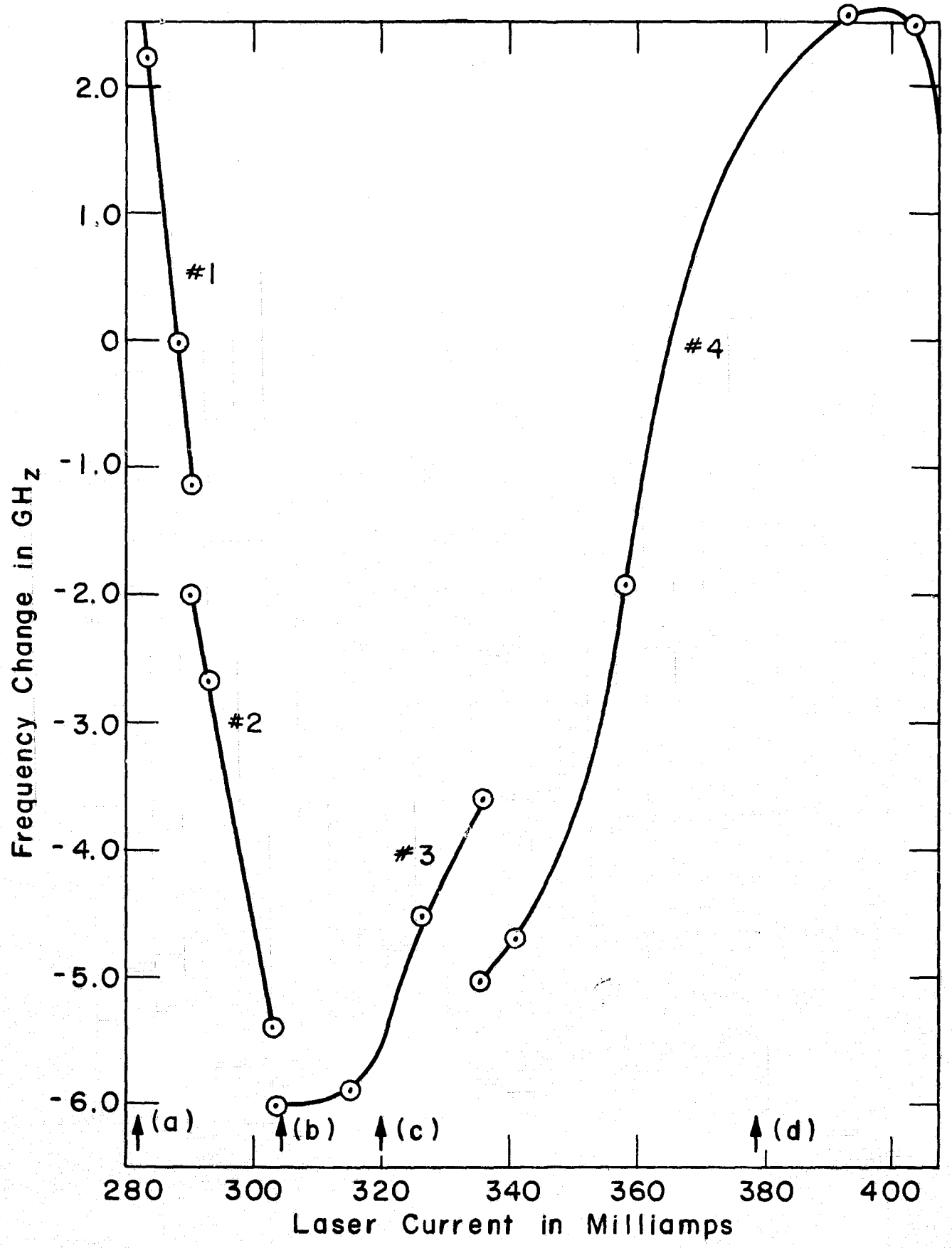

Figure 4-14 Frequency Change of Laser with Current

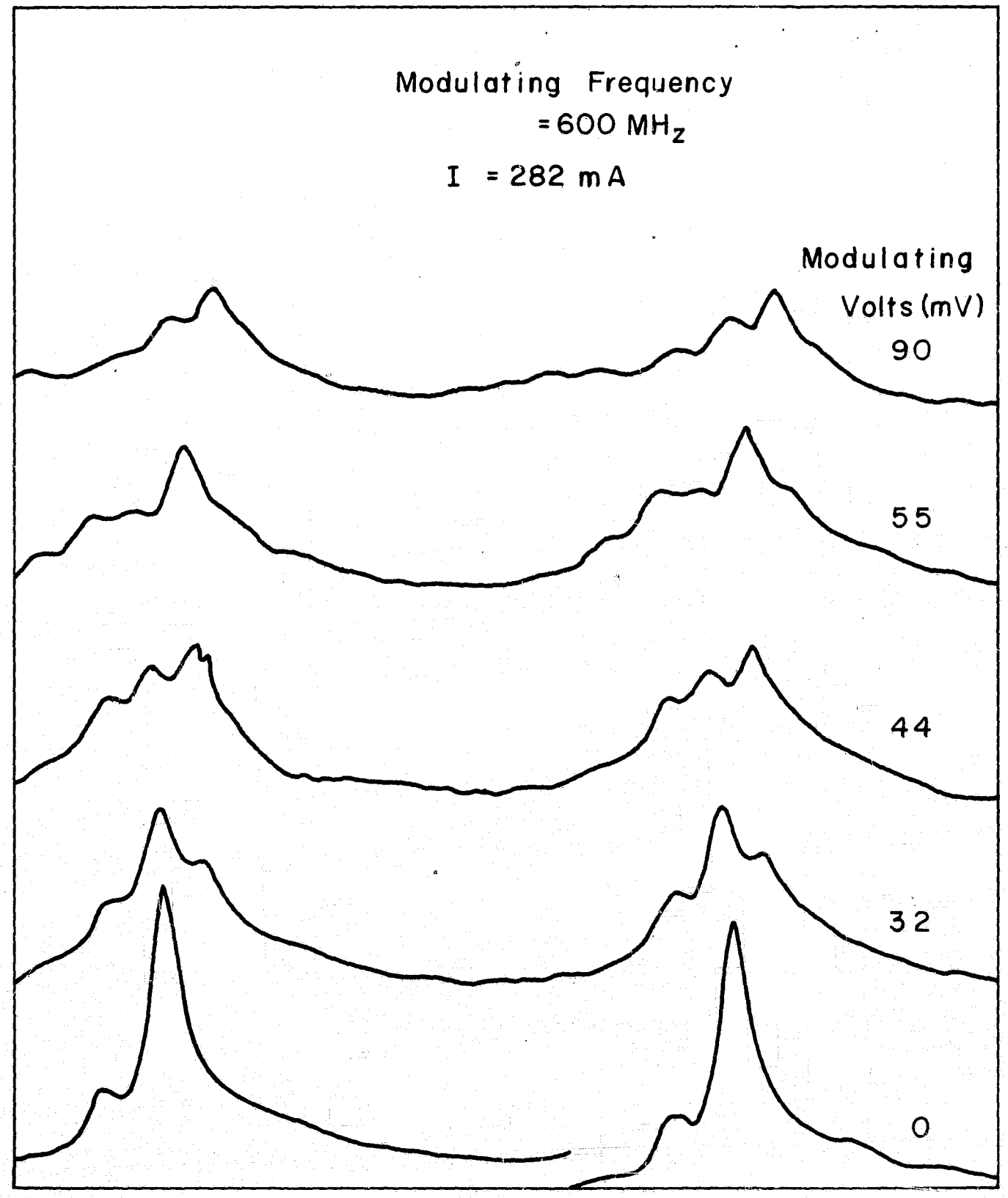

Figure 4-15(a) The Effect of Bias Point on the Spectrum of an Injection Modulated Laser

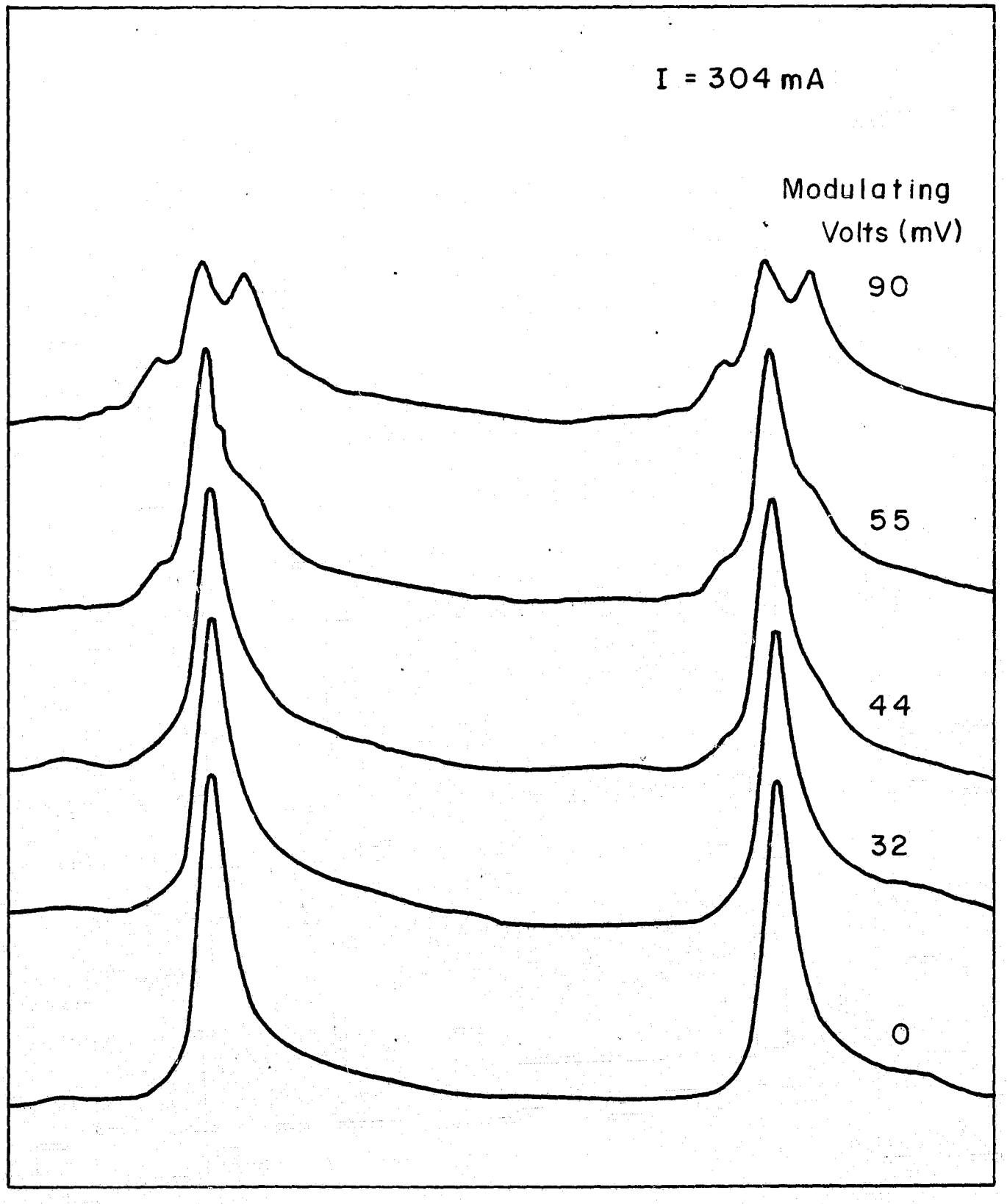

Figure 4-15 (b) The Effect of Bias Point on the Spectrum of an Injection Modulated Laser

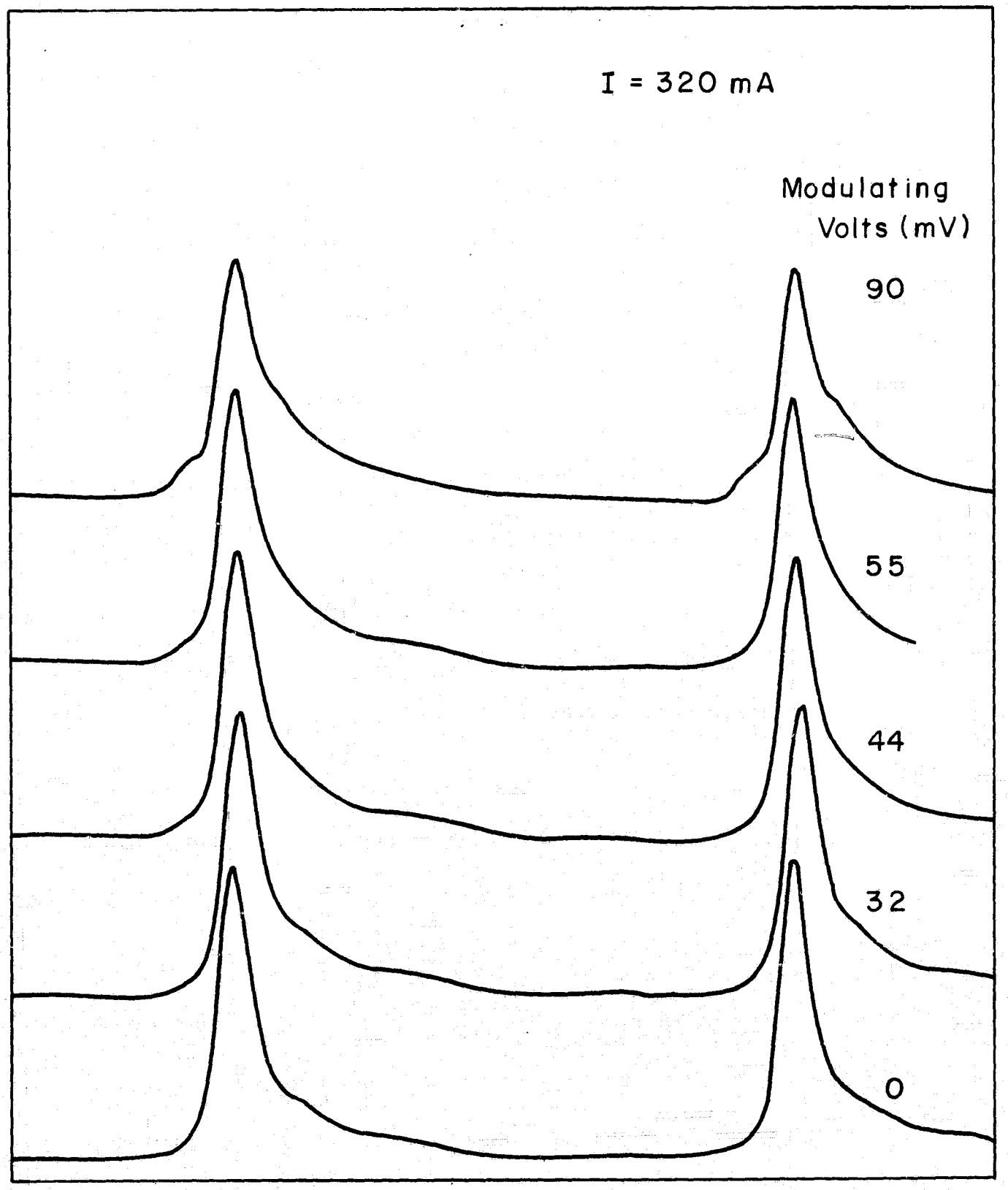

Figure 4-15 (c) The Effect of Bias Point on the Spectrum of an Injection Modulated Laser

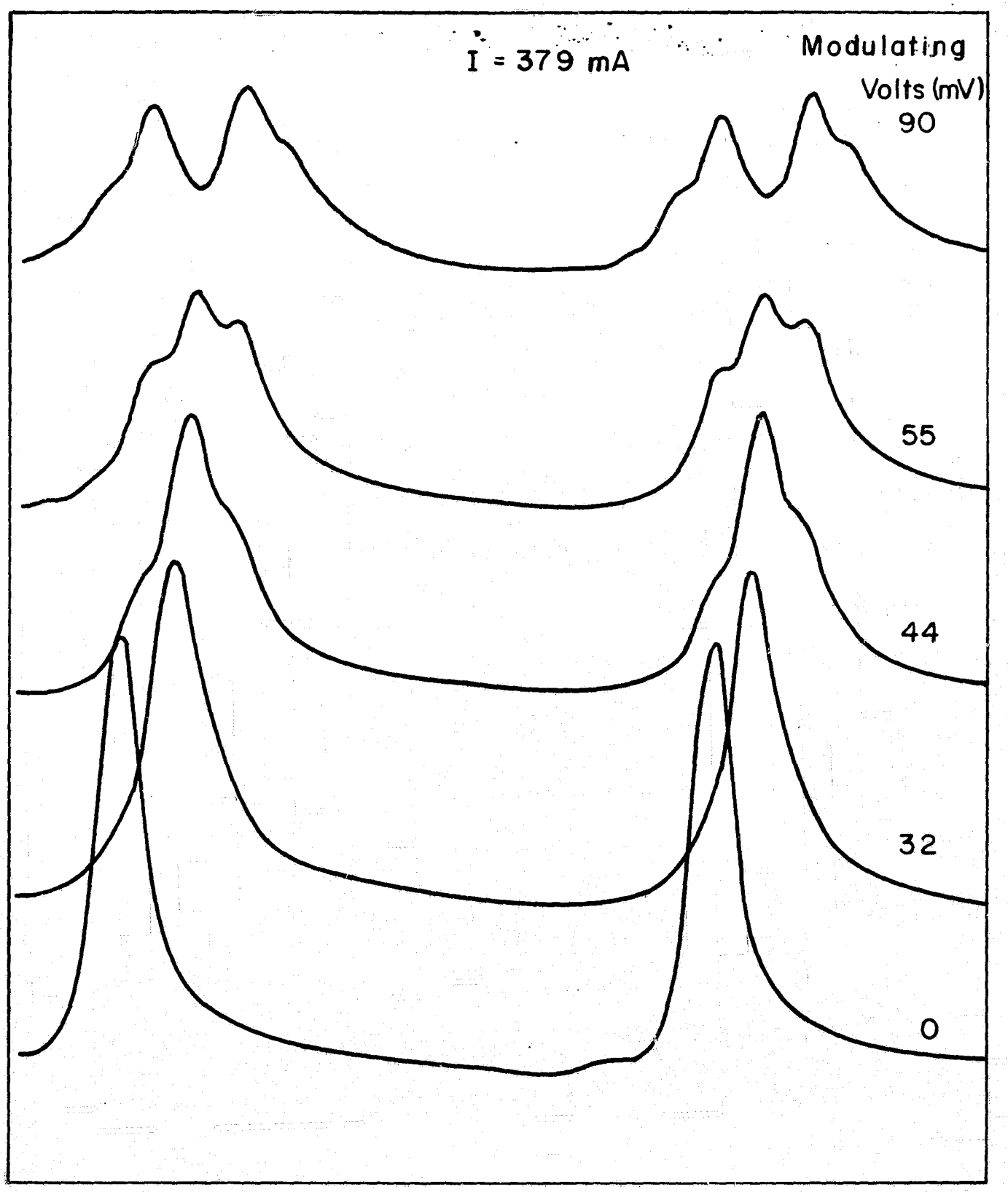

Figure 4-15 (d) The Effect of Bias Point on the Spectrum of an Injection Modulated Laser

References

1. T. L. Paoli and J. E. Ripper, Applied Physics Letters 15, 3, 105 (1 Aug. 1969).

2. M. R. Johnson and N. Holonyak, Jr., Journal of Applied Physics 39, 3, 3977 (July 1968).

3. N. G. Basov, O. V. Bogdankevich, V. A. Goncharov, B. M. Lavrushin, and V. Yu. Sudzilovskii, Soviet Physics-Doklady 11, 6, 522 (Dec. 1966).

CHAPTER FIVE

Spectral Shift Under Pulsed Emission

1. Introduction

One of the disadvantages associated with semiconductor lasers is the necessity of cooling in order to obtain cw operation. So far operation at room temperature has been possible only under pulsed conditions. Thus if a modulated semiconductor laser were to be used as a transmitter at room temperature, it would have to be operated in a pulsed condition. The frequency information would then have to be demodulated on a pulsed basis.

In order to ascertain the feasibility of demodulating such an optical signal, a high resolution study of the spectral shift under pulsed conditions was made. Previous measurements on the pulsed spectral shift of semiconductor lasers used spectrometers. The standard technique requires that the pulsed light be passed through the spectrometer and the behavior of the detected light pulse be watched as a function time during the pulse at different wavelengths. Usually, in order to obtain a large enough shift to be measured, the laser injection level must be high so that several modes of the laser may be oscillating simultaneously. The spectral shift must then be inferred from the enhancement of the long wavelength modes. The procedure is as follows: When the injection to a junction laser is pulsed, the temperature at the junction rises during the course of the pulse. This temperature rise causes a shift in the dielectric constant. Thus in order to maintain the resonance condition in the cavity, the laser frequency must follow the change in the dielectric constant. This it can do, since the gain profile of semiconductor lasers is broad. In gallium arsenide the laser frequency decreases with temperature. Thus when a GaAs laser is pulsed the frequency will be decreasing with time. Suppose this light is passed through a Fabry-Perot interferometer. The interferometer has a transfer

function

$$h(\nu) = \frac{1}{1+\left[\frac{2F}{\pi}\sin\pi\frac{\nu}{f}\cos\theta\right]^2} \qquad 5\text{-}1$$

F = Finesse
f = Free Spectral Range
ν = Frequency
θ = Incident Angle

For F large, this consists of a series of peaks separated by a distance f in frequency. Thus as the laser frequency decreases, the output of the interferometer will consist of a series of peaks, occurring every time

$$\nu(t) = m f \qquad \text{for } \theta = 0 \qquad m = \text{integer} \qquad 5\text{-}2$$

Thus by counting the peaks the total frequency shift during the pulse may be determined. By observing the position in time at which the peaks occur, the instantaneous frequency can be seen and thus the change in dielectric constant with time may be calculated. Furthermore, a continuous plot of frequency change versus time may be obtained by scanning the interferometer. Suppose one mirror is mounted on a piezoelectric slab, then by applying a d.c. voltage to the slab we can change the position of the resonance frequency

$$f = \frac{c}{4nR} \qquad 5\text{-}3$$

c = velocity of light
n = dielectric constant
R = distance between mirrors

This formula applies for spherical Fabry-Perot interferometer. Application of a d.c. voltage causes a shift in R such that $\Delta R/R \ll 1$

$$f' = \frac{c}{4n(R+\Delta R)} \qquad 5\text{-}4$$

$$f' \approx f - \frac{\Delta R}{R} f \qquad 5\text{-}5$$

$$f' \approx f \qquad 5\text{-}6$$

For resonance now

$$\nu'(t) = m f' \qquad 5\text{-}7$$

$$\nu'(t) = mf - \frac{\Delta R}{R} mf \qquad 5\text{-}8\ (a)$$

$$\text{or} \quad \nu(t) - \Delta\nu = mf - \frac{\Delta R}{R} mf \qquad 5\text{-}8\ (b)$$

thus although the distance between peaks remains constant, the position of the peaks will shift since m>>1. Furthermore, by changing the applied dc voltage and noting the direction of the peak shift, we can also tell whether the frequency increases or decreases with time.

2. Temperature Rise at the Junction Under Pulsed Injection

In order to calculate the temperature rise at the junction and correlate it with the deserved spectral shift, three models of heat folow in the laser are considered along with their applicability to the case at hand. The three models considered are (a) linear flow of heat from the junction to the laser surface which is maintained at the heat sink temperature[1], (b) linear flow in a semi-infinite medium[2], and (c) flow from a spherical heat source[3].

(a) Linear Flow of Heat from the Junction to the Laser Surface Which is Maintained at the Heat Sink Temperature

Consider a gallium arsenide injection laser soldered onto a heat sink at x=0. The p-n junction lies in the plane $x=\ell$ with the p-side adjacent to the heat sink. Current flows into the laser at the end x=L via a thin wire and out at x=0. The temperature rise ΔT at the junction $x=\ell$ must be calculated while a pulse of current (I) is passed throug the laser. It is assumed that the end of the laser x=0 is maintained at the temperature T_B of the heat sink. In practice, however, there will always be a temperature drop across the solder layer between the laser and heat sink. For cw operation, thermal gradients in the solder layer are important. However, under pulsed operation, these gradients are unimportant provided the solder layer is either thin or several diffusion lengths away, the diffusion length being the distance heat travels during the pulse. For short pulses and most junction depths, the second condition is often

satisfied. For the lasers used in this experiment, $\ell=2.5\mu$. At 77°K the diffusion length for a 1 μsec pulse is 17μ so this second condition was not satisfied, and it was found that the observed spectral shift was due to thermal gradients in the solder layer since this was also fairly thick. Heat is generated in the laser in three ways. First there is the heat generated at the junction due to the quantum efficiency of the recombination process being less than one. Secondly there is the heating associated with the bulk resistance of the laser and thermally that due to contact resistance and the temperature rise of the heat sink. At the low current densities used, bulk heating may be neglected. Since the rate of heating produced is

$$Q_{bulk} = I^2 R_b \qquad R_b \approx 0.14\ \Omega \quad 5\text{-}9$$

$$= 0.14 \text{ watts} \qquad I = 1 \text{amp} \quad 5\text{-}10$$

while that produced at the junction is

$$Q_j \approx IV = 1.5 \text{ watts} \qquad I = 1 \text{amp} \quad 5\text{-}11$$

At high current densities, however, the bulk heating cannot be neglected. Neglecting the contact resistance and the temperature rise of the heat sink for the moment, the only source of heat left is that produced at the junction. The temperature rise in the heat sink and solder layer are calculated later and used as boundary conditions instead of equation 5-13. Since, experimentally, a small temperature rise in the junction was observed, it is assumed that the thermal conductivity k_p specific heat C and hence $D = k_p/C$ the diffusion constant are constant throughout the pulse at any heat sink temperature.

It is assumed that the heat flows linearly through the laser into the heat sink. The equation to be solved is this

$$k_p \frac{\partial^2 \Delta T}{\partial x^2} - C \frac{\partial \Delta T}{\partial t} = -J \qquad 5\text{-}12$$

where J is the bulk heating and will be neglected. The boundary conditions are

$$\Delta T = 0 \qquad \text{at } x=0 \quad \text{for all } t \qquad 5\text{-}13$$

$$\Delta T = 0 \qquad \text{for all } x \quad \text{for } t<0 \qquad 5\text{-}14$$

and

$$k_p \left.\frac{\partial \Delta T}{\partial x}\right|_{x=\ell} = \frac{Q}{A} \qquad \begin{matrix} Q = \text{rate of heating} \\ A = \text{junction area} \end{matrix} \qquad 5\text{-}15$$

which accounts for junction heating. Neglecting J we have for the temperature rise $\Delta T = T - T_B$

$$\frac{\partial^2 \Delta T}{\partial x^2} = \frac{1}{D}\frac{\partial \Delta T}{\partial t} \qquad 5\text{-}16$$

If we assume $\Delta T = \Theta(t)X(x)$, then we may write

$$\frac{1}{X(x)}\frac{\partial^2 X(x)}{\partial x^2} = \frac{1}{D\,\Theta(t)}\frac{\partial \Theta(t)}{\partial t} = -\alpha \qquad 5\text{-}17$$

where α is a constant

$$\therefore \quad \Theta(t) = e^{-D\alpha t} \qquad \text{for } \alpha \neq 0 \qquad 5\text{-}18$$

and

$$\Theta(t) = 1 \qquad \text{for } \alpha = 0 \qquad 5\text{-}19$$

Solving for X

$$\frac{\partial^2 X(x)}{\partial x^2} + \alpha X(x) = 0 \qquad 5\text{-}20$$

$$\therefore \quad X(x) = \begin{cases} A_\alpha e^{i\sqrt{\alpha}x} + B_\alpha e^{-i\sqrt{\alpha}x} & \text{for } \alpha \neq 0 \\ A_1 x + A_2 & \text{for } \alpha = 0 \end{cases} \qquad 5\text{-}21$$

$$\therefore \quad \Delta T = A_1 x + A_2 + \sum_\alpha e^{-D\alpha t}\left(A_\alpha e^{i\sqrt{\alpha}x} + B_\alpha e^{-i\sqrt{\alpha}x}\right) \qquad 5\text{-}22$$

To determine the unknown constants the boundary conditions 5-13 and 5-15 may be used. 5-13 gives

$$A_2 = 0 \qquad 5-23$$

and

$$A_\alpha + B_\alpha = 0 \qquad 5-24$$

From 5-15

$$k_p A_1 + \sum_\alpha 2i\, A_\alpha \sqrt{\alpha}\, \cos(\sqrt{\alpha}\, l)\, e^{-D\alpha t} = \frac{q}{A} \qquad 5-25$$

$$\therefore \quad A_1 = \frac{q}{A k_p} \qquad 5-26$$

$$\cos(\sqrt{\alpha}\, l) = 0 \qquad 5-27$$

$$\sqrt{\alpha} = \frac{2n+1}{2}\,\frac{\pi}{l} \qquad 5-28$$

$$\therefore \quad \Delta T = \frac{q x}{A k_p} + \sum_{\substack{n=-\infty \\ n\neq 0}}^{\infty} \gamma_n \sin\frac{(2n+1)\pi x}{2l}\, e^{-\frac{(2n+1)^2}{4}\frac{\pi^2}{l^2} D t} \qquad 5-29$$

finally at t=o and for all x, $\Delta T = 0$

$$0 = \frac{q x}{A k_p} + \sum_{\substack{n=-\infty \\ n\neq 0}}^{\infty} \gamma_n \sin\left(\frac{2n+1}{2}\,\frac{\pi x}{l}\right) \qquad 5-30$$

$$\therefore \quad \gamma_n = -\frac{4l}{\pi^2}\,\frac{(-1)^n}{(2n+1)^2}\,\frac{q}{A k_p} \qquad 5-31$$

$$\therefore \quad \Delta T = \frac{q l}{A k_p}\left[\frac{x}{l} - \frac{8}{\pi^2}\sum_{n=1}^{\infty}\frac{(-1)^n}{(2n+1)^2}\sin\frac{(2n+1)\pi x}{2l}\, e^{-\frac{(2n+1)^2\pi^2}{4l^2} D t}\right] \qquad 5-32$$

at the junction x=ℓ we have

$$\Delta T(\ell,t) = \frac{Q\ell}{A k_p}\left[1 - \frac{8}{\pi^2}\sum_{n=1}^{\infty}\frac{e^{-\frac{(2n+1)^2\pi^2 Dt}{4\ell^2}}}{(2n+1)^2}\right] \qquad 5\text{-}33$$

This form of the solution is useful for long times, i.e. $Dt \geq \ell^2$. An equivalent solution may be obtained which is useful for short times by using Laplace transforms

$$\Delta T(x,t) = \frac{2Q}{A k_p}(Dt)^{1/2}\left[\sum_{n=0}^{\infty}(-1)^n\left(i\,\mathrm{erfc}\frac{(2n+1)(\ell-x)}{2(Dt)^{1/2}} - i\,\mathrm{erfc}\frac{(2n+1)(\ell+x)}{2(Dt)^{1/2}}\right)\right] \qquad 5\text{-}34$$

at the junction x=ℓ this reduces to

$$\Delta T(\ell,t) = \frac{2Q}{A k_p}\left(\frac{Dt}{\pi}\right)^{\frac{1}{2}}\left[1 + 2\pi^{\frac{1}{2}}\sum_{n=1}^{\infty}(-1)^n\,\mathrm{ierfc}\frac{n\ell}{(Dt)^{1/2}}\right] \qquad 5\text{-}35$$

for short times such that $(Dt)^{1/2} < \ell$

$$\Delta T(\ell,t) = \frac{2Q}{A k_p}\left(\frac{Dt}{\pi}\right)^{\frac{1}{2}} \qquad 5\text{-}36$$

While from 5-33 for long times such that $(Dt)^{1/2} > \ell$

$$\Delta T_{\infty}(\ell,t) = \frac{Q\ell}{A k_p} \qquad 5\text{-}37$$

This is the maximum temperature rise at the junction during the pulse.

(b) Linear Flow in a Semi-infinite Medium

In this model it is assumed that heat is generated at the junction and flows linearly into a semi-infinite medium. This situation corresponds to the case where the junction is far from the heat sink and the pulse time $t << \frac{\ell^2}{D}$. In this case heat does not reach the boundary so that the model should give good agreement for short times. The problem now reduces to solving

with

$$\frac{Q_o}{A} = k \left.\frac{\partial \Delta T}{\partial x}\right|_{x=\ell} \qquad 5-39$$

note that the heat flow

$$\frac{Q}{A} = k \left.\frac{\partial \Delta T}{\partial x}\right|_{x} \qquad 5-40$$

also satisfies 5-38 with $Q=Q_o$ at $x=\ell$. The solution of 5-38 for Q gives

$$\frac{Q}{A} = \frac{Q_o}{A} \operatorname{erfc} \frac{(x-\ell)}{2(Dt)^{1/2}} \qquad 5-41$$

$$\therefore \quad \Delta T = \frac{Q_o}{kA} \int_{x-\ell}^{\infty} \operatorname{erfc} \frac{(x-\ell)}{2(Dt)^{1/2}} \, dx \qquad 5-42$$

$$\Delta T = \frac{2Q_o}{kA} (Dt)^{1/2} \operatorname{ierfc} \frac{(x-\ell)}{2(Dt)^{1/2}} \qquad 5-43$$

or

$$\Delta T = \frac{2Q_o}{kA} \left[\left(\frac{Dt}{\pi}\right)^{1/2} e^{-\frac{(x-\ell)^2}{4Dt}} - \frac{(x-\ell)}{2} \operatorname{erfc} \frac{(x-\ell)}{2(Dt)^{1/2}} \right] \qquad 5-44$$

that at $x=\ell$

$$\Delta T = \frac{2Q_o}{kA} \left(\frac{Dt}{\pi}\right)^{1/2} \qquad 5-45$$

which gives the temperature rise at the junction. Note that this is identical to 5-36 so that the second term in 5-35 represents the effect the boundary has on the temperature rise.

(c) Heat Flow from a Spherical Source

The temperature rise at the junction has been calculated in (a) under two main assumptions (i) the end of the laser x=0 is held at the heat sink temperature (ii) linear heat flow from the junction. In the actual case, there are temperatu.

gradients in the solder layer and heat sink. These must be accounted for and may be used as boundary conditions to solve for the temperature rise at the junction. For the heat sink and thick solder layers, lateral diffusion of heat must be accounted for.

From equation 5-33, the temperature rise at the junction stabilizes for times such that $\frac{Dt}{\ell^2} > 1$. This time may be computed for the lasers used at 77°K as

$$t_o = \frac{\ell^2}{D} = 2.1 \times 10^{-8} \text{ secs} \qquad \ell = 2.5\mu \quad D = 3 \text{ cm}^2/\text{sec} \qquad 5\text{-}46$$

This time is well below the time resolution of the experiment and it is clear that the boundary condition 5-13 is not valid. We thus consider now the temperature rise of the heat sink. This may be done as follows: By differentiating 5-32 the heat flow at $x=\ell$ may be found as

$$\frac{Q}{A}(x=0) = \frac{Q}{A}\left[1 - \frac{4}{\pi}\sum_{n=1}^{\infty}\frac{(-1)^n}{(2n+1)} e^{-(2n+1)^2\frac{\pi^2}{4}\left(\frac{Dt}{\ell}\right)^2}\right] \qquad 5\text{-}47$$

for $t \gg t_o$ which conforms to the experimental situation

$$\frac{Q}{A}(x=0) \longrightarrow \frac{Q}{A}$$

Thus we have the problem of solving the temperature rise in the heat sink when heat is supplied at a constant rate Q/A. In order to simplify the problem and take into account the spreading of the heat in the heat sink, we consider the heat to be produced in a sphere of radius a surrounded by a heat sink of thermal conductivity k_i and diffusivity D_i. The problem is thus reduced to solving the equation

$$\frac{1}{r^2}\frac{\partial}{\partial r}\left(r^2\frac{\partial \Delta T}{\partial r}\right) = \frac{1}{D_i}\frac{\partial \Delta T}{\partial t} \qquad 5\text{-}48$$

with the boundary condition

$$+ 4\pi r^2 k_i \frac{\partial \Delta T}{\partial r} = Q' \quad \text{at } r = a \qquad 5\text{-}49$$

and requiring

$$T \to 0 \quad \text{as} \quad r \to \infty \qquad 5\text{-}50$$

putting $u = \Delta T r$ reduces the problem to solving

$$\frac{\partial^2 u}{\partial r^2} = \frac{1}{D_i} \frac{\partial u}{\partial t} \qquad 5\text{-}51$$

with

$$r \frac{\partial u}{\partial r} - u = \frac{-Q'}{4\pi k_i} \qquad \text{at } r = a \qquad 5\text{-}52$$

Equations 5-51 and 5-52 may be solved by Laplace transforms. Defining

$$\bar{u}(p) = \int_0^\infty e^{-pt} u(t)\, dt \qquad 5\text{-}53$$

5-51 becomes

$$\frac{\partial^2 \bar{u}(q)}{\partial r^2} - q^2 \bar{u}(q) = 0 \qquad q = \sqrt{\frac{p}{D_i}} \qquad 5\text{-}54$$

where the additional constant u(t=o) arising from the transform of the time derivative of u is zero since $\Delta T(t=o)=0$. Equation 5-52 thus becomes

$$r \frac{\partial \bar{u}(q)}{\partial r} - \bar{u}(q) = \frac{-Q'}{4\pi k_i p} \qquad 5\text{-}55$$

The solution of 5-54 taking into account the boundary condition 5-50 is

$$\bar{u}(q) = A_q e^{-qr} \qquad q > 0, \text{ real} \qquad 5\text{-}56$$

from 5-52 we find

$$-(qr+1)\, \bar{u}(q)\Big|_{r=a} = -\frac{Q'}{4\pi k_i p} \qquad 5\text{-}57$$

$$\bar{u}(q)\,|_{r=a} = \frac{Q'}{4\pi k_i p(1+aq)} \qquad 5\text{-}58$$

$$\bar{u}(q) = \frac{Q'}{4\pi k_i a p\left(\frac{1}{a}+q\right)} \qquad 5\text{-}59$$

$$u(r,t) = \frac{Q'}{4\pi k_i}\left[\operatorname{erfc}\frac{(r-a)}{2(D_i t)^{1/2}} - e^{\left(-\frac{r-a}{a}+\frac{D_i t}{a^2}\right)}\operatorname{erfc}\left[\frac{r-a}{2(D_i t)^{1/2}}+\left(\frac{D_i t}{a^2}\right)^{\frac{1}{2}}\right]\right] \qquad 5\text{-}60$$

$$\therefore \quad \Delta T(r,t) = \frac{Q'}{4\pi k_i r}\left[\operatorname{erfc}\frac{(r-a)}{2(D_i t)^{1/2}} - e^{\left(-\frac{r-a}{a}+\frac{D_i t}{a^2}\right)}\operatorname{erfc}\left[\frac{(r-a)}{2(D_i t)^{1/2}}+\left(\frac{D_i t}{a^2}\right)^{1/2}\right]\right] \qquad 5\text{-}61$$

at the surface $r=a$

$$\Delta T(a,t) = \frac{Q'}{4\pi k_i a}\left[1 - e^{\frac{D_i t}{a^2}}\operatorname{erfc}\left(\frac{D_i t}{a^2}\right)^{1/2}\right] \qquad 5\text{-}62$$

The original problem of finding the temperature rise at the junction may thus be solved with the boundary condition at x=0 in place of 5-13

$$\Delta T(x=0) = \frac{Q' a}{4\pi a^2 k_i}\left[1 - e^{\frac{D_i t}{a^2}}\operatorname{erfc}\left(\frac{D_i t}{a^2}\right)^{\frac{1}{2}}\right] \qquad 5\text{-}63$$

The solution of 5-22 with the boundary condition 5-63 inserted instead of 5-13 leads to

$$\Delta T(x,t) = \frac{Q\ell}{A k_p}\left[\frac{x}{\ell} - \frac{8}{\pi^2}\sum_{n=1}^{\infty}\frac{(-1)^n}{(2n+1)^2}\sin\frac{(2n+1)\pi x}{2\ell}\, e^{-\frac{(2n+1)^2\pi^2}{4\ell^2}(D_i t)^2}\right]$$

$$+ \frac{Q'}{4\pi a^2}\frac{a}{k_i}\left[1 - e^{\left(\frac{D_i t}{a^2}\right)}\operatorname{erfc}\left(\frac{D_i t}{a^2}\right)^{\frac{1}{2}}\right] \qquad 5\text{-}64$$

The temperature rise at the junction is thus given by

$$\Delta T(\ell,t) = \frac{Q\ell}{A k_p}\left[1 - \frac{8}{\pi^2}\sum_{n=1}^{\infty}\frac{e^{-\frac{(2n+1)^2 D t}{4\ell^2}}}{(2n+1)^2}\right] + \frac{Q'}{4\pi a^2}\frac{a}{k_i}\left[1 - e^{\frac{D_i t}{a^2}}\operatorname{erfc}\left(\frac{D_i t}{a^2}\right)\right] \qquad 5-65$$

If now the temperature rise ΔT_{solder} in the indium solder layer is taken into account, 5-65 will have this as an additional term. For thin solder layers, the linear flow model should give the temperature. Moreover, experimentally the solder layer was made thick due to the difficulty of bonding the lasers onto a sapphire substrate. Thus the lateral diffusion of heat must be accounted for in a manner similar to that used for the temperature rise in the heat sink. The general temperature rise at the junction may thus be written

$$\Delta T = \Delta T_{GaAs} + \Delta T_{HS} + \Delta T_{Solder} \qquad 5-66$$

where ΔT_{GaAs} and ΔT_{HS} are given by 5-33 or 5-35 and 5-65 respectively and

$$\Delta T_{Solder} = \frac{Q}{A}\frac{a}{k_z}\left[1 - e^{\frac{D_z t}{a^2}}\operatorname{erfc}\left(\frac{D_z t}{a^2}\right)^{\frac{1}{2}}\right] \qquad 5-67$$

where k_z = thermal conductivity of indium; D_z = diffusivity of indium. The value of $\frac{Q}{A}$ is given by

$$\frac{Q}{A} = \frac{I V (1-\eta)}{h s\left[1+\left(\frac{k_n}{k_p}\right)^2\right]} \qquad 5-68$$

where I = junction current, V = junction voltage = 1.48 volts; η = quantum efficiency, h = cavity length, s = stripe width and k_p = thermal conductivity of $\frac{n}{p}$ type GaAs and A = hs = $2\pi a^2$.

The bracketed factor in the denominator of 5-68 accounts for the fact that heat flows from the junction into the n region as well as the p region. Also in 5-68, the energy converted to photons has been taken into account by introducing the quantum efficiency. Thus we approximate the observed temperature rise at the junction as

$$\Delta T = \frac{IV(1-\eta)}{hs\left[1+\left(\frac{k_n}{k_p}\right)^{\frac{1}{2}}\right]}\left[1 - e^{D_2 t/a^2}\,\mathrm{erfc}\left(\frac{D_2 t}{a^2}\right)^{\frac{1}{2}}\right] \qquad 5\text{-}69$$

From equations 5-69 and 5-66, it may be seen that the temperature rise at the junction may be minimized by (i) making the solder layer as thin as possible and using in solder with high thermal conductivity and (ii) placing the junction as close as possible to a heat sink with large thermal conductivity. For the lasers used, where the junction was very close to the heat sink, the temperature rise due to the thermal conductivity of the gallium arsenide was small and essentially constant for the times involved in the experiment. The main contribution to the temperature rise was due to the heating in the solder layer. This situation contrasts that of Engeler and Garfinkel[1] where the junction was far enough from the heat sink that the main contribution to the junction heating arose from the thermal conductivity of the laser itself. Note that the fundamental assumption made of constant conductivity and diffusivity is not true at high injection levels where the temperature rise at the junction is large. For this case the approach of Engeler and Garfinkel[1] may be used to obtain a numerical solution.

The main features of 5-33, 5-65, 5-66 and 5-67 show that for short times the temperature rise by $\Delta T \propto t^{1/2}$ while for longer times the temperature rise

saturates at the cw value

$$\Delta T_{cw} = \frac{IV(1-\eta)}{hs\left[1+\left(\frac{k_n}{k_p}\right)^{1/2}\right]}\left[\frac{l}{k_p}+\frac{a}{k_i}+\frac{a}{k_i}\right] \qquad 5\text{-}70$$

Figure 5-1 shows how the temperature varies with time for different models. Curve (1), for linear flow in a semi-infinite slab, gives a temperature rise which increases indefinitely with time at $t^{1/2}$. Curve (11), the temperature rise due to the thermal conductivity of GaAs, rises as for the semi-infinite slab but saturates near $(Dt/a^2)^{1/2} = 1$. Finally, the temperature rise for spherical flow of heat in a semi-infinite slab gives a much slower temperature rise reflecting the lateral diffusion of the heat.

3. Experiment

Gallium Arsenide lasers of the stripe geometry were indium bonded on to either a sapphire or a copper heat sink and cooled in a dewar to 77°K or 4.2°K. In the lasers used, the p-layer was 2.5μ thick and the lasers were mounted p-side down on the heat sink. Electrical contact was made to the n-side of the laser via a thin gold wire which was indium bonded to the laser. The heat sink was clamped in a copper block, which was cooled via the cold finger method. The bias to the laser could be pulsed by placing the laser in series with a 50Ω resistor which was connected to the output of a Hewlett-Packard Model 214A pulse generator. By monitoring the voltage across the series resistor, the current through the laser could be seen to be constant during the pulse. The pulsed output from the laser was focused by a short focal length lens onto the center of a spherical Fabry-Perot interferometer which had a free spectral range of 7.5 GHz. One mirror of the interferometer was mounted on a piezoelectric slab so that the interferometer could be scanned by applying a voltage to the slab and moving the mirror backwards and forwards. Light passing through the interferometer on axis

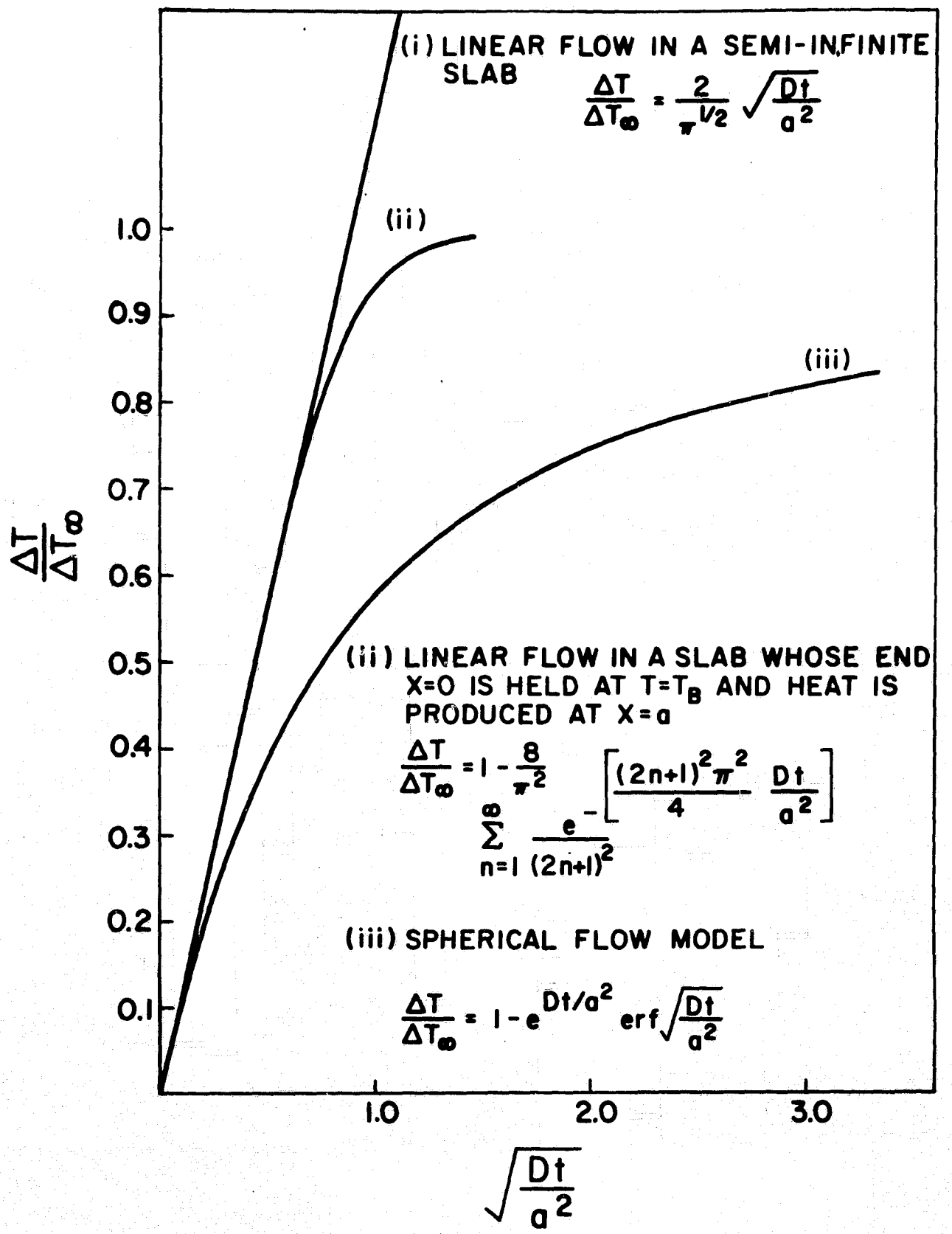

THEORETICAL HEAT FLOW CURVES

FIGURE 5-1

was detected by a silicon photodetector placed directly behind the interferometer. The output from the photodetector was passed into a Tektronix 555 Oscilloscope with a 1A7 plug-in unit. The X-axis of the oscilloscope was triggered from the output of the pulse generator. When the signal-to-noise ratio was good, photographs of the oscilloscope display were taken. When the signal-to-noise ratio was bad or when the light pulse shape was to be recorded on a graph, the output of the 1A7 plug-in was fed into a Princeton Applied Research Boxcar Integrator and then to the Y-axis of an x-y recorder. The X-axis of the recorder was operated from the Boxcar scan ramp. The Boxcar Integrator was operated in the recurrent mode. The signal from the time base ramp was used to trigger the pulse generator. The position of the pulse with respect to this trigger could be adjusted using the pulse position control on the generator so that the pulse occurred during the time base ramp. The operation of the Boxcar was thus as follows: at the start of a time base a trigger was sent to the pulse generator. At a later time, controlled by the pulse position knob on the pulse generator, a pulse was sent through the laser and simultaneously the x-axis of the oscilloscope was triggered. The output pulse from the photodetector was amplified by the 1A7 plug-in and fed into the Boxcar integrator. The signal was then amplified in the Boxcar integrator and applied to the input of a gated amplified. The length of time the amplifier gate was open could be controlled with the gate width switch on the Boxcar integrator, while the time at which it opened with respect to the start of the time base could be adjusted using the scan time control. The output of the Boxcar integrator, for gate widths small compared to detail in the pulse, reproduced the pulse shape at a rate which could be recorded on an x-y recorder. The signal was fed into the y-axis of the recorder while the x-axis was driven from the scan ramp jack which produced a voltage proportional to the position of the open gate. Thus by using either the Boxcar and recorder or by observing the oscilloscope display, the time behavior of the light pulse passed through the interferometer could be observed.

As noted earlier, during the pulse, the laser frequency decreases at a rate proportional to the temperature rise at the junction calculated in equation 5-69. Thus frequency changes rapidly at the beginning of the pulse and more slowly toward the end. Since the transfer function of the interferometer for light on the axis consists of a series of peaks separated in frequency by the free spectral range f = 7.5 GHz in our case, light will be transmitted by the interferometer only when the laser frequency is some multiple of f. Thus every time the laser frequency decreases by f a peak of light will be passed by the interferometer. The interferometer thus acts as a frequency marker, marking off frequency intervals of f. The output of the interferometer should thus consist of a set of peaks, the time between successive peaks increasing according to 5-69.

Results

The change in frequency of a semiconductor laser during pulsed operation, arises through the temperature dependence of the dielectric constant. Thus the time behavior of the spectral output may be written

$$\nu(t) = \nu_0 + \frac{d\nu}{dt}\,\Delta T(t) \qquad 5\text{-}71$$

Using 1-19 and neglecting thermal expansion

$$-\frac{d\ln\nu}{dT} = \frac{1}{2}\frac{d\ln\varepsilon}{dT} \qquad 5\text{-}72$$

$$\text{but } \varepsilon = \varepsilon(\nu, T)$$

$$\therefore \quad \frac{d\ln\varepsilon}{dT} = \frac{\partial\ln\varepsilon}{\partial T} + \frac{\partial\varepsilon}{\partial\nu}\frac{d\nu}{dT} \qquad 5\text{-}73$$

$$\therefore \quad \frac{d\nu}{dT} = -\frac{1}{2}\,\frac{\nu_0\,\frac{\partial\varepsilon}{\partial T}}{\varepsilon\left[1+\frac{\nu}{\varepsilon}\frac{\partial\varepsilon}{\partial\nu}\right]} \qquad 5\text{-}74$$

$$\nu(t) = \nu_0 - \frac{\frac{1}{2}\frac{\nu_0}{\varepsilon}\frac{\partial \varepsilon}{\partial T}}{1 + \frac{\nu}{\varepsilon}\frac{\partial \varepsilon}{\partial \nu}} \Delta T(t) \qquad 5\text{-}75$$

where ΔT is given by 5-69

$$\text{but} \quad -\left.\frac{\partial \varepsilon}{\partial T}\right|_{\nu} = \left.\frac{\partial \varepsilon}{\partial \nu}\right|_{T} \left.\frac{\partial \nu}{\partial T}\right|_{\varepsilon} \qquad 5\text{-}76$$

assuming that the dielectric constant change is one solely to the shift in the absorption edge,

$$\frac{\partial \varepsilon}{\partial T} = -\frac{\partial \varepsilon}{\partial \nu}\frac{1}{h}\frac{dE_g}{dT} \qquad 5\text{-}77$$

$$\therefore \quad \nu(t) = \nu_0 + \frac{\frac{\nu_0}{2\varepsilon}\frac{\partial \varepsilon}{\partial \nu}}{1 + \frac{\nu_0}{2\varepsilon}\frac{\partial \varepsilon}{\partial \nu}} \frac{1}{h}\frac{dE_g}{dT} \Delta T(t) \qquad 5\text{-}78$$

Using the results of Eugeler and Garfinkel for[4] GaAs

$$\frac{\frac{\nu_0}{2\varepsilon}\frac{\partial \varepsilon}{\partial \nu}}{1 + \frac{\nu_0}{2\varepsilon}\frac{\partial \varepsilon}{\partial \nu}} = 0.35 \qquad 5\text{-}79$$

$$\frac{dE_g}{dT} = -2 \times 10^{-4} \text{ ev/}^{\circ}\text{K} \quad \text{at } 77^{\circ}\text{K} \qquad 5\text{-}80$$

$$\nu(t) - \nu_0 = -16.7\, \Delta T(t) \quad \text{GHz at } 77^{\circ}\text{K} \qquad 5\text{-}81$$

Table 5-1 shows values of k, c and D at different temperatures for different materials. Using in 5-69, the values V = 1.48 volts, h = 380μ, s = 12.7μ,

$a = \frac{hs}{2\Pi} = 27.5\mu$.

$t_o = a^2/D_2 = 9.7$ μsecs at 77°K which are applicable for lasers L-15 and L-23 5-82

$$\nu(t) - \nu_0 = -614\, I(1-\eta)\left[1 - e^{t/t_0}\, \text{erfc}\left(\frac{t}{t_0}\right)^{\frac{1}{2}}\right] \quad \text{GHz at } 77^{\circ}\text{K}$$

TABLE 5-1. – THERMAL CONSTANTS FOR VARIOUS SUBSTANCES

Substance	Density (P) gms/ c. c.	Temperature T ^{o}K	Thermal conductivity watts/cm ^{o}K	Specific heat C Joules/cm^3 ^{o}K	Diffusivity D = k/c cm^2/ sec
GaAs	5.36	4.2	0.025	2.8×10^{-4}	89
P Type		77	2.41	0.93	2.59
		300	0.47	1.73	0.27
In	7.33	4.2	8.52	7.4×10^{-3}	1.09×10^{3}
		77	1.09	1.395	0.574
		300	0.25	1.816	0.1376
Sapphire	4.00	4.2	1.1	8.35×10^{-4}	1.3×10^{3}
		77	7.8	0.269	29.1
		300	2	3.11	0.64
Copper	8.93	4.2	120	0.89×10^{-3}	135×10^{3}
		77	6	1.75	3.43
		300	~3	3.45	1.15

As will be seen below, comparison of equation 5-82 with the experimental results at 77°K shows good agreement.

Figures 5-2a to 5-2d show the variation in time of the light intensity passed through a Fabry-Perot interferometer from laser L-15 which was pulsed at liquid nitrogen temperatures. The top trace in the four photographs shows the current passed through the laser while the bottom trace gives the output of the photodetector placed behind the Fabry-Perot interferometer. The peaks occur every time the laser frequency equals some multiple of the interferometer's resonant frequency which, for the interferometer used, was 7.5 GHz. It can clearly be seen that the frequency change with time is fast at the beginning of the pulse and slows down as time progresses. In the four pictures 5-2a to 5-2d the current is kept constant but the pulse length (and horizontal time) scale are changed. The repartition frequency was kept low enough so that the junction temperature had returned to the heat sink temperature before the heat pulse arrived. That this was true, was determined noting that the peak positions were not affected by increasing the pulse length up to a certain value. Figures 5-3a to 5-3d show the effect of scanning the interferometer on the observed peak positions for the same laser L-15 at 77°K. Here the current is held fixed through the pulse and the position of one mirror is changed from picture to picture. The corresponding total frequency shift is noted with each picture. It can be seen that the mirror is moved almost through one free spectral range. By examining the movement of the peaks it can be determined that the frequency is decreasing with time for if we look at one of the modes, the fifth for instance, it moves to earlier times as the resonance frequency is increased. Hence the laser frequency does in fact decrease with temperature. Figures 5-4a to 5-4d show the time behavior of the laser intensity as a function of current. These

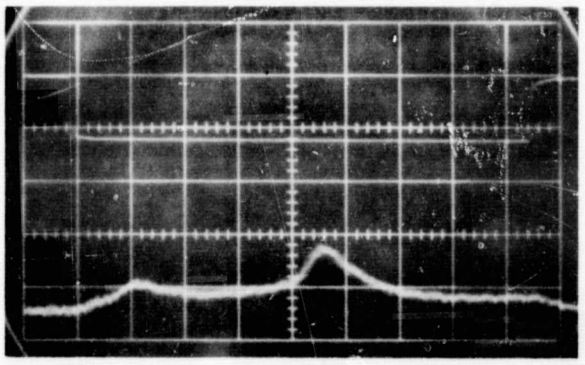

1 2 3

(a)

HORIZONTAL SCALE = 0.5 μs/cm

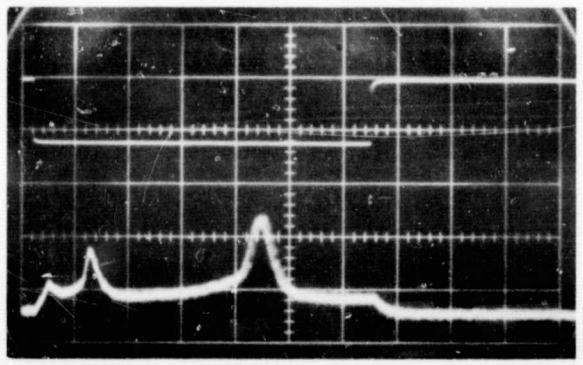

2 3 4

(b)

HORIZONTAL SCALE = 2 μs/cm

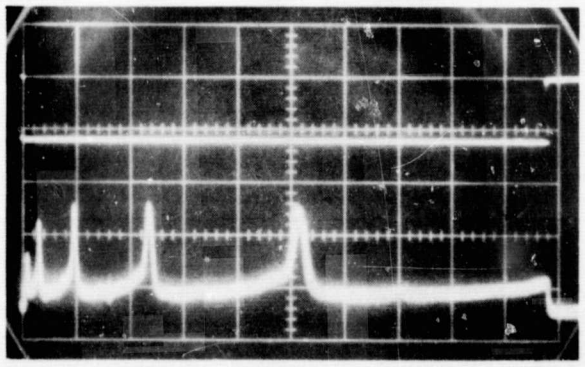

4 5 6 7

(c)

HORIZONTAL SCALE = 20 μs/cm

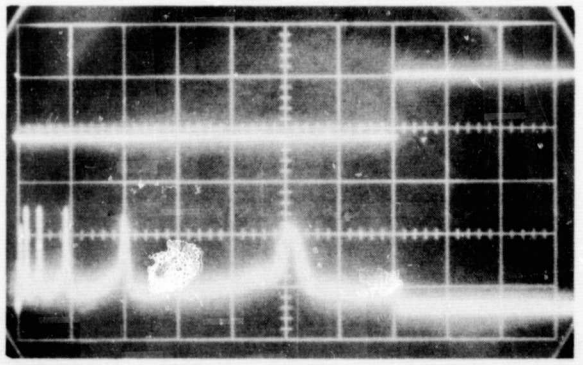

567 8 9

(d)

HORIZONTAL SCALE = 100 μs/cm

L-15

TOP TRACES: LASER CURRENT PULSE: VERTICLE SCALE - 20V/cm
BOTTOM TRACES: LIGHT OUTPUT FABRY-PEROT INTERFEROMETER
LASER CURRENT = 240 mA VERTICLE SCALE - 1 mV/cm
T = 77°K

FIG. 5-2 SPECTRAL SHIFT OF LIGHT FROM A PULSED INJECTION LASER AS MEASURED WITH A FABRY-PEROT INTERFEROMETER

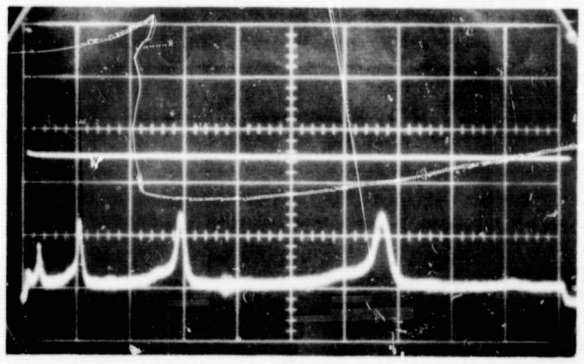

5

(a)

MIRROR VOLTAGE = 0

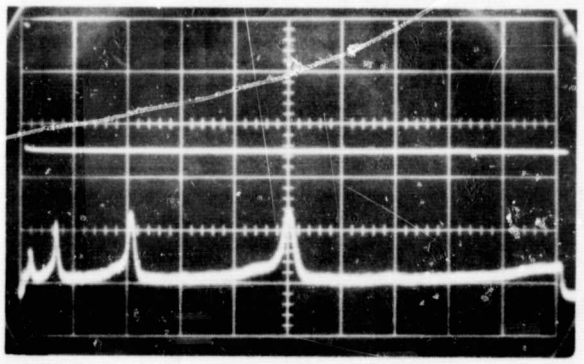

5

(b)

MIRROR VOLTAGE = 15.5 VOLTS

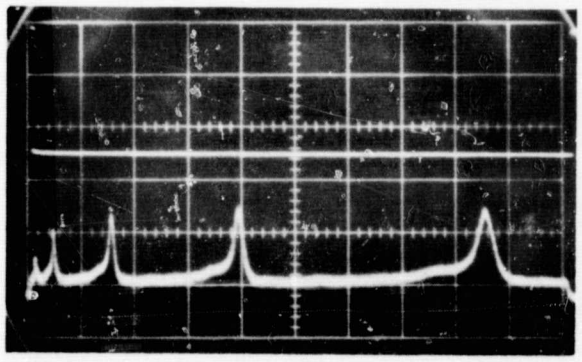

5 8

(c)

MIRROR VOLTAGE = 27.5 VOLTS

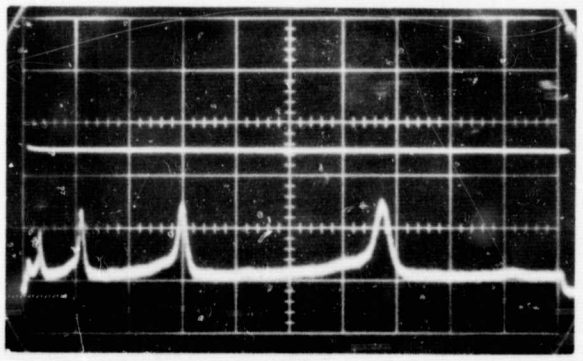

5 6

(d)

MIRROR VOLTAGE = 44 VOLTS

L-15
HORIZONTAL SCALE: 10 μs/cm
LASER CURRENT: 230 mA
T = 77 °K

FIG. 5.3 SCANNING OF A PULSED INJECTION LASER BY MOVING FABRY-PEROT INTERFEROMETER MIRROR

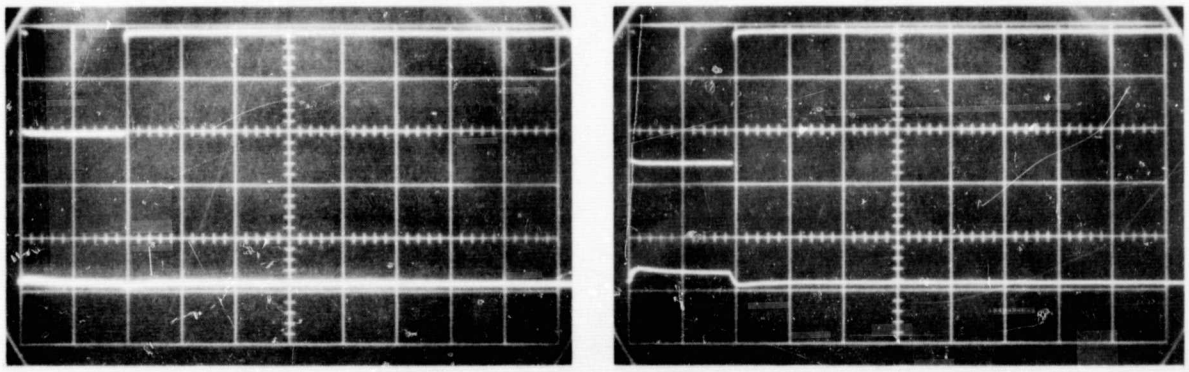

(a)
LASER CURRENT = 200 mA

(b)
LASER CURRENT = 260 mA

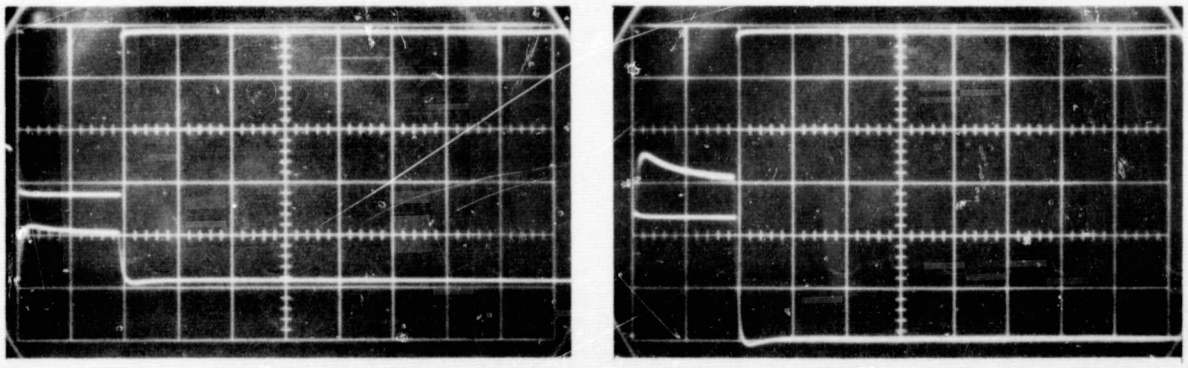

(c)
LASER CURRENT = 320 mA

(d)
LASER CURRENT = 360 mA

L-15
TOP TRACES: LASER CURRENT PULSE: VERTICAL SCALE - 5 V/cm
BOTTOM TRACES: LASER LIGHT PULSE: VERTICAL SCALE - 10 mV/cm
HORIZONTAL SCALE: 20μs/cm
T = 77°K

FIG. 5-4 LIGHT INTENSITY FROM A PULSED INJECTION FOR DIFFERENT CURRENTS

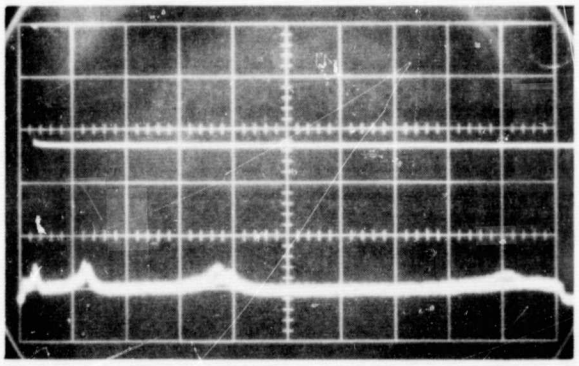

(a) 5
LASER CURRENT = 230 mA

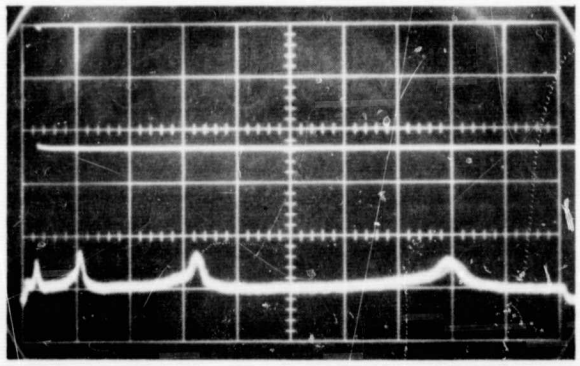

(b) 5
LASER CURRENT = 235 mA

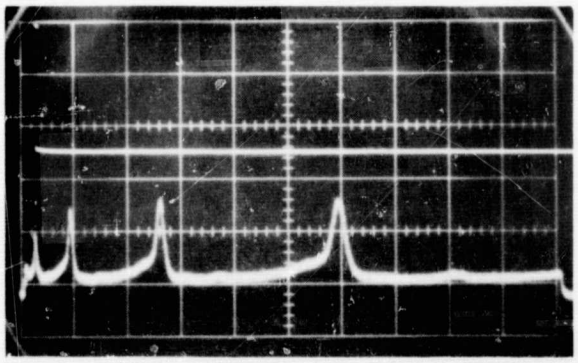

(c) 5
LASER CURRENT = 250 mA

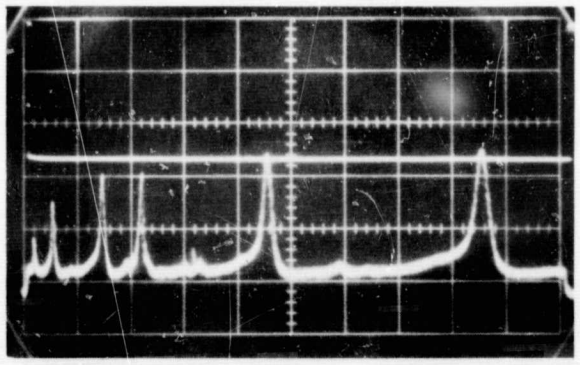

(d) 5
LASER CURRENT = 265 mA

L-15
TOP TRACES: LASER CURRENT - VERTICAL SCALE - 10 V/cm
BOTTOM TRACES: LASER OUTPUT PASSED THROUGH FABRY-PEROT INTEROMETER VERTICAL SCALE - 1 mV/cm
HORIZONTAL SCALE: 10 μs/cm

FIG. 5-5 THE EFFECT OF INJECTION CURRENT ON THE MODE FREQUENCY OF A PULSED INJECTION LASER AT T = 77°K

traces were obtained by focussing the laser beam directly onto a photodiode. It can be seen that the light pulses are reasonably flat with a slightly higher intensity at the beginning of the pulse for higher currents. The peaks observed in figures 5-2 and 5-3 are thus definitely caused by the transmission characterisitcs of the Fabry-Perot interferometer.

The behavior of laser frequency was also observed as the current was changed. As can be seen from figures 5-5a to 5-5d the peaks initially move toward the left as the current is increased and then reverse direction and move toward the right. This behavior was observed both in laser L-15 and L-23 (figure 5-6) at 77°K. It is due to a shift in the laser starting frequency, initially toward lower frequencies and then toward higher frequencies. This phenomenon is also observed on a cw basis. The shift toward higher frequencies is the normal behavior and is accounted for by a filling of the states in the conduction band since the maximum in the laser gain curve moves toward higher energies with current. The shift toward lower energies is discussed in Chapter IV. This behavior can be seen the graphs of figure 5-6. Initially (figure 5-6a) the laser is below threshold and only spontaneous emission is emitted. As the current is increased laser threshold is reached and the laser peaks appear in the trace. The peaks move toward the front of the pulse at first, as noted with laser L-15 but then move toward the rear. Figure 5-7 shows a plot of frequency change versus time for several currents. These results were taken from figure 5-6. The vertical distance between curves is the actual change in the laser frequency for a given instant in tiem, when the laser current is changed. A similar graph in figure 5-8 shows the results for figure 5-5 while figure 5-9 shows those for figure 5-3 where the interferometer was scanned. Note that by scanning, the laser frequency change with time may be followed continuously.

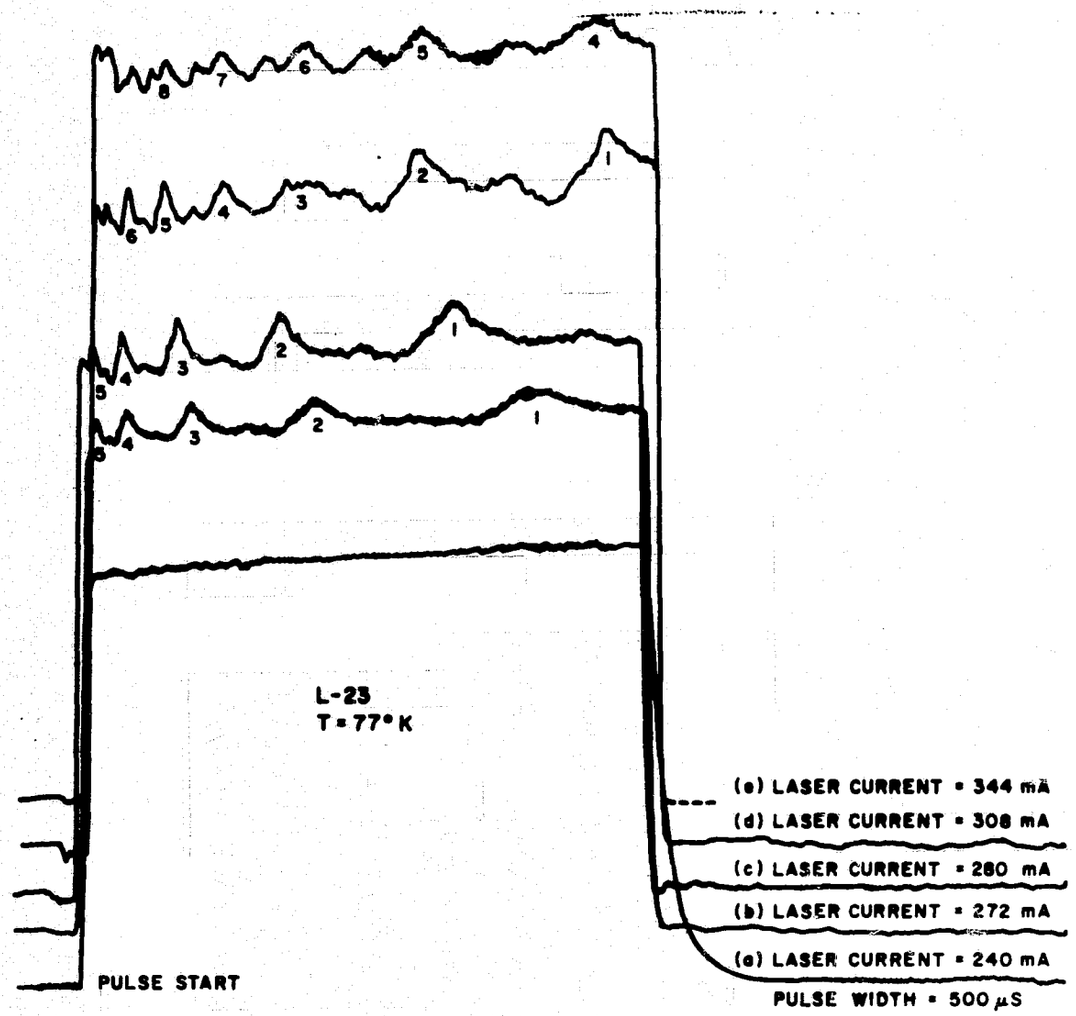

SHIFT OF LASER STARTING FREQUENCY WITH LASER CURRENT

FIGURE 5-6

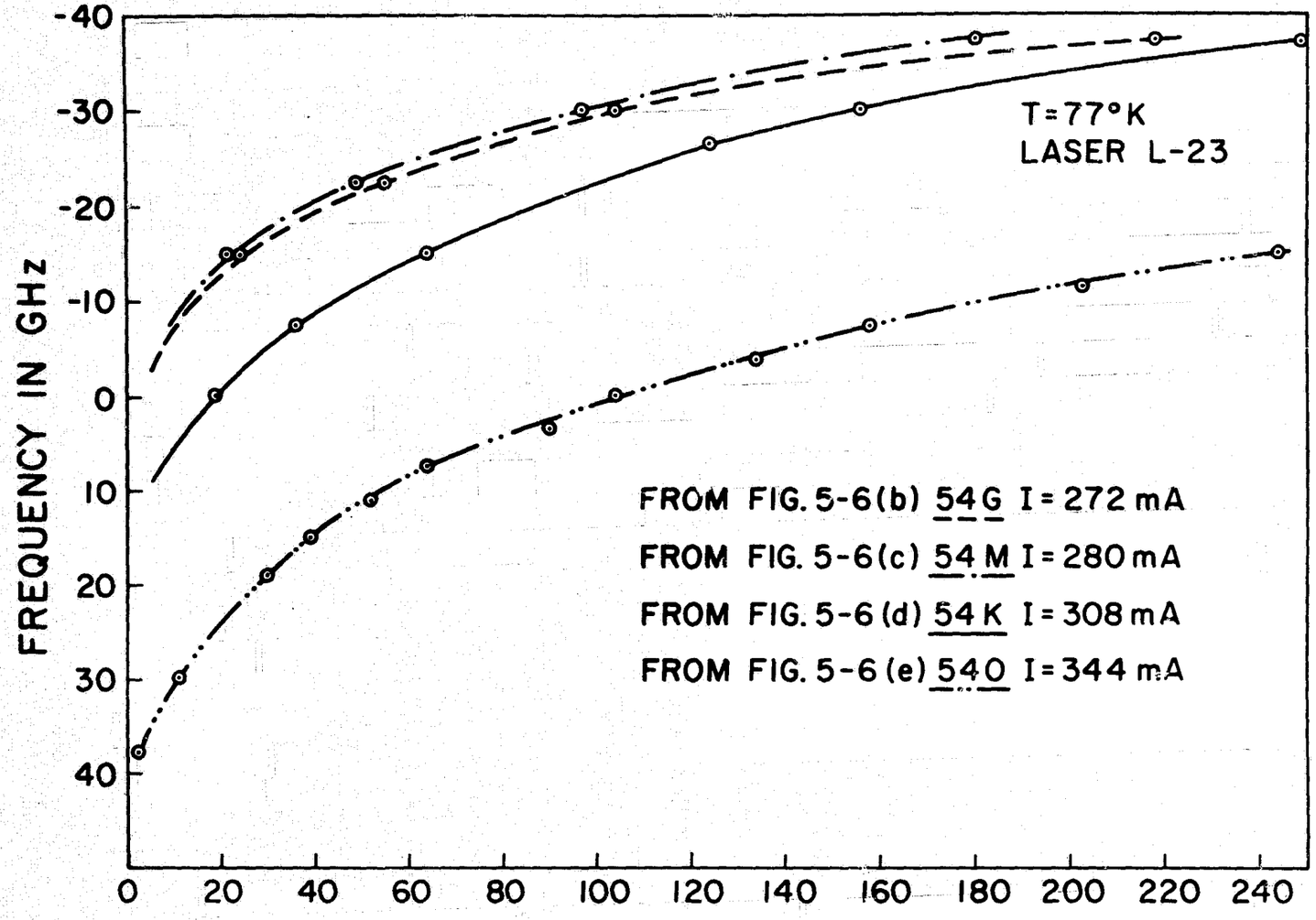

FREQUENCY CHANGE WITH TIME
DURING PULSED OPERATION
FIGURE 5-7

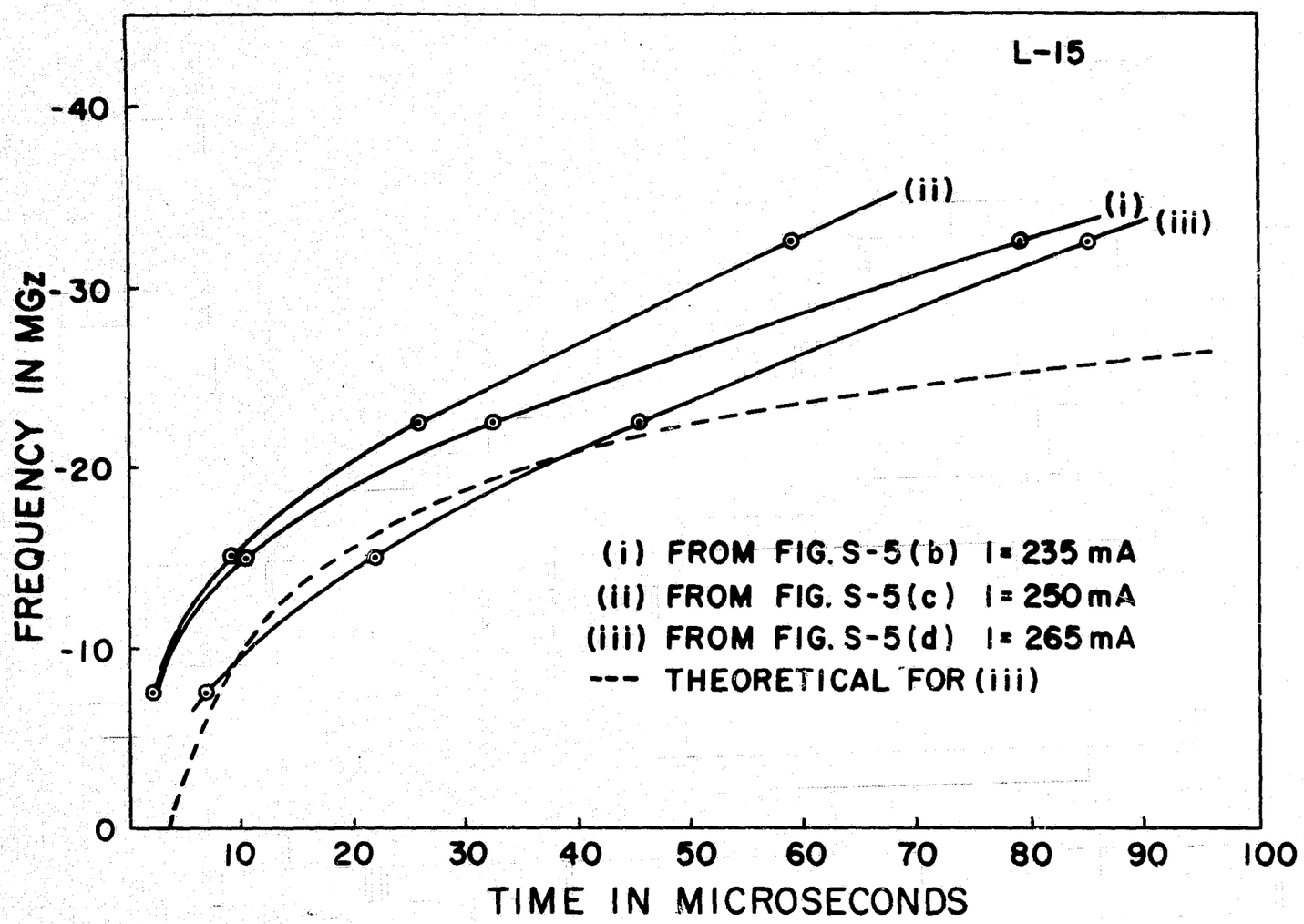

FREQUENCY SHIFT WITH TIME
FOR PULSED OPERATION AT 77°K

FIGURE 5-8

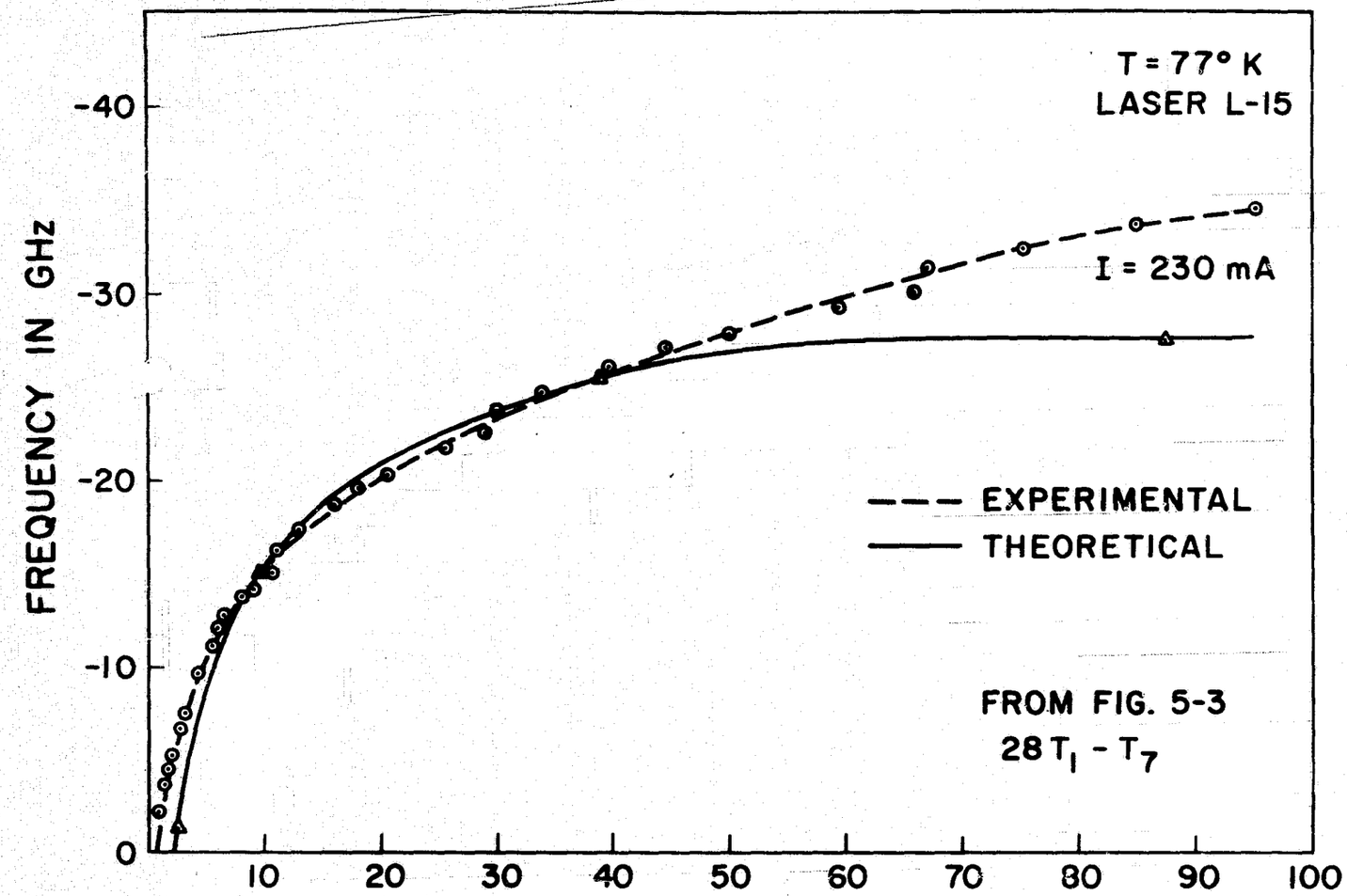

FREQUENCY CHANGE WITH TIME DURING
PULSED OPERATION

FIGURE 5-9

In order to elucidate the behavior of laser frequency further, two mere graphs, figures 5-10 and 5-11, were drawn from the data in figure 5-6 and other data taken in the same run but not shown in figure 5-6. In figure 5-10, the frequency change is plotted as a function of current at different instants during the pulse. This figure clearly shows the inital shift toward lower frequencies followed by the shift toward higher frequencies. In figure 5-11, the position in time of each peak (a fixed frequency) is plotted against current. For low currents the peak positions move toward shorter times reflecting the shift toward lower freqeuncy. As the current increases, however, the peaks move toward longer times. This latter behavior is just the reverse of what would be expected if the laser starting freqeuncy was fixed and the total frequency change was due soley to the temperature change at the junction with current.

The results presented so far were taken for duty cycles low enough that heating from the previous pulse was negligible. This condition could easily be verified by increasing the pulse repartition frequency. At some frequency, the peaks would start to shift toward shorter times due to the additional heating caused by the previous pulse. Figures 5-12a to 5-12d and accompanying curve figure 5-13 show the effects of keeping the repartition frequency fixed and varying the pulse length. As the pulse length is increased the peaks move toward the front of the pulse reflecting the increase in heating. Eventually the increase in heating becomes so great that laser action ceases altogether.

Comparison of equation 5-82 with the experimental results was made in the following manner. From figures 5-7, 5-8, and 5-9, the frequency change at two times t_o and $4t_o$ were noted and related via figure 5-1 to the maximum frequency change. Knowing the current, the quantum efficiency η was calculated and equation 5-82 then plotted against time. This is shown in figure 5-8 and 5-9. The value of the quantum efficiency calculated is

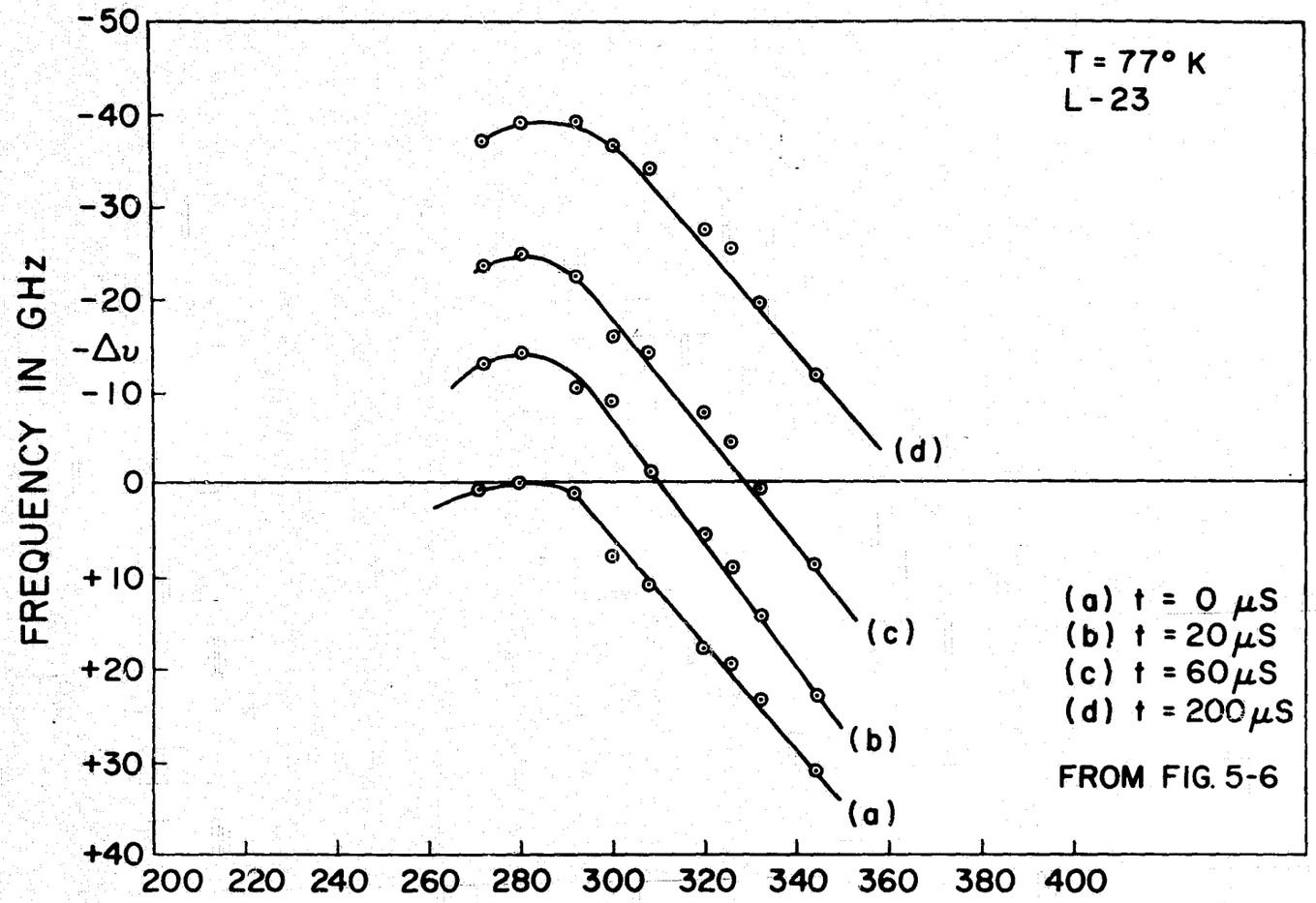

FREQUENCY CHANGE OF LASER WITH CURRENT
AT DIFFERENT INSTANTS OF TIME

FIGURE 5-10

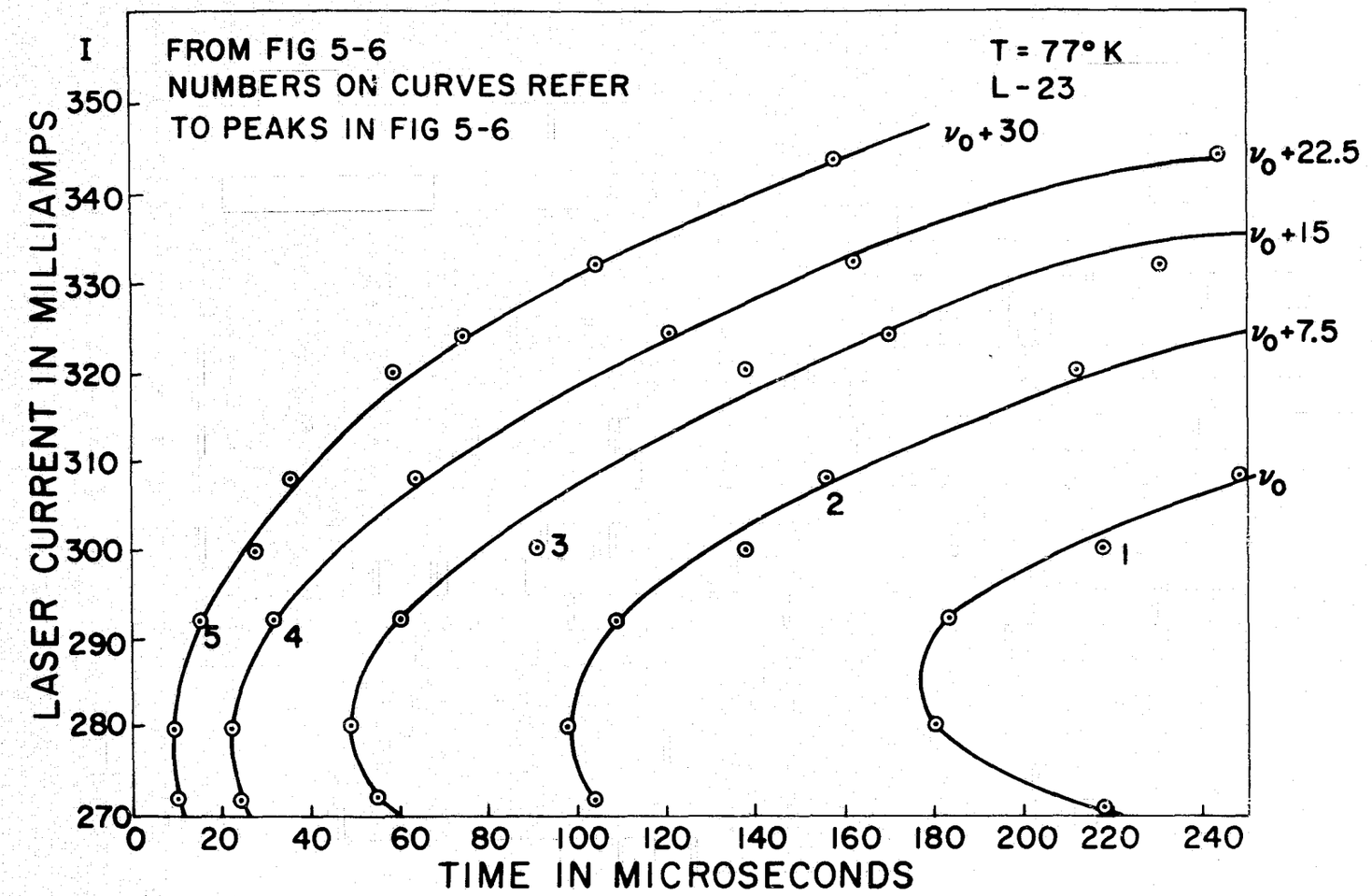

THE TIME AT WHICH THE LASER REACHES
CERTAIN FIXED FREQUENCIES AS A FUNCTION OF CURRENT

FIGURE 5-11

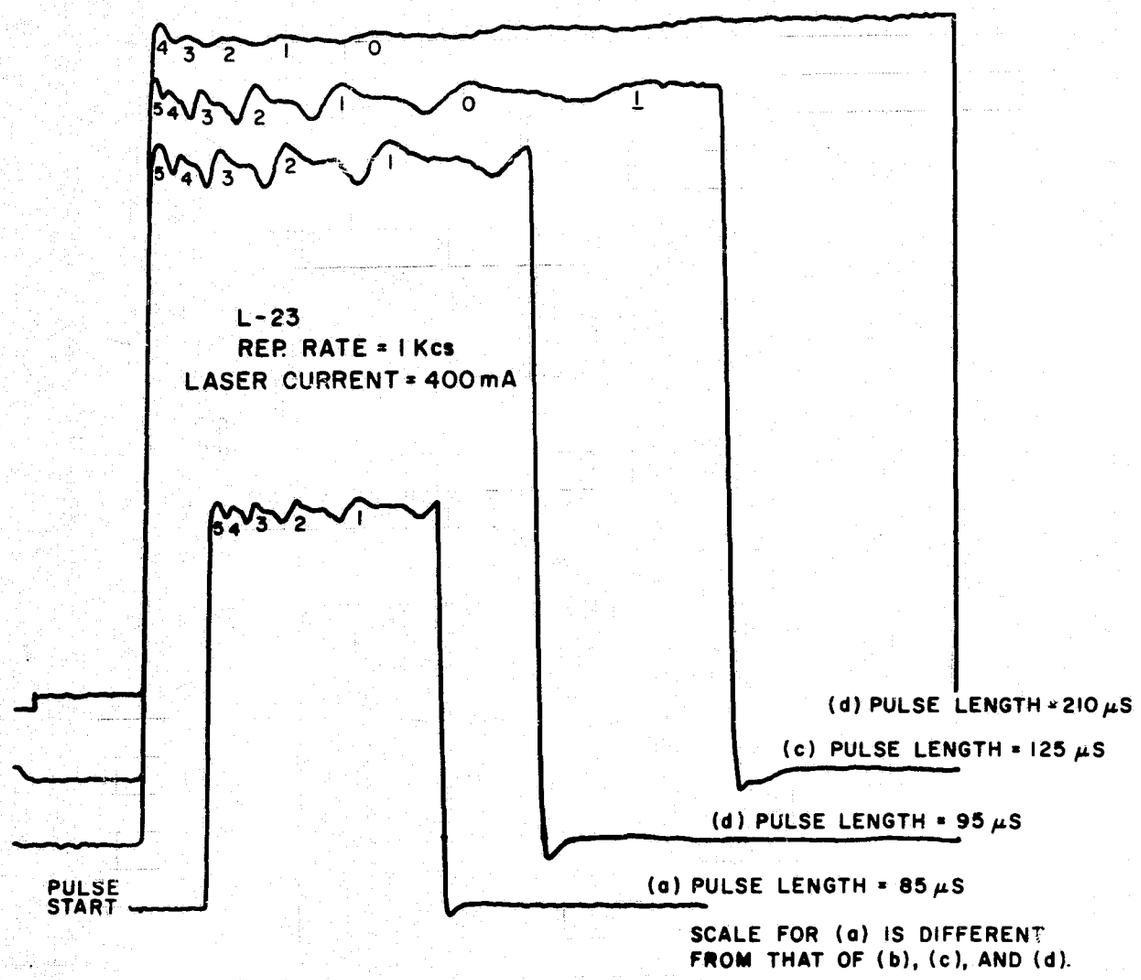

EFFECT OF PULSE LENGTH ON THE SPECTRAL SHIFT AT T = 77° K

FIGURE 5-12

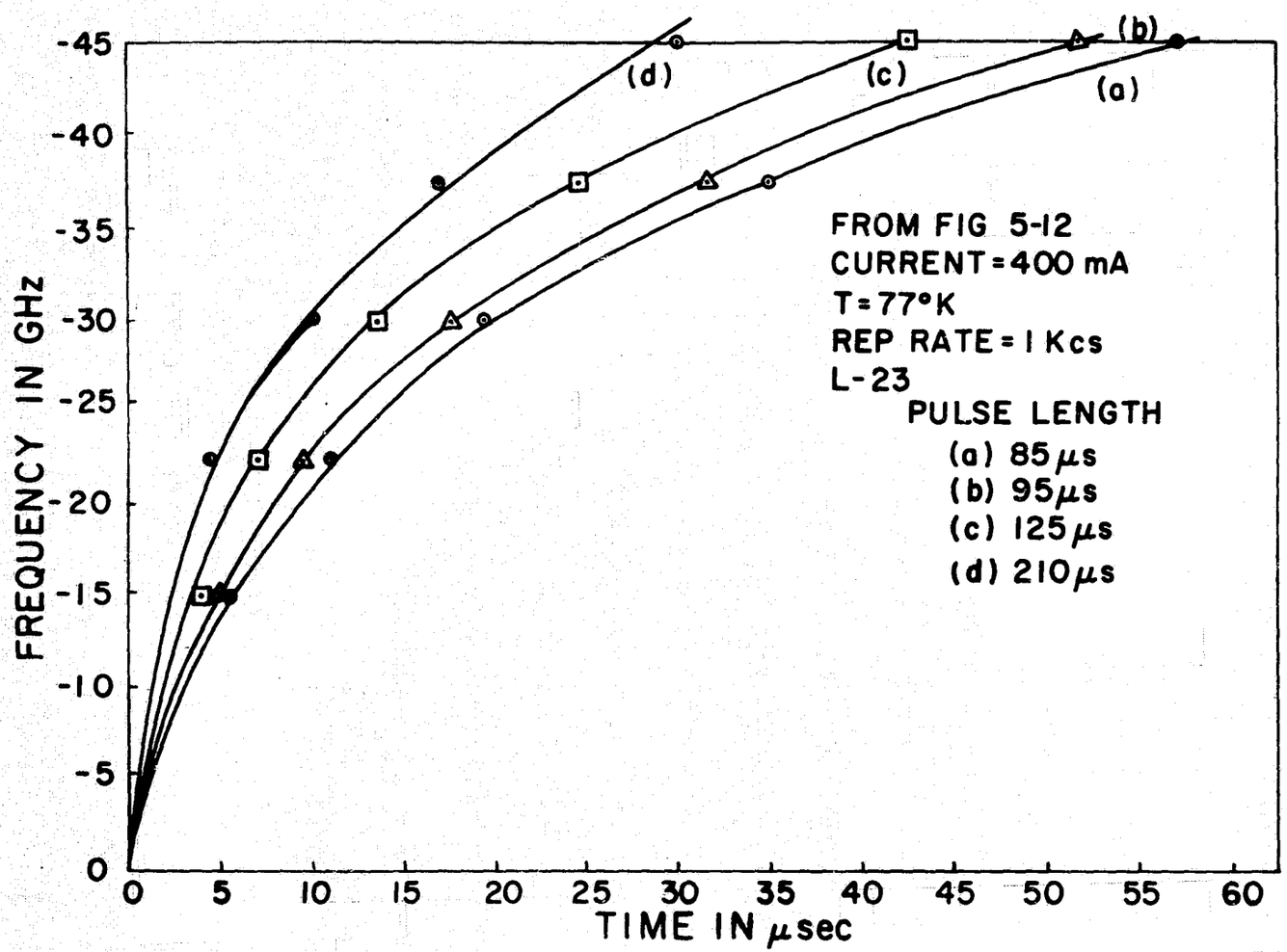

FREQUENCY SHIFT VERSUS TIME
FOR VARYING PULSE LENGTHS

FIGURE 5-13

undoubtedly too high, although no independent measurements of η have been made on these lasers, but considering the assumptions made in calculating the temperature rise, the agreement with the observed results is good. For longer times, the spectral shift is more rapid than would be predicted on the spherical flow model. This behavior is to be expected, however, from the examination of curves (11) and (111) in figure 5-1, since the actual flow would like somewhere between the linear and spherical flows. Table 5-2 shows the calculated maximum frequency shift and corresponding temperature rise for different currents. The calculated values of η are also given. Figure 5-14 shows these maximum frequency shifts plotted against the laser current to obtain an average value for the quantum efficiency.

Measurements of the spectral shift under pulsed operations were also made at 4.2°K. Data was recorded both using a boxcar integrator and by direct observation of the photodiode output on an oscilloscope. The observed spectral shifts are much smaller than those obtained at 77°K as can be seen by comparing figure 5-15 with figure 5-6. This would be expected because (i) D is much larger so the temperature rise is more rapid and (ii) $\frac{dEg}{dT}$ is smaller $\approx 2\times10^{-5}$ ev/°K^4 at 10°K. However, the maximum spectral shifts calculated from 5-82 are too small to account for the observed shifts. It thus seems likely that the observed shifts are due to small pockets at the interfaces of the solder layer. The graphs of figure 5-15 show the appearance of second laser mode. This and the original mode merge to form one peak in figure 5-15c. At this point they are separated by an integral number of free spectral ranges. Unfortunately, without the aid of a spectrometer the actual frequency difference cannot be measured.

Owing to the slow variation of frequency with time in figure 5-15, the position of the peaks is extremely sensitive to temperature variations. Thus thermal drifting of the laser temperature was sometimes observed due to

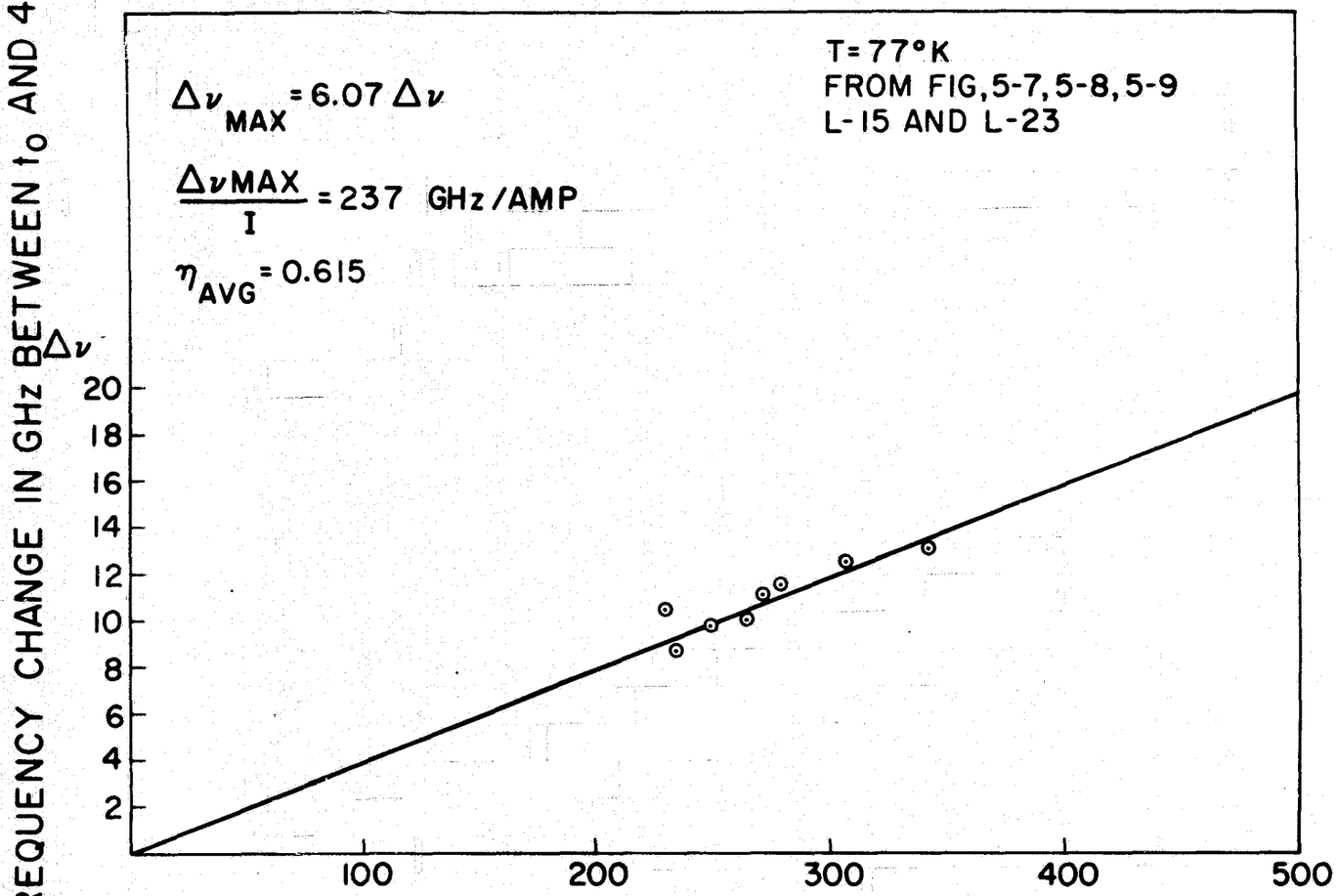

MAXIMUM FREQUENCY SHIFT Vs CURRENT

FIGURE 5-14

TABLE 5-2. – CALCULATED VALUES OF QUANTUM EFFICIENCY

Figure	Laser current mA	$\Delta\nu$ max GHz	ΔT max ^{o}K	η	Laser
5-7 (b)	272	72.2	4.33	.568	L-23
5-7 (c)	280	74.6	4.47	.566	L-23
5-7 (d)	308	81.4	4.88	.568	L-23
5-7 (e)	344	95.3	5.70	.548	L-23
5-8 (i)	235	54.6	3.27	.621	L-15
5-8 (ii)	250	66.7	4.00	.565	L-15
5-8 (iii)	265	68.0	4.08	.581	L-15
5-9	230	63.8	3.82	.545	L-15

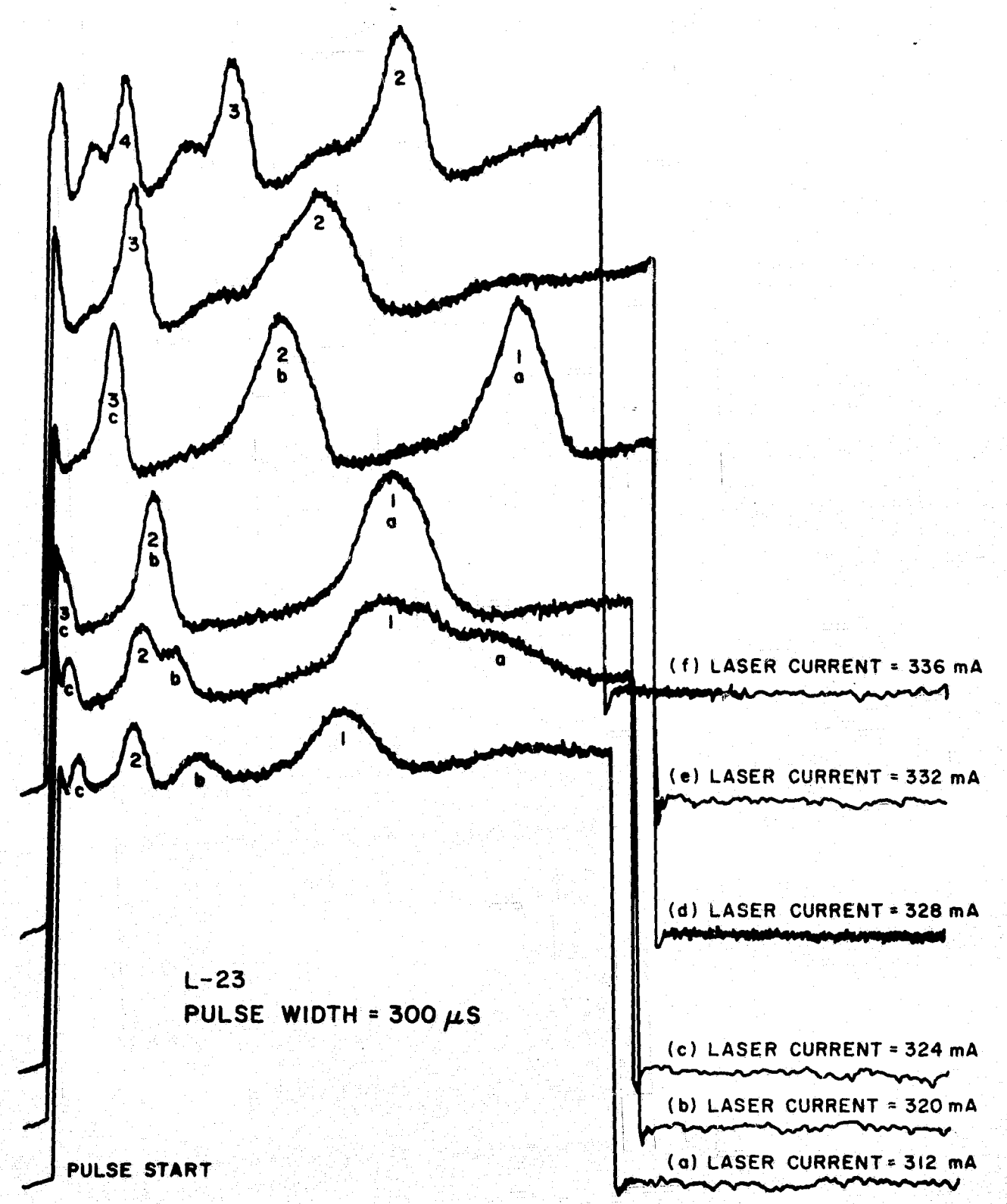

FREQUENCY DEPENDENCE OF PULSED LASER WITH INCREASING CURRENT AT 4.2°K

FIGURE 5-15

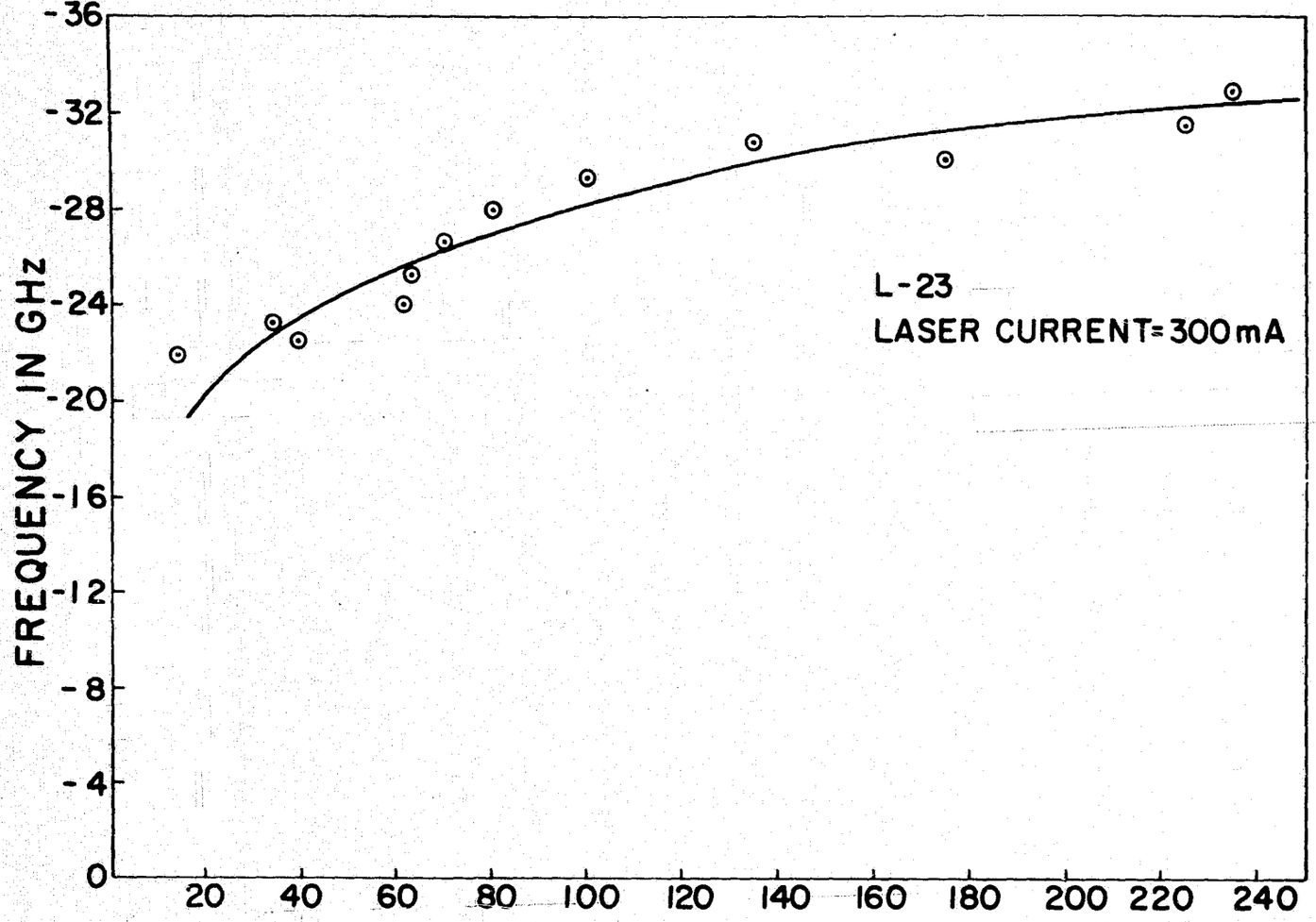

FREQUENCY CHANGE WITH TIME
DURING PULSED OPERATION AT 4.2°K

FIGURE 5-16

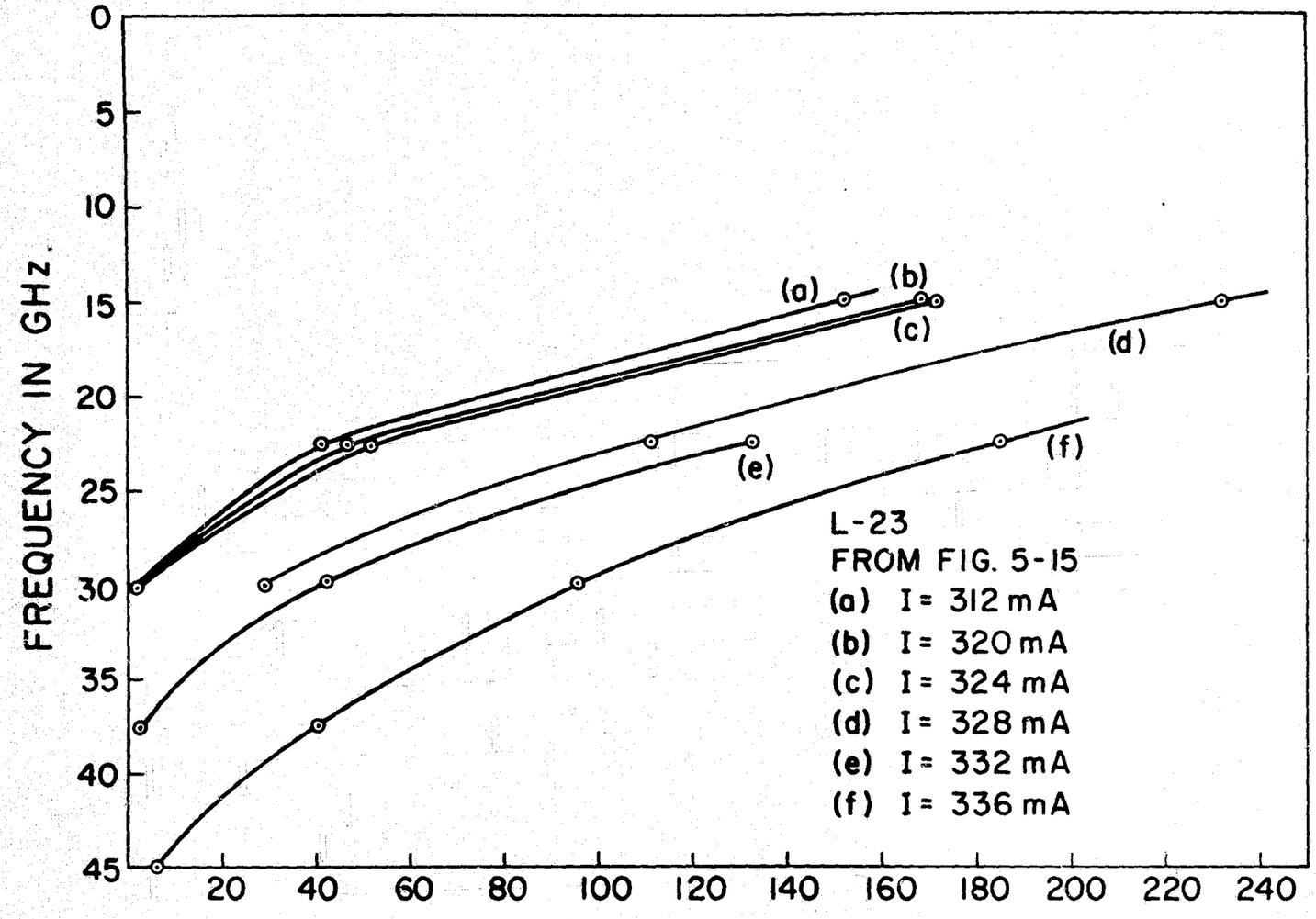

FREQUENCY CHANGE WITH TIME
FOR DIFFERENT CURRENTS AT 4.2°K
FIGURE 5-17

instabilities in the cryogenic cooling. Consequently, the traces obtained using the boxcar integrator, which required many minutes to plot, necessitate great temperature stability. Figure 5-16 shows a plot of freqeuncy change versus time at I = 300ma obtained by scanning the interferometer as mentioned previously. The data was taken over a period of several hours and the data points reflect the above mentioned temperature fluctuations. Figure 5-17 shows similar data for different currents.

Application to room temperature operation

The results presented above were taken at 4.2°K and 77°K. At room temperature, the threshold current densities required for pulsed lasing operation are very high $\sim 10^5$ amps/sq. cm. and thus laser heats up rapidly. Pulse lengths are thus required to be short, typically less than 100 ns. Since the thermal diffusivity of GaAs is small at 300°K (0.27 $cm^2 sec^{-1}$)[1], the diffusion length $L = \sqrt{kt}$ is of the order of 1μ for t = 40ns. If pulse lengths shorter than 40ns are used, thermal diffusion may be neglected and the temperature rise may be estimated by solving

$$C \frac{\partial \Delta T}{\partial t} = \frac{Q}{A \varepsilon} \qquad 5\text{-}83$$

where ε is the thickness of the active region

$$\Delta T(t) = \frac{Q t}{A C \varepsilon} \qquad 5\text{-}84$$

Using a typical current threshold values J ≃ 10^5 amps/cm^2 and C = 1.73 $\frac{J}{°K\,cm^3}$ and ε = 1μ

$$\frac{d\,\Delta T(t)}{dt} \approx 0.87\ °K/ns \qquad 5\text{-}85$$

Using the room temperature value for the band edge shift of 2.5Å/o_k, and the mode frequency shift of 0.35 times the band edge shift, we find

$$\frac{d\nu}{dt} \approx 30 \quad GHz/ns \qquad 5\text{-}86$$

Spectral shifts this rapid may be observed if (i) the Fabry-Perot interferometer has a large free spectral range say 100-150 GHz might be a good choice and (ii) sampling techniques are used. Interferometers with this large a free spectral range can be made, but measurements at 300°K were not performed since neither equipment with the necessary speed nor a suitable interferometer was available.

6. Detection of Sidebands During Pulsed Operation

In order to determine the feasibility of detecting sidebands under pulsed operation, the following experiment was conducted. A pulse of current was sent through a 50 ohm resistor in series with a GaAs laser so that it lased in a pulsed mode. The amplitude of the current pulse was chosen so that the laser remained in a single mode. A modulating signal at a frequency of 480 MHz was capacitatively coupled from a signal generator to the laser bias head. The pulsed, modulated light was passed through a Fabry-Perot interferometer, as mentioned before, and the output of the photodetector placed behind the interferometer was monitored on an oscilloscope. The modulating signal was increased, keeping the current pulse constant. Figure 5-18 shows a series of five pictures as the modulating voltage is increased. The horizontal time scale is 10 μsec/cm and the vertical scale 20 μV/cm. Figure 5-18a shows the output when no modulation is applied. The increasing time difference between peaks is due to the saturation of the laser temperature rise. As the modulating signal is increased, sidebands appear on either side of the carrier frequency. The first zero of the carrier can be seen in fig. 5-18d. In fig. 5-18e the first sidebands are zero.

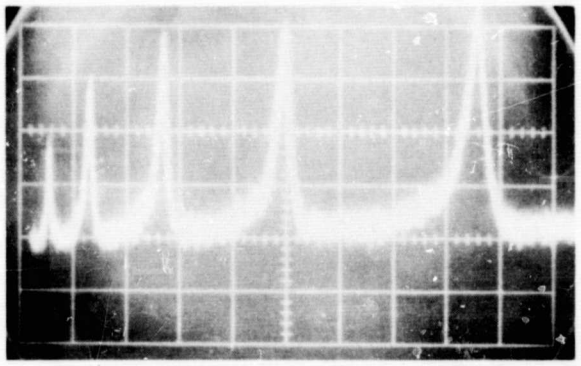

(a)
MODULATION VOLTAGE = 0

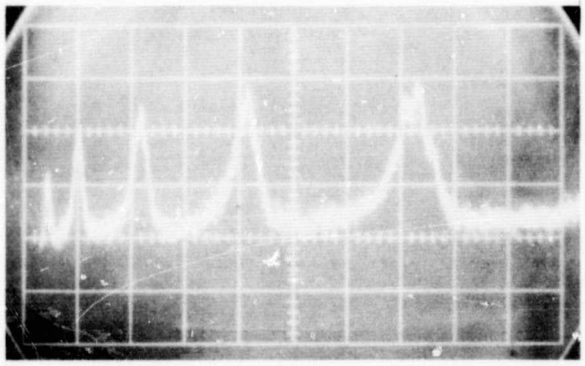

(b)
MODULATION VOLTAGE = 34 mV

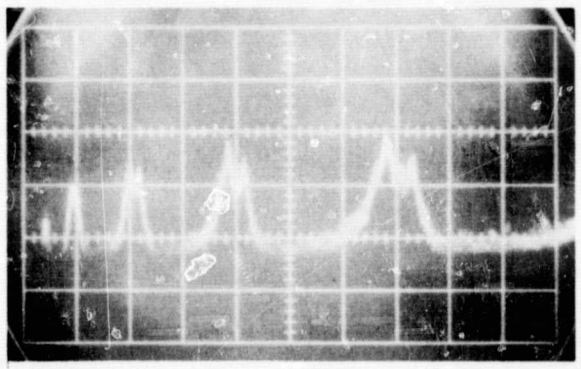

(c)
MODULATION VOLTAGE = 50 mV

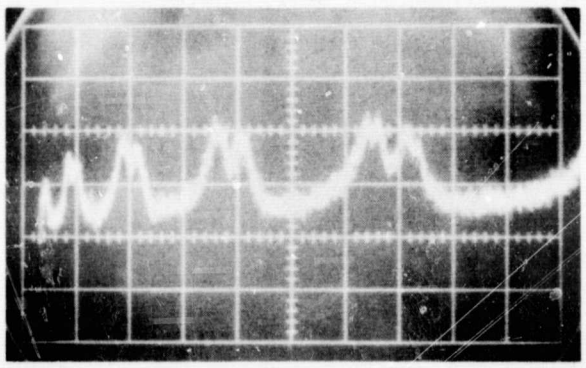

(d)
MODULATION VOLTAGE = 70 mV

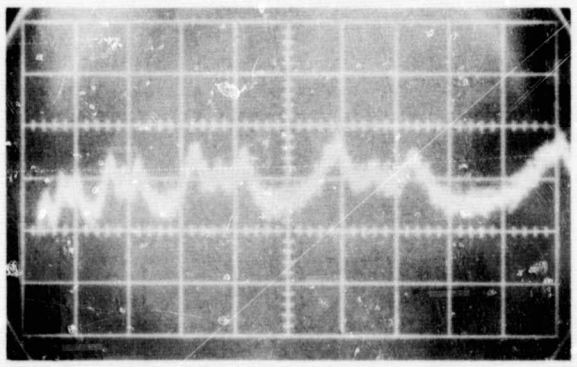

(e)
MODULATION VOLTAGE = 130 mV

L-26
HORIZONTAL SCALE : 10 μs/cm
VERTICAL SCALE : 20 μV/cm
LASER CURRENT = 220 mA
T = 77°K

FIG. 5-18 MODULATION OF A PULSED INJECTION LASER AT 480 MHz

The reverse of this experiment, where the laser was operated cw and the modulating signal was pulsed, was also performed to demonstrate how power is pumped from the carrier to the sidebands. The output from the photodetector was amplified by a Tektronix 1A7 plug-in amplifier and fed to the Boxcar Integrator along with a trigger pulse. The output of the Integrator was fed to the Y-axis of an X-Y recorder while the interferometer scanning voltage was fed to the X-axis. D.C. signals were filtered out in the plug-in amplifier and prevented from reaching the Boxcar Integrator. As the interferometer was swept the X-Y recorder plotted changes in light intensity against frequency. Figure 5-19 shows such a plot where a modulating frequency of 1 GHz was used. The negative peak corresponds to the intensity pumped from the carrier frequency into the sidebands by the modulating signal. The positive peaks on either side of the carrier are due to the first sidebands.

7. Conclusions

It has been shown that the spectral shift under pulsed operation of a semiconductor laser may be measured using a Fabry-Perot interferometer. Furthermore, the laser fires, from pulse to pulse, consistently into the same starting frequency. The spectral shift observed at 77°K was consistent with that calculated from the temperature change of indium binding layer. At 4.2°K the observed shift was attributed to pockets in this layer. Frequency sidebands were observed under pulsed operation showing the feasibility of detecting frequency modulation when the laser is pulsed. Also it is shown that the same technique may be used at room temperature.

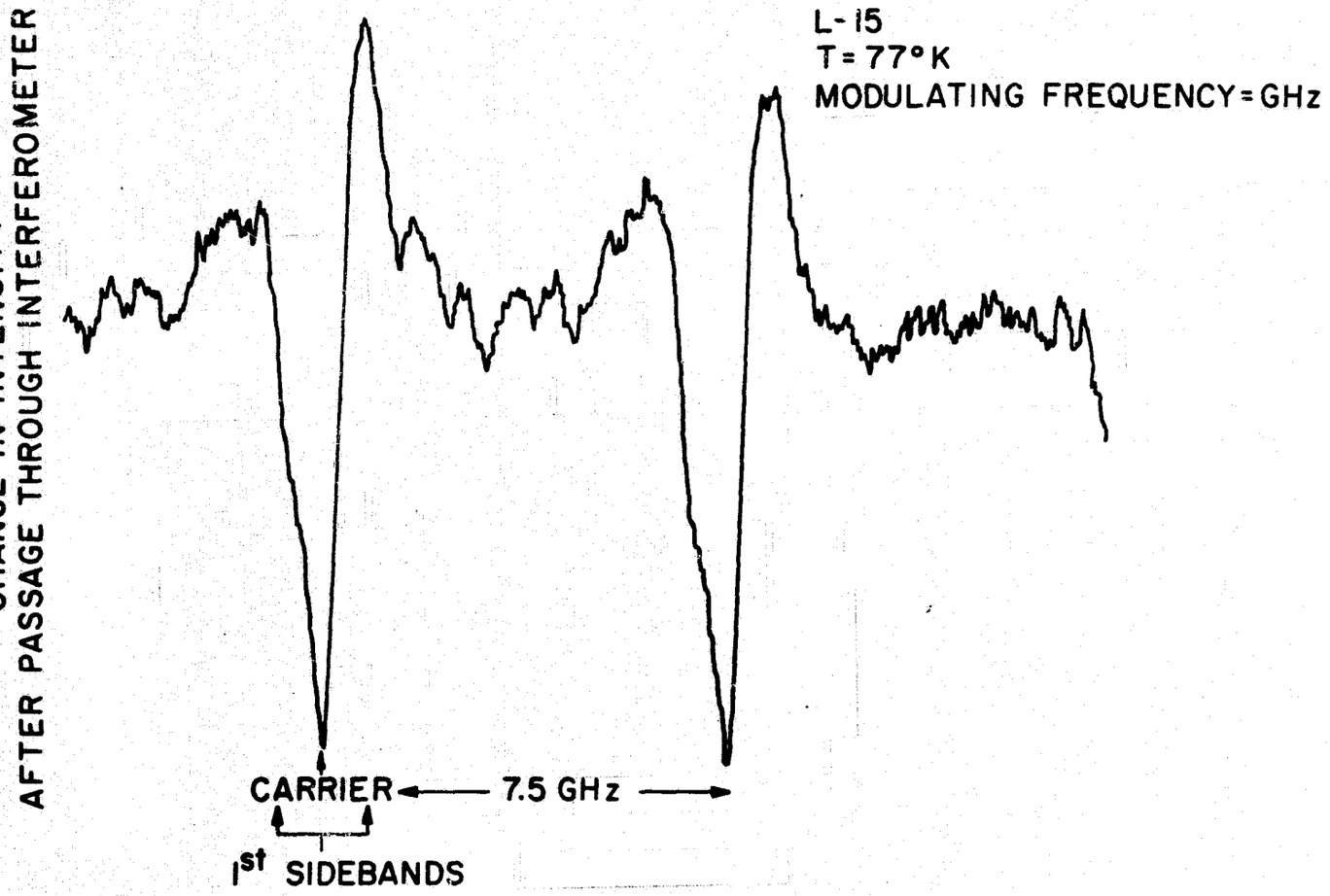

PULSED MODULATION
ON A CW SEMICONDUCTOR LASER

FIGURE 5-19

References

1. W. Engeler and M. Garfinkel, Solid State Electronics 8, 585 (1965).

2. M. S. Carslow and J. C. Jaeger, "Conduction of Heat in Solids," Oxford University Press (1959).

3. W. Engeler and M. Garfinkel, Journal of Applied Physics 34, 2746 (1963).

Biographic Note

Colin G. Whitney was born in London, England, on July 2, 1944. In June 1966, he receive his B.S. degree in physics from the Massachusetts Institute of Technology and in September 1966 began a doctoral program in the Physics Department at the Massachusetts Institute of Technology. From September 1966 to September 1967 he held a MIT Woodrow Wilson Fellowship and was elected member of the Society of Sigma Xi in June 1970. His publications to date are: "Direct Frequency Modulation of a Semiconductor Laser by Ultrasonic Waves", IEEE Journal of Quantum Electronics, QE-2, 9, 603 (September 1966); "Frequency Modulation and Demodulation of a Gallium Arsenide Injection Laser Using Ultrasonic Waves", IEEE Journal of Quantum Electronics, QE-3, 5, 202 (May 1967); "Resolution of Sidebands in a Semiconductor Laser Frequency Modulated by Ultrasonic Waves", presented at the IEEE Semiconductor Laser Conference, Mexico, December 1969, and published in the IEEE Journal of Quantum Electronics, June 1970.

Unclassified

Security Classification

DOCUMENT CONTROL DATA - R & D

(Security classification of title, body of abstract and indexing annotation must be entered when the overall report is classified)

1. ORIGINATING ACTIVITY *(Corporate author)*
Massachusetts Institute of Technology

2a. REPORT SECURITY CLASSIFICATION
Unclassified

2b. GROUP
NA

3. REPORT TITLE
The Behavior of Laser Modes in a Medium with Time Varying Dielectric Constant

4. DESCRIPTIVE NOTES *(Type of report and inclusivn dates)*
Technical Report

5. AUTHOR(S) *(First name, middle initial, last name)*
Colin Gordon Whitney

6. REPORT DATE	7a. TOTAL NO. OF PAGES	7b. NO. OF REFS
25 Aug 70	168	

8a. CONTRACT OR GRANT NO.	9a. ORIGINATOR'S REPORT NUMBER(S)
DA-31-124- ARO-D-92	NA
b.	
c.	9b. OTHER REPORT NO(S) *(Any other numbers that may be assigned this report)*
d.	4109.12-P

10. DISTRIBUTION STATEMENT
Approved for public release; distribution unlimited.

11. SUPPLEMENTARY NOTES	12. SPONSORING MILITARY ACTIVITY
	U. S. Army Research Office-Durham Box CM, Duke Station Durham, North Carolina 27706

13. ABSTRACT

The effect, on semiconductor laser modes, of a time-varying modulation of the complex dielectric constant of the active region of the laser, is considered. It is seen that the main effect is to produce frequency modulation associated with modulation of the real part of the dielectric constant while modulation of the imaginary part gives rise to amplitude modulation. Two methods for producing the modulation are considered. The first, pressure via ultrasonic waves, produces pure frequency modulation in impure material. The second, modulation of the injection, results in both amplitude and frequency modulation.

Experiments to confirm this analysis were carried out on a cw GaAs injection laser. The modulated laser spectrum was observed with a Fabry-Perot Interferometer. Pressure modulation was seen to give frequency modulation with little distortion, while for injection modulation, ratio of the amplitude modulation index to frequency modulation index was found to be about 0.1.

High resolution measurements on the pulsed spectral shift of a GaAs laser at 77°K and 4.2°K were performed using a Fabry-Perot interferometer. The feasibility of detecting modulation on a pulsed semiconductor laser was demonstrated.

14. KEY WORDS

Gallium arsenide lasers
Light modulation
Frequency modulation
Laser beams
Dielectric properties

DD FORM 1 NOV 65 1473 REPLACES DD FORM 1473, 1 JAN 64, WHICH IS OBSOLETE FOR ARMY USE.

Unclassified